C.E. Davies

ERRATA

p 31, line 17 for "gasbourne" read 'gasborn'.

p 64 Equation E.3.28 should read $\tau_m = \sum_{t=0}^{t=\tau} (N_{or} \Delta t) = N_{or} \tau$

p 64 Equation E.3.29 should read $\tau_a = \sum_{t=0}^{t=\tau} (N_{op} \Delta t) = N_{op} \tau$

p 77, under "conditions", for "402 m" read '402 μm'.

p 109, line 20 for "bahaviour" read 'behaviour'.

p 128 Equation E.A.2.3 should read $R_r = \pi D_t \, e \sigma (T^4 - T_w^4)$

p 129 Equation E.A.2.8 should read $R_{nr} = \pi D_t e \sigma (T_{nr}^4 - T_w^4)$

p 155, line 6 for "0.4 x $10^{-3} m^3/s$ " read '0.4 x $10^{-4} m^3/s$ '.

THE DESIGN, CONSTRUCTION AND COMMISSIONING OF A PILOT PLANT FOR THE FLUIDISED BED COMBUSTION OF GASIFIED FUEL OIL.

A Thesis submitted for the degree

DOCTOR OF PHILOSOPHY

University of London

by

CLIVE ERIC DAVIES

B.Sc., A.C.G.I.

Department of Chemical Engineering

and Chemical Technology,

Imperial College of Science and Technology,

London S.W.7.

January, 1976.

TO DIANA

ABSTRACT

A fluidised bed combustor, 0.61 m in diameter, has been designed and built to burn a reducing gas formed by the gasification of residual fuel oil. The oil is spray atomised in a high intensity combustion chamber, and the gasified oil containing large quantities of solid carbon is passed into a fluidised bed where it is mixed with air. A distributor plate having ceramic tuyeres has been designed to promote good gas-air mixing close to the bottom of the bed to encourage the complete combustion of the gas and air in the bed. Commissioning trials have been carried out, and a plant incorporating the combustor is now ready for experimental tests.

A model has been developed to study the effect of changes in distributor plate geometry, and orifice non-operation on the efficiency of combustion of coalescing bubbles of gas and air on a distributor plate. It has been shown that orifice separation, and a delay time between the commencement of operation of air and gas orifices, can both strongly affect combustion efficiency. The model has been applied to the distributor plate designed in this work to illustrate the interaction of the system variables. The results show the importance of the relative numbers of air and gas orifices in a distributor plate which injects air and gas separately into a fluidised bed on gas combustion efficiency, and also on the combustion of any solid carbon in the gas feed.

LIST OF CONTENTS

LIST OF FIGURES

LIST OF TABLES

ACKNOWLEDGEMENT

The stimulating supervision of Dr. Paul Eisenklam has made my period of research memorable and instructive.

The interest shown in the project by Professor A.R. Ubbelohde and Professor R.W.H. Sargent was greatly appreciated, and the co-operation of members of the departmental staff at all times has been invaluable.

Thanks are given to Mr. J.S. Oakley for his constant interest in the work, and to Mr. H. Simmons and Mr. R. Davis for their contributions to the construction of the plant. My colleagues, N. Munz and D. Rodriguez, have assisted in the preparations for the experimintal trials, and have provided interesting company and lively disussion during all stages of the project.

Financial support was received from a college bursary, The World University Service, The British Council, The Courtaulds Fund, and Professor A.R. Ubbelohde.

I would like to thank the members of my family, in particular my wife, Diana, for their understanding and encouragement at all times.

NOTATION

All dimensions are in terms of S.I. units except where otherwise specified.

Primary Units:

Length	L	meter	m
Mass	M	kilogram	kg
Time	T	second	s
Temperature	θ	degree Kelvin	K

Derived Units:

Force	F	newton	$N = kg\,m\,s^{-2}$
Energy	E	joule	$J = Nm$
Power	P	watt	$W = Js^{-1}$

Symbol	Significance	Dimensions
a	Number of moles of air used in oil gasification per carbon atom in fuel.	
a_b	Mass of air in bubble.	M
b	Number of moles of carbon dioxide in gasified oil per carbon atom in fuel.	
c	Number of moles of carbon monoxide in gasified oil per carbon atom in fuel.	
c_b	Concentration of combustible gas in bubble.	ML^{-3}
c_{bo}	Concentration of combustible gas in bubble at distributor plate.	ML^{-3}

c_d	Discharge coefficient.	
c_p	Mean molal heat capacity of the gasified oil.	$EM^{-1}\,\Theta^{-1}$
C_s	Percentage of carbon in solids.	
d	Number of moles of water vapour in gasified oil per carbon atom in fuel.	
d_{or}	Orifice diameter.	L
d_{org}	Diameter of gas orifice.	L
d_p	Mean particle diameter.	L
d_t	External diameter of tuyere.	L
D_b	Bubble diameter.	L
D_r	Diameter of fluidised bed	L
e	emissivity	
E_p	Gas combustion efficiency on a distributor plate.	
$\bar{E}_p$	Mean gas combustion efficiency on a distributor plate (E.3.44, p 70).	
f	Number of moles of hydrogen in gasified oil per carbon atom in fuel.	
f_b, f_{bi}	Mass of fuel in a bubble.	M
F_p	Mass flowrate of fuel to particulate phase.	MT^{-1}
F_1	Mass flowrate of fuel to gasifier.	MT^{-1}
g	Acceleration due to gravity.	LT^{-2}
G_b, G_{bi}, G_{bj}	Volumetric flowrate to bubble.	L^3T^{-1}
h	Number of atoms of solid carbon in gasified oil per carbon atom in fuel.	
H_b	Height of fluidised bed.	L
ΔH_b, ΔH_{bi}	Heat released in bubble per unit mass of fuel.	EM^{-1}

ΔH_{ov}	Maximum heat release per unit mass of fuel.	EM^{-1}
ΔH_p	Heat released in particulate phase per unit mass of fuel.	EM^{-1}
H_r	Heat of reaction.	EM^{-1}
H_s	Percentage of hydrogen in solids in gasified oil.	
i	Number of moles of methane in gasified oil per carbon atom in fuel.	
i^*	Percentage by volume on a dry basis of methane in gasified oil.	
j	Number of moles of sulphur dioxide in gasified oil per carbon atom in fuel.	
k, k_1, k_2, k_3	constants	
k_{bc}	Volume of gas exchanged between bubble and cloud per unit volume of bubble per unit time.	T^{-1}
k_{bp}	Volume of gas exchanged between bubble and particulate phase per unit volume of bubble per unit time.	T^{-1}
k_{cp}	Volume of gas exchanged between cloud and particulate phase per unit volume of bubble per unit time.	T^{-1}
K_d	Grate flow factor (E.2.4, p 35)	$L^2T^{-1}F^{-\frac{1}{2}}$
l_t	Length of horizontal duct in tuyere.	L
L	Jet length.	L
M_s	Mass of solids produced in oil gasification per unit mass fuel burnt.	
n	Average number of carbon atoms per molecule of fuel.	

n_b	Number of bubbles formed during an extended period of plate operation.	
N	Number of tuyeres on a distributor plate.	
N_a	Number of air orifices on plate.	
N_c	Average number of product bubbles on plate.	
N_{dc}	Number of successive dual bubble coalescences undergone by bubble leaving region of distributor plate.	
N_{op}	Number of operative orifices on a distributor plate.	
N_{or}	Number of orifices on a distributor plate.	
p	Proportion of orifices in array that are operative.	
p_a	Proportion of air orifices in array that are operative.	
p_g	Proportion of gas orifices in array that are operative.	
$\bar{P}$	Heat release rate in fluidised bed.	P
ΔP_b	Pressure drop across fluidised bed.	FL^{-2}
ΔP_{bmf}	Pressure drop across a fixed bed in the entrance region of a fluidised bed, at incipient flow from each orifice (E.2.5, p 36).	FL^{-2}
ΔP_d	Pressure drop across the distributor plate.	FL^{-2}
ΔP_s	Pressure drop across a preferential gas path in a fluidised bed (E.2.5 p 36).	FL^{-2}
Q	Heat removed from the gasified oil per carbon atom in the fuel.	EM^{-1}

Q_g	Heat removed from the gasified oil in the the gas plenum chamber per unit mass of fuel.	EM^{-1}
Q_i	Heat removed from the gasified oil in the cooling tube per unit mass of fuel.	EM^{-1}
Q_r	Heat removed from the gasified oil in the fluidised bed per unit mass of fuel.	EM^{-1}
Q_s	Sensible heat of the gasified oil per unit mass of fuel.	EM^{-1}
Q_{s1}	Sensible heat of the gas stream burnt with the stoichiometric air requirement in the second stage, per unit mass of fuel.	EM^{-1}
Q_{sa}	Sensible heat of the gasified oil under adiabatic conditions per unit mass of fuel.	EM^{-1}
Q_{sa1}	Sensible heat of the gasified oil at an equivalence ratio of one under adiabatic conditions per unit mass of fuel.	EM^{-1}
Q_t	Total heat removed from gasified oil per unit mass of fuel.	EM^{-1}
r_b	Radius of bubble.	L
r_c	Radius of bubble cloud.	L
R_a	Mass flowrate of air to fluidised bed.	MT^{-1}
R_{ab}	Mass flowrate of air to bubble phase.	MT^{-1}
R^*_{ab}	Mass flowrate of air to bubble phase from single orifice.	MT^{-1}
R_g	Mass flowrate of gas to fluidised bed.	MT^{-1}
R_{gb}	Mass flowrate of gas to bubble phase.	MT^{-1}
R^*_{gb}	Mass flowrate of gas to bubble phase from single orifice.	MT^{-1}
R_{gp}	Mass flowrate of gas to particulate phase.	MT^{-1}
s	Height above distributor plate in fluidised bed.	L
t	Time.	T

t_a	Time air orifice operates.	T
t_b	Formation time of product bubble.	T
t_d	Delay time.	T
t_{da}	Delay time at air orifice.	T
t_{dg}	Delay time at gas orifice.	T
t_g	Time gas orifice operates.	T
T	Gas temperature.	Θ
T_a	Air temperature.	Θ
U	Superficial velocity.	LT^{-1}
U_a	Absolute velocity of rise of bubble in bubbling bed.	LT^{-1}
U_b	Velocity of rise of single bubble.	LT^{-1}
U_g	Superficial velocity calculated on the basis of the unreacted gas.	LT^{-1}
U_m	Superficial velocity above which all tuyeres are continuously operative.	LT^{-1}
U_{mf}	Superficial velocity at incipient fluidisation.	LT^{-1}
U_{or}	Fluid velocity at orifice.	LT^{-1}
V	Bubble volume.	L^3
w	Air to fuel mass ratio for stoichiometric combustion.	

Greek letters.

β	Angle of repose.	
ϵ, (ϵ_{mf})	Bed voidage at (incipient fluidisation)	
θ	Half angle of cone at top of tuyere.	
λ	Orifice separation.	L
μ_f, (μ_f^T)	Fluid viscosity, (at temperature T).	FTL^{-2}

ρ_f	Fluid density.	ML^{-3}
ρ_o	Fluid density at orifice.	ML^{-3}
ρ_p	Particle density.	ML^{-3}
τ	Extended period of operating time.	T
τ_a	Actual time orifices are operative during τ.	T
τ_m	Maximum operative time for whole plate during τ.	T
ϕ	Equivalence ratio, defined: $\left[\frac{\text{Mass of air required for stoichiometric combustion}}{\text{mass of air supplied}}\right]$	
ϕ_1	Gasifier equivalence ratio.	
ϕ_b	Equivalence ratio of product bubble.	
ϕ_g	Equivalence ratio of gas.	
ϕ_p	Equivalence ratio of particulate phase.	
χ	Ratio of open area of distributor plate to total area (E.2.5 p 36).	

A bar $\bar{}$ over a letter signifies an average value.

CHAPTER ONE

INTRODUCTION

Fluidised bed combustion has received extensive research attention in the last two decades. The high heat transfer rates and combustion efficiencies attainable, allow a reduction in plant size, and accompanying reductions in capital cost. Pollution control with both inert and chemically active beds provides an economic solution to the increasingly stringent legal requirements governing atmospheric emissions, and these together with additional associated benefits make the method of burning a fuel in a fluidised bed very attractive.

Residual fuel oil is cheap, and therefore economically favourable. However, the higher oxides of metal impurities contained in the oil cause high temperature fireside corrosion. These oxides are only formed in the presence of free oxygen, and at high temperatures, and a two stage system may be employed to ensure that they are not produced. The fuel is burnt with less than the stoichiometric amount of air and passes via a heat exchanger to a second combustor where more air is added to make up the stoichiometric requirement and release the remaining calorific content of the gasified fuel. In an experimental investigation of a two stage system firing residual fuel oil, Archer and Eisenklam (1) found that solid carbon formed in cracking reactions and from incompletely burnt oil drops was only partially removed by a tunnel type combustor used as a second stage, although under certain conditions solid emissions were reduced below the statutory limit.

The object of this research has been to design, construct, and commission a versatile fluidised bed combustor. This is to be the second stage to the gasifier described in reference (1), and used in a long term

investigation of the suitability of fluidised bed combustion as a method for burning fuel oil gasified in a high intensity combustor.

A fluidised bed 610mm (2ft) in diameter to which gasified fuel and air are fed through separate arrays of tuyeres on the distributor plate, and in which mixing and combustion take place, has been designed and built, and a plant incorporating this combustor has been commissioned.

A model has been developed to study the effect of distributor geometry and air and gas inlet conditions on the efficiency of the combustion in gas bubbles on a distributor plate, and the results applied to the calculation of the theoretical efficiency of gas combustion in the combustor. Theoretical gas combustion efficiencies were found to vary between 100% and 76% for gasifier equivalence ratios between 1.1 and 1.55 and oil flows between 2.5 g/s and 3.5 g/s, and corresponding heat release rates were calculated to lie between 1.6 kw and 11 kw.

The fluidised bed reactor is now ready for pilot scale work to establish:

(i) the combustion efficiencies obtainable in the reactor.

(ii) whether soot can be burnt effectively in the bed, and the behaviour of ash that is formed.

(iii) the thermal stability of this type of reactor to low temperature operation.

CHAPTER TWO

LITERATURE REVIEW

The purpose of this review is to examine the suitability of the method of fluidised bed combustion for completing the combustion of oil gasified in a conventional burner, and to establish criteria for the design of a combustor to do this.

2.1. Gasification of Residual Fuel Oil in a High Intensity Combustor.

Residual fuel oil is the residue from the distillation of crude oil, in which inorganic and organo-metallic impurities in the crude are concentrated by the stripping of light petroleum fractions. It is the manifestation of these impurities as the cause of high-temperature fireside corrosion of boiler tubes and turbine blades that offsets the attractiveness of the low cost of residual fuels. Because of their high viscosity, residual fuels must first be preheated and then blast atomised with air, steam or a mixture of both, before combustion will satisfactorily occur.

High intensity combustors are designed with careful internal contouring and air-jet location to eliminate dead volume and promote intense mixing of fuel and air. Complete combustion is obtained with minimal excess air, and heat release rates per unit combustor volume are high. Ewings (2) describes three such combustors and reviews some commercial applications for this type of oil burner.

In designing a two stage combustion system, it is important to be able to estimate the quantity of any interstage heat transfer, as this can determine the stability of the second stage. The design of a fluidised bed for a specified mass throughput requires a knowledge of the properties of the gases entering the bed through the distributor plate, and data on

the chemical and thermal properties of the products of the High Duty Combustion Chamber* that is used as the gasifier in this work are available from previous experimental studies. The H.D.C.C. is depicted in Fig. 1.1. The oil used was an Admiralty reference fuel code named Vanilla, and its specification is given in Appendix 1.

2.1.1. Composition and Temperature of Gasified Oil. Archer et al.(1) atomised the fuel with steam, and found that the carbon monoxide, carbon dioxide, hydrogen and water vapour in the products of the gasifier were within $\pm$ 2% of the values predicted by the water gas equilibrium, and that temperatures corresponded well with theoretical values. A second stage converter was placed after the gasifier, and heat was removed between the stages. The compositions and temperatures of emissions from the converter were those predicted by the water gas shift reaction.

Johns (3) atomised the fuel with air and found that the temperatures reached by the gasified oil were close to those predicted by equilibrium existing between the carbon monoxide, carbon dioxide, hydrogen and water vapour in the gasified oil.

2.1.2. Solids Produced. Htun (4) measured the solid loading of the combustion products, and regressions of data obtained by him have been given in reference (1). For air atomised flames:

$$M_s = 0.041\ \phi_1^2 - 9.6\ F_1 - 0.0074 \qquad \text{E 2.1.}$$

where:

M_s Mass of solid produced per mass fuel gasified.

F_1 Oil flowrate to the gasifier (kg/s).

ϕ_1 Equivalence ratio of the gasifier.

Equivalence ratio, ϕ, is defined;

$$\phi = \frac{\text{mass of air required for stoichiometric combustion}}{\text{mass of air supplied}}$$

---

* The H.D.C.C. was manufactured by Urquharts (1926) Ltd., Perivale, Middlesex.

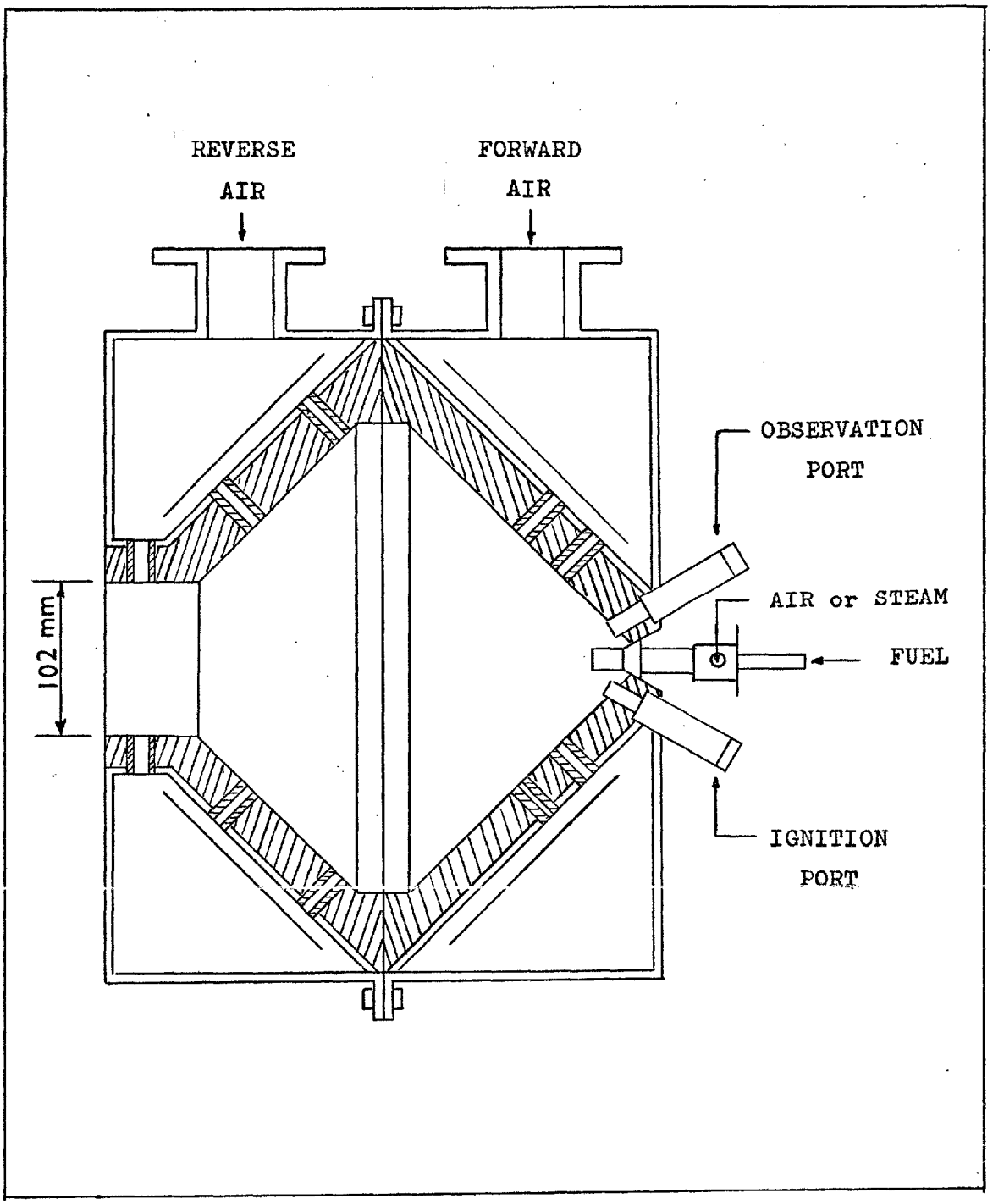

FIG. 1.1: H.D.C.C. GASIFIER.

2.1.3. Heat Transfer from Combustion Products. Dombrowski and Johns (5) varied the air to fuel ratio and flowrate of oil to the H.D.C.C. and measured the amount of heat removed from the combustion products by a known length of cooling tube. They measured the temperature of the cooled gases, and then used a numerical method of stepwise integration along the length of the cooling tube to deduce values of a temperature independant gas emissivity. They did not take the condition of the inside of the tube into account, and thus their results are a funotion of their experimental equipment and the method by which they were calculated. However, the same tubes are available for use in this work and reapplication of their methods to the results they computed should enable the temperature of the gases entering the fluidised bed and the total interstage head transfer to be found.

2.2. Two Stage Combustion.

The high flame temperatures and a presence of free oxygen in the combustion products that together cause high temperature corrosion when residual fuels are burnt, may both be avoided by employing multistage systems. High grade heat is removed between the stages, and the full heat of combustion of the fuel is released by the staged addition of the stoichiometric air requirement. The simplest and most practicable multi-stage unit is a two stage system.

2.2.1. Corrosion Inhibition. Htun (4) observed that sodium vanadyl vanadate which is responsible for high temperature corrosion, was only formed under oxidising conditions. Rodriguez (6) has considered the thermodynamics of vanadium oxidation in combustion systems and has shown that when equilibrium prevails, vanadium pentoxide is only produced under

certain oxidising conditions.

A two stage system for the combustion of residual fuel oil has been described by Archer and Eisenklam (1). They found that the system was successful in inhibiting the formation of corrosive metal salts and oxides. Rodriguez (6) carried out further experiments on the same rig used in reference (1) and did not detect vanadium pentoxide in solids collected from the system exhaust.

2.2.2. Solid and Gaseous Pollutants. Archer et al. (1) noted that they could operate their two stage system so that the solids in the second stage emissions were below the statutory limit of 0.4% of the mass of fuel (7), but that the converter could not burn all the solid carbon produced in the outdated first stage. The converter was a tunnel type burner and consisted of a well mixed reactor followed by a plug flow section. Grout (8) has recommended the redesign of the second stage, and the removal of the plug flow section as he found that it did not improve combustion efficiency.

Many fuels have high sulphur contents, and consequently the flue gases of installations firing such fuels have unacceptably high levels of sulphur oxides. As expected, sulphur trioxide was not detected in the exhaust of the H.D.C.C. firing residual fuel with a sulphur content of 2.4% by weight (1), but sulphur dioxide was produced, and is itself a highly undesirable pollutant.

Rodriguez (6) measured both first stage and second stage NO_x levels, and showed that emissions from the second stage operating at an equivalence ratio of one were well below those recorded for a single combustor fired at the same equivalence ratio. The use of two stage combustion for NO_x pollution control has also been noted by Bartok et al. (9), and as with corrosion inhibition, it is the limited oxygen availability in the sub-stoichiometric first stage, and elimination of high temperatures, that encourages low NO_x readings.

It is clear that two stage combustion offers a solution to the problem of high temperature corrosion, and has the added benefit of reducing NO_x emissions. But the solid loading of the exhaust of the pilot scale plant considered in this review is high, and is only below the legal limit under certain operating conditions. Combustion control cannot prevent the formation of sulphur dioxide, and the removal of this pollutant from the products of combustion must be achieved by chemical or physical methods.

2.3. Fluidised Bed Combustion and Pollution Control.

Fluidised beds have been used in sulphur and nitrogen oxide pollution control, and the use of a chemically active fluidised bed in a two stage system carries the prospect of clean power production from residual fuels rich in pollution and corrosion generating inorganic elements.

The principle of a two stage system having a fluidised bed second stage and a conventional gasifier has been discussed by Eisenklam and Archer (10), but the operation of this type of system has not been reported.

Fluidised bed combustion has received extensive world wide research attention over the last twenty years. The list of potential advantages of fluidised bed combustors over conventional systems is long, but most stem from the high heat transfer rates attainable, and the encouraging results of ventures into pollution control using fluidised systems. Most of the research in this field has been concerned with the fluidised bed combustion of coal, and progress to 1969 has been reviewed by Skinner (11). The Proceedings of three invited conferences in fluidised bed combustion (12) held under the auspices of the E.P.A. of the United States were predominantly descriptions of commercial coal fired systems, and in the Institute of Fuel Symposium Series No. 1 (13), the majority of papers again relate

to the fluidised bed combustion of coal.

The combustion of a solid fuel requires gas-solid contact, whereas when liquid (14) and gaseous fuels are used, the combustion reaction demands contact of gaseous species only. Although the mechanisms of combustion are different, the principle of using a fluidised bed for reducing the level of gaseous pollutants formed in combustion reactions is successful whether a solid (13), liquid (15) (16), or gaseous fuel is used. Natural gaseous fuels do not usually exhibit the high sulphur levels of coal or oil, but regenerative fluidised beds have been used for the removal of sulphur dioxide from the simulated exhaust of conventional plant (17), and sulphur dioxide added to natural gas was almost completely absent when the gas was burnt in a bed of limestone (18). Low NO_x emissions have been recorded both from fluidised beds of inert particles, (19), (20), and chemically active materials (18).

Lunn et al. (16) have noted that when residual fuel oil was burnt in a bed containing limestone, up to 70% of the sodium and 99% of the vanadium in the oil was retained by the bed material.

2.4. Fluidised Bed Combustion of Gases.

This subject may be split into two subdivisions; the combustion of premixed air and gas, and the combustion of gas and air added separately to the bed. Several investigators have established that premixed gas and air may be completely burnt in very shallow fluidised beds, whilst it has also been reported that deeper beds must be used when the gases are not premixed.

2.4.1. Premixed Reactants. Cole and Essenhigh (21) burning natural gas in a square combustor, 0.13 m^2 (1.4 ft^2) in cross-sectional area, were

able to obtain complete combustion in beds as shallow as 0.025 m, and Broughton (20) notes that combustion of gas-air mixtures was completed 0.05 m above the distributor plate of a 100 mm diameter bed. Elliot and Virr (19) give a similar result in noting the completion of combustion 0.013 m (½ in) above the distributor in beds of small diameter. In all cases, a porous-plate type of distributor was used.

2.4.2. Separate Air and Gas Injection. Tamalet (22) found that at low superficial velocities, the pattern of gas injectors in a pilot unit could still be seen at the top of a bed 0.686 m (2 ft 3 in) deep, but that modifications to the distributor (not described) did result in complete combustion within the bed.

In preliminary studies of gas combustion in fluidised beds, Cole and Essenhigh (21) used a perforated distributor and injected air and gas separately. The distributor chosen was a square plate set with a 9 x 9 array of horizontally perforated hollow studs on a 0.038 m (1.5 in) square pitch. 17 of the 81 studs supplied gas, and the remaining 64, air. This design proved unsatisfactory as flames were seen to stabilise on the bed surface in a pattern corresponding to the layout of the gas inlets.

Reh (23) measured combustion efficiency and temperatures in a 813 mm (32 in) diameter bed firing town gas. It was fluidised by an air flow distributed evenly over its base and the gas was injected through a centrally located tuyere. Efficiency was measured as the percentage of unburned carbon in samples of gas withdrawn at various levels, and increased with increasing bed height. The superficial velocity, U, of the gases was varied, and at a given bed height the efficiency fell with increasing U. The amount of unburnt carbon in the gases at the surface of the bed which was 1.52 m (5 ft) deep, varied from

5% when U was 1.3 m/s (4.2 ft/s), to 20% when U was 2.2 m/s (7.2 ft/s).

A novel type of distributor that is suitable for use at high temperatures has been invented by Evans (24). This device consists of two concentric pipes each pierced by a number of holes. The fluidising gas flows down the central pipe and into the annular space between the pipes, and thence into the bed. By placing the pipes so that the holes in the outer pipe face downwards, it is claimed that satisfactory fluidisation with no back flow of solids into the pipes, is achieved.

Singh et al. (25) used pipes of this kind to inject air and gas separately into fluidised beds. Two beds were used, one rectangular 960 mm x 610 mm, and the other circular and 360 mm in diameter. Experimental results were published for studies on the circular bed. A single central pipe distributor was used to inject LPG into the bed, and air was fed through two pipe distributors located on 85 mm centres on either side of the gas pipe and 100 mm below it. The reported data indicate that the extent of reaction is a strong function of bed height, and that there is some height at which mixing is completed and beyond which no increase in combustion efficiency is observed. For the conditions investigated this was an unspecified height somewhere between 0.09 m and 0.275 m.

The work reported here on separate gas and air injection is characterised by incomplete combustion, with the pattern of the gas injectors visible at the bed surface, or by deep beds required for high combustion efficiency. All the distributors that were described, supplied gas to an area at the base of the bed smaller than that to which they fed the air required for combustion.

Although it is apparent that complete inbed combustion is accomplished more easily when gas and air are premixed rather than mixed in the bed, certain applications of fluidised bed combustion do require that the fuel gas and air be injected separately. In larger installations particularly, the safety problems associated with the handling of inflammable gas

mixtures encourage the development of distributors capable of bringing about efficient inbed combustion of unpremixed gaseous fuels.

2.5. Design Requirement in this Work.

The products of the H.D.C.C. gasifier are hot, and contain suspended carbon particles. They are delivered at 5 kN/m^2 (20 in water gauge).

The option of premixing the reactants is removed, as this would result in immediate ignition. The air supplied to the second stage is the stoichiometric requirement of the gasified fuel, and as the gas phase reactions are almost instantaneous, most of the available oxygen would be immediately consumed, and only that required by the unburnt solid carbon would remain. The mixing chamber would thus itself act as a second stage, whereas the possibility of collecting the carbon in the gas feed on the particles in the bed and circulating these to regions rich in oxygen where the carbon burns off, points to a design in which the air and gas are mixed inside the bed.

The use of packed beds and all types of moving beds for the collection of gasbourne suspensions has been extensively surveyed by Meisen and Mathur (26) and a spouted bed process for the removal of carbon and tar from a cracked hydrocarbon gas has been described by Suzukawa et al. (27).

The first objective of this work is therefore to design a combustor capable of burning the gasified oil inside the bed, and also suitable for the sudy of the behaviour of the carbon suspended in the gas feed.

2.6. The Distributor Plate.

The importance of this was illustrated in section 2.4.2. The following pages assess the suitability of different types of distribution

devices for use with hot dusty gases supplied at low pressure, and also discuss existing models of the bubbling behaviour of a distributor plate. These models were used both in the design of the distributor, and in a theoretical study of bubble coalescence on the plate, carried out to examine the effect of distributor design and flow maldistribution on combustion efficiency.

2.6.1. Functions. The distributor must serve several purposes simultaneously, and these are listed by Whitehead (28). It should distribute the fluidising fluid evenly so as to promote fluidisation as opposed to spouting and channelling, and so that stagnant zones at the bottom of the bed are avoided. In most operations it is also desirable that the bed solids should not run back into the plenum chamber, either during operation or in periods of start up or shut down. Radial mixing in fluidised beds is poor, and when a gas and air are to be injected separately and burnt, the distributor should ensure that the mixing of the fuel and air over the whole cross-section of the bed in the plate region is good.

A designer may influence the performance of a distributor by varying the number, location and geometry of the fluid inlets, the shape of the distributor in the region of the injection points, and the pressure drop across the distributor.

2.6.2. Configuration in Specialised Applications. The most common forms of distributor found in small scale laboratory systems are the porous plate and multi-orifice plate. These are cheap and simple to construct, but the porous plate has a high associated pressure drop, and is unsuitable for use with dusty gases, and the multi-orifice plate allows flowback of solids into the plenum chamber when non-operational, and under some

fluidising conditions.

The large scale operations encountered in industrial practice, have led to the development of a number of specialised distributors, and a selection of these is described by Kunii and Levenspeil (29). Whitehead (28) also reviews several types of distributor, and gives particular attention to gas injection to fluidised beds through multi-tuyere arrays. Plates set with tuyeres are attractive for several reasons. The individual tuyeres may be removed for inspection, cleaning or alteration; the flow through each tuyere and its operation may be monitored, and banks of tuyeres may be connected to independent manifolds.

The bubble cap is a popular type of tuyere, and has successfully been used in lime calciners where staged beds are fluidised by the dusty gas from the unit below. Johnson and Davison (30) adopted this form of distributor to combat problems encountered with a perforated plate used in a study of iron ore reduction in fluidised beds. Holes up to 6.4 mm ($\frac{1}{4}$ in) in perforated plates in 610 mm (2 ft) diameter beds were quickly blocked by carbonaceous deposits laid down from the fluidising gas. Metal and ceramic bubble caps operated for longer than perforated plates, but they too choked after an unsatisfactorily short time. $7\frac{1}{2}$ hours in the case of the ceramic bubble cap, was the longest recorded running time. The fluidising gas was generated by the gasification of coal and had a solid loading of $17 g/m^3$ at the delivery temperature of 1000 C. Further attemptswere made to devise a method of fluidising a bed of haemetite with the reducing gas rich in particulate carbon, and all failed including the use of a mechanical self cleaning grid that remained clean, but did not give good fluidisation.

2.6.3. Bubble Formation. According to the two phase theory of fluidisation, gas in excess of that required for incipient fluidisation passes through the bed in the form of bubbles. These are initiated in the region of the distributor plate, and during their passage through the bed grow in size by coalescence with other bubbles, though some bubble splitting also occurs.

Harrison and Leung (31) have investigated bubble formation at an orifice in a fluidised bed, and suggest that bubbles are formed in the same way as in an inviscid liquid of zero surface tension. Bubble growth under these conditions may be described by balancing the buoyancy force of the bubble and the upward mass acceleration of the surrounding liquid (32), giving an equation for the upward motion of the bubble:

$$Vg = \frac{d}{dt}\left(kV\frac{ds}{dt}\right) \qquad \text{E.2.2.}$$

where:

g Acceleration due to gravity.

k Constant.

s Distance above the distributor.

t Time.

V Bubble volume.

If the bubble is fed at a constant volumetric flowrate, G, the volume of the bubble at any time is Gt, and E.2.2 may be integrated with the boundary conditions;

$$t = 0, \quad \frac{ds}{dt} = 0, \quad s = 0, \quad V = 0$$

to give:

$$V = \left(\frac{48k^3}{\pi}\right)^{\frac{1}{5}} \frac{G^{\frac{6}{5}}}{g^{\frac{3}{5}}} \qquad \text{E.2.3.}$$

Leung (33) has applied this result to the design of multi-orifice distributors required to give a specified bubble size range, and has shown the use of the equation is consistent with the experimental bubble size data reported by Whitehead and Young (34).

Watson and Harrison (35) have extended equations derived for single bubbles to cover bubble interaction on a multi-orifice plate, assuming that when two bubbles touched they coalesced instantaneously.

2.6.4. Bubbling Mode. Experiments with both multi-tuyere assemblies and multi-orifice plates have indicated that bubbles only form continuously at all the orifices or tuyeres when a certain superficial velocity is reached.

Whitehead and Dent (36) studied multiple-tuyere assemblies that served as distributors in 4 square fluidised beds. These operated isothermally and varied in cross-section from .092 m^2 (1 ft^2) to 5.9 m^2 (64 ft^2), and contained sand to depths of 1.22 m (4 ft). They deduced the semi-empirical equation E.2.4, relating the various parameters that affected the superficial velocity, U_m, above which all tuyeres were continuously operative.

$$\frac{U_m}{U_{mf}} = 0.7 + \left[\frac{0.49 + 3.23.10^{-7}\ N^{0.22}\ K_d \rho_p H_b}{U^2_{mf}}\right]^{\frac{1}{2}} \qquad \text{E.2.4.}$$

where:

H_b Bed height (ft).

K_d Grate flow factor, $\frac{60U}{(\Delta P_d)^{\frac{1}{2}}}$

N Number of tuyeres in the assembly.

ΔP_d Pressure drop across the distributor, (ins water gauge).

U Superficial velocity, (ft/s).

U_{mf} Superficial velocity at incipient fluidisation, (ft/s).

ρ_p Particle density, (lb/ft^3).

It was found that the stability of the distributor was dependent on its resistance to fluid flow rather than the efflux velocity of the gases leaving the tuyere, and this suggests that E.2.4 could be used with distributors having tuyeres of different design to those providing the data used in its derivation.

Fakhimi and Harrison (37) investigated the mode of operation of the orifices in a perforated plate, and derived a relationship between the proportion of bubbling orifices and the properties of the distributor and particles used. Good agreement was found between experimental results and an expression deduced in a theoretical study of the plate region, viz.;

$$\frac{N_{op}}{N_{or}} = \frac{\left[\frac{U}{U_{mf}} - 1\right]}{\left[1 + \frac{2\chi^2}{\rho_f U_{mf}} (\Delta P_{bmf} - \Delta P_s)\right]^{\frac{1}{2}} - 1} \qquad E.2.5.$$

where:

N_{op} Number of operative orifices on the distributor plate.

N_{or} Total number of orifices, in the plate.

ΔP_{bmf} Pressure drop across a fixed bed in the entrance region at incipient flow from each orifice.

ΔP_s Pressure drop across a preferential gas path through the fluidised bed.

χ Ratio of the open area of the plate to the area of the plate.

This equation is in accord with the findings of Whitehead and Dent (36).

It was observed (36) that the location of defluidised zones moved randomly when U was less than U_m, and in another publication Whitehead et al. (38) note that flow maldistribution at the distributor can lead to the nonrandom location of nonoperative tuyeres. Fakhimi and Harrison (37) do not report any random movement of the location of nonoperative orifices in the plates they studied.

2.6.5. Pressure Drop. In section 2.6.4 it was recorded that the flow resistance of the distributor rather than the velocity of the gases entering the fluidised bed determined its stability to flow maldistribution. The ratio of the pressure drop across the distributor plate, ΔP_d, to the pressure drop across the bed ΔP_b is a useful index of the quality of fluidisation to be expected. The selection of the critical pressure ratio has been the subject of much comment, and opinion as to the value this ratio should take has been divided.

Gregory (39) notes the emergence of a high pressure drop school advocating that this ratio should be greater than 0.4, and a low pressure drop school favouring a value of the ratio less than 0.2, as design criteria for good fluidisation. The work of Hiby (40) with a small scale system employing a porous plate distributor, and more recently Whitehead et al. (38), has attempted to formalise the selection of pressure drop ratio in terms of the measurable hydrodynamic characteristics of a fluidised system.

Hiby (40) worked with a small fluidised bed having a controlled independant feed to the central section, and deduced pressure ratio criteria for good gas distribution. Near incipient fluidising conditons,

a ratio of 0.15 was acceptable, whilst when $(\frac{U}{U_{mf}})$ was much greater than 1, it could be as low as 0.015.

Zuiderweg (41) derives almost identical criteria from the results of Whitehead and Dent (36) for multiple-tuyere arrays.

In a study of arrays of tuyeres, Whitehead et al. (38) measured flow and pressure maldistribution for values of $(\frac{U}{U_{mf}})$ greater than 2. They found that pressure maldistribution was an inherent property of deep fluidised beds and hence for a given bed depth, the pressure ratio was set by the acceptable flow maldistribution at the operating velocity. In their experiments $(\frac{\Delta P_d}{\Delta P_b})$ varied from 0.03 to 2.4. For a bed 1.09 m (43in) deep in which 5% of the mean flow through a tuyere was the tolerable flow maldistribution, they calculated a critical ratio of 0.13, which supports a value of critical pressure ratio of less than 0.2 as a criterion for design.

Whitehead (28) notes the use of low pressure drop distributors in shallow beds.

2.7. Conclusions.

(i) The composition, temperature and solid burden of the products of the H.D.C.C. gasifier used in this work may be found from theoretical and empirical relations, and the heat transfer in cooling tubes placed after the gasifier can be predicted.

(ii) A two stage system with interstage heat removal can be employed to inhibit the formation of higher metal oxides and salts that cause high temperature corrosion, and at the same time reduce NO_x emissions to the atmosphere. A chemically active fluidised bed operating as a second stage combustor could also reduce the level of sulphur dioxide in the exhaust, when high sulphur fuels are used. The ability of

particulate systems to collect mists and dusts dispersed in the gases passing through them, suggests that a fluidised bed could capture and burn the soot in the products of the H.D.C.C. gasifier.

(iii) In this design the air and gas must be mixed inside the fluidised bed. When gas and air are injected separately the relative disposition of the injectors on the distributor plate is important as it strongly affects gas-air mixing in the bed. The effect of distributor design on mixing in the region of the plate should be investigated.

(iv) The ratio of the pressure drop across the distributor to the pressure drop across the bed that gives good fluidisation can be smaller than 0.2, and the superficial velocity above which all tuyeres in an array are continuously operative, may be estimated. The size and frequency of bubbles forming on a distributor plate can be predicted from first principles.

CHAPTER THREE

DESIGN THEORY

AND

MODELLING

3.1. Temperature and Composition of Gasified Oil.

The method used for evaluating the composition and temperature of gasified residual fuel oil is described in detail in reference (1), and outlined on page A 4 - 5 in Appendix 8. The reaction may be represented by the equation:

$$\frac{1}{n}\ (C\ H_{1.532}\ S_{0.0104})_n + a(O_2 + 3.76N_2) \longrightarrow bCO_2 + cCO + dH_2O + fH_2 + 3.76\ a\ N_2 + hC + iCH_4 + jSO_2 \qquad \text{E.3.1.}$$

where n is the average number of carbon atoms per molecule of fuel and the coefficients a,b,c,d,f,h,i,j are the number of moles of each chemical species present in the reactants or products.

E.3.1 includes the presence of solid carbon, methane and sulphur dioxide in the gasified fuel, and when the material balance equations for carbon and hydrogen were written, h and i were obtained from empirical relationships.

The equation E.2.1 was used in conjunction with a regression based on data presented by Htun (4), p149 to find h. The carbon content of the solids is expressed by:

$$C_s = 106 - 17.3\phi_1 + 3.9\phi_1^2 \quad , \quad \phi_1 > 1 \qquad \text{E.3.2.}$$

Where C_s is the percentage of carbon that was detected in the solids.

Htun (4) detected small quantities of hydrogen in the solids, and this was also included in the material balances:

$$H_s = 0.504 - 0.9654\phi_1 + 0.584\phi_1^2 \quad , \quad \phi_1 > 1 \qquad \text{E.3.3.}$$

where H_s is the percentage of hydrogen that was detected in the solids.

Only very small quantities of methane were recorded by Htun (4), p148, and i was found from an equation fitted to the data in reference (4):

$$i^* = 0.2\phi_1 \quad , \quad \phi_1 > 1 \qquad \text{E.3.4.}$$

where i^* is the mole % methane expressed on a dry basis.

Johns (3) has shown that neglect of the sulphur present in the fuel does not make any significant difference to the temperatures reached in the gasification, so sulphur dioxide has not been considered when calculating the sensible heat of the gasified oil.

An option was included in the program which was written to calculate gas compositions and temperatures for the conditions encountered in this work, to allow gas compositions to be found at specified temperatures. This option was used in the stepwise integration along the length of the interstage cooling tubes (Appendix 2).

An additional term, Q, was also included in equation A9 in Appendix 8 to account for the heat removed from the gas stream:

$$T = T_a + \left(\frac{H_r - Q}{c_p}\right) \qquad \text{E.3.5.}$$

where:

c_p Mean heat capacity of the gasified oil.

H_r Heat released in the reaction per carbon atom in the fuel.

Q Heat removed from the gasified oil per carbon atom in the fuel.

T Temperature of the gasified oil.

T_a Temperature of the air, equal in all calculations to the thermodynamic reference temperature of 298 K.

3.2. Heat Transfer.

The products of the H.D.C.C. gasifier contain suspended solids consisting of carbon formed in cracking reactions, and char formed from incompletely burned fuel drops. These suspended carbon particles give the combustion products a high emissivity, e, and in estimating the heat transfer that occurs in the exchangers placed after the gasifier, it is necessary to consider both the convective and radiant contributions. The method of integrating along the length of the cooling tube described in reference (5) is outlined in Appendix 2.

Some heat is also taken out of the gas stream in the gas plenum chamber and fluidised bed, (see Fig. 4.1 for a labelled drawing of the fluidised bed combustor), and estimates of this have been made for the

case of the fluidised bed combustor surrounded by a water jacket.

3.2.1. Effect of Cooling Tube Length. Three cooling tubes of length 1.22 m (4 ft), 0.61 m (2 ft), and 0.305 m (1 ft) respectively, were available for use in this work, and the combination of all three was found to be very convenient geometrically in making the connection of the gasifier to the fluidised bed combustor. The effect of increasing the length of the interstage cooling tube above the 1.22 m used in previous two stage work (1) was examined.

Data points for emissivities found at oil flows and equivalence ratios in the range considered in this design, viz.

$$1.1 \leq \phi_1 \leq 1.6 \quad , \quad 2 \text{ g/s} \leq F_1 \leq 3.5 \text{ g/s}$$

were taken from reference (3), p104. A regression of emissivity data that includes these points has also been given in reference (5). These emissivities are listed in table 1, together with the predicted heat transfer in the cooling tubes arranged in series. Over the range of conditions considered, the total amount of heat transferred from the gas stream was predicted to vary linearly with the first stage equivalence ratio. This is illustrated in Fig. 3.1. Fig. 3.2. is a typical plot of the cumulative percentage of the total heat transferred in the combined tubes as a function of length along the tube, and it shows that the addition of tube after the 1.22 m exchanger has little effect, as more than 85% of the total heat transfer in the combined tubes takes place in the first 1.22 m.

TABLE 1 : PREDICTED INTERSTAGE HEAT TRANSFER IN COOLING TUBE

F_1 (g/s)	ϕ_1 (-)	e (-)	Q_i (kJ/kg)
2.43	1.09	0.3501	23,504
3.05	1.139	0.3616	21,318
2.96	1.24	0.3780	19,241
3.48	1.14	0.5571	22,112
2.59	1.13	0.7577	24,378
2.96	1.33	0.3766	17,305
3.21	1.53	0.8145	15,550

F_1, ϕ_1, e , presented in reference (3). Q_i, calculated by the method in Appendix 2 for 2.13 m cooling tube.

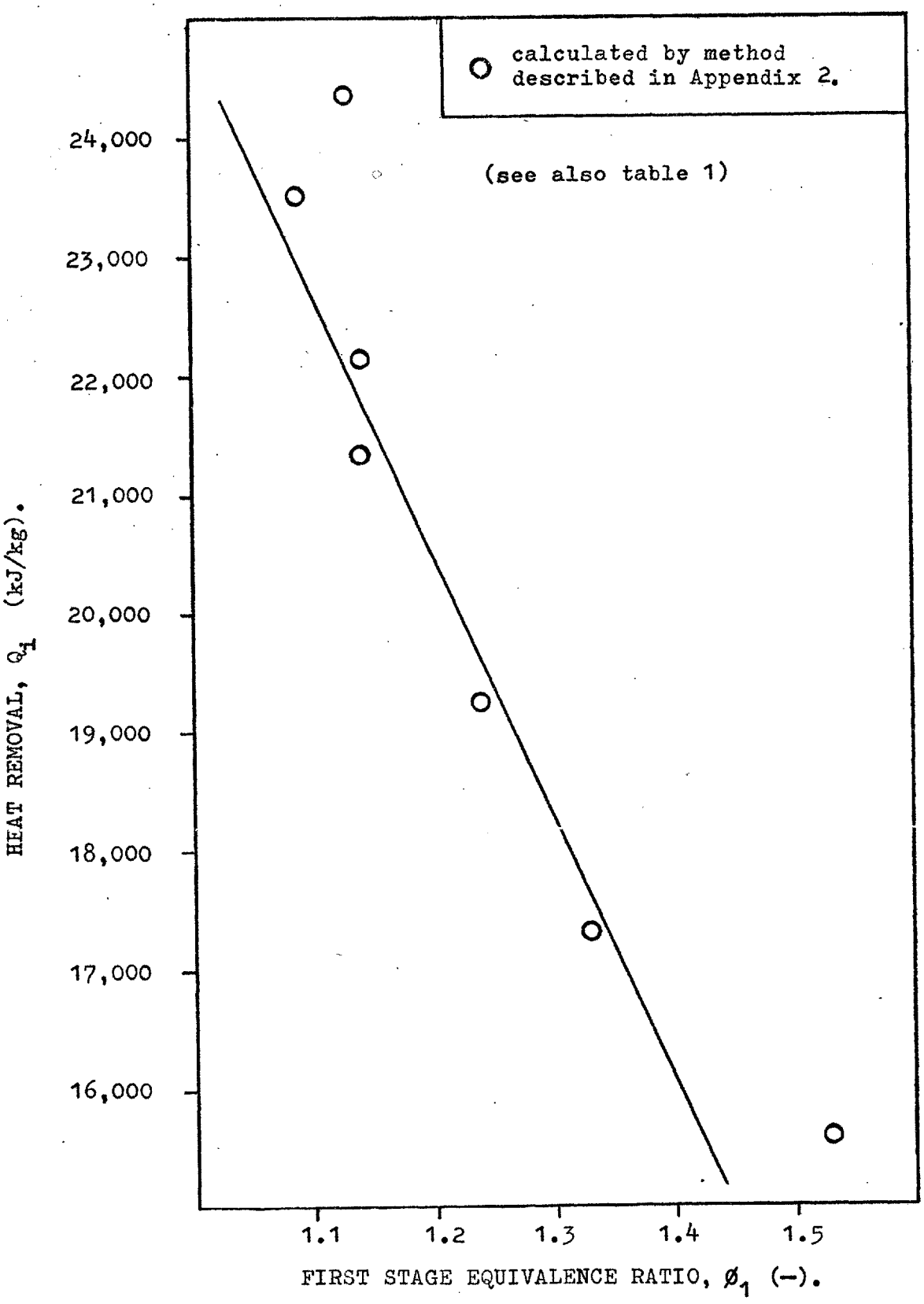

FIG. 3.1: INTERSTAGE HEAT REMOVAL BY 2.13 m COOLING TUBE.

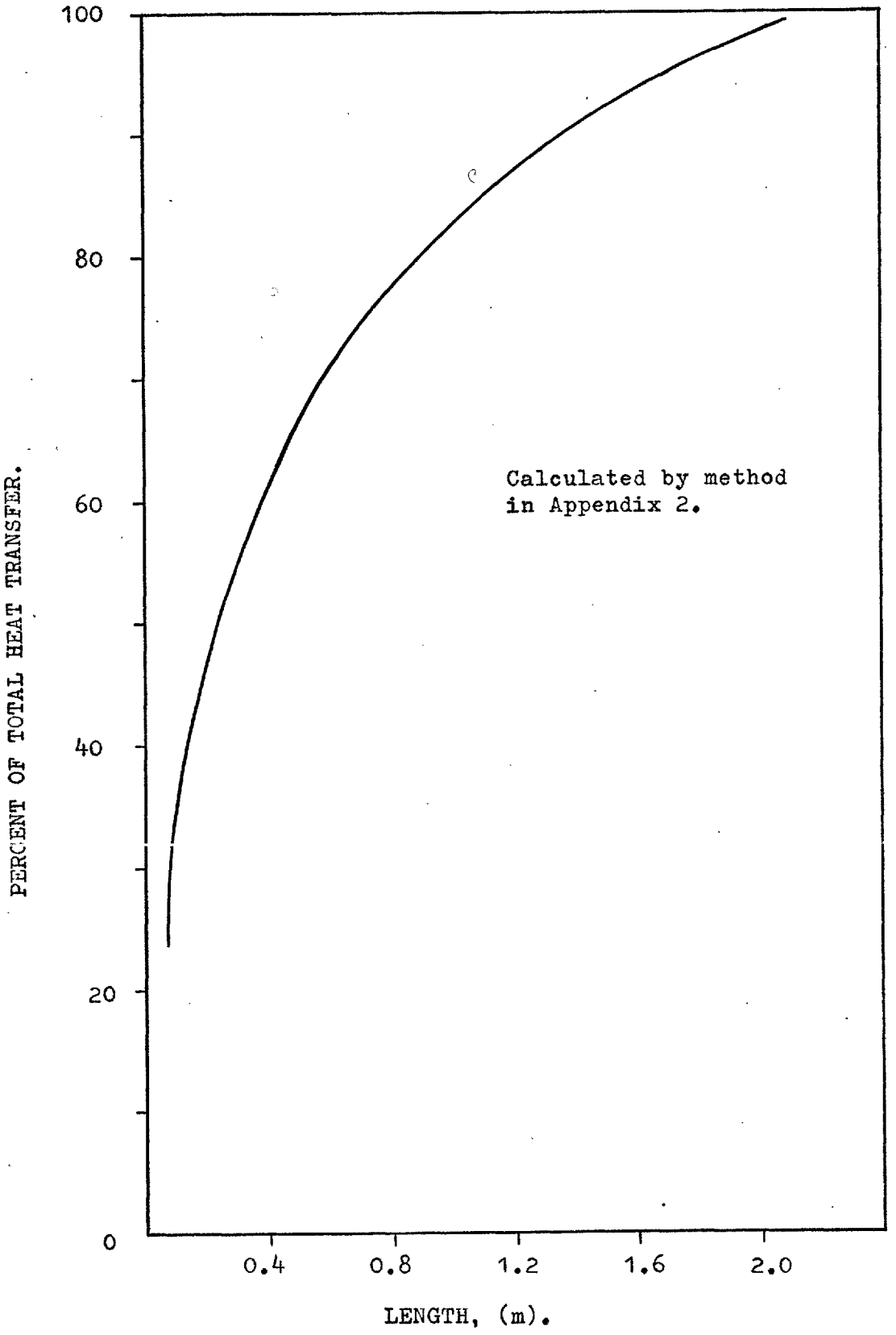

FIG. 3.2: CUMULATIVE HEAT TRANSFER IN 2.13 m COOLING TUBE.

3.2.2. Gas Plenum Chamber and Fluidised Bed. Estimates of the heat transfer through the refractory lining of the gas plenum chamber to a surrounding water jacket were made by solving E.3.6:

$$Q_s = Q_{sa} - Q_i - Q_g \qquad \text{E.3.6.}$$

where;

Q_s Sensible heat of the gas stream.

Q_{sa} Sensible heat of the gas stream for adiabatic conditions.

Q_i Heat removed in the interstage cooling tube.

Q_g Heat transferred through the refractory lining of the gas plenum chamber to a surrounding water jacket.

E.3.6 may be applied to the products of the gasifier operating at any specified oil flow rate and equivalence ratio. It was assumed that the temperature in the gas plenum was uniform, and that all resistance to heat transfer was in the refractory lining.

A similar approach was adopted in estimating the heat loss from a bed in the combustor which was taken to be 0.305 m deep. In this case, it was also assumed that complete combustion occurred in the bed, and that the temperature throughout the bed was uniform. Radiation exchange between the bed surface and the lid and walls of the combustor above the bed was not considered. The heat loss in the gas plenum chamber, Q_g, obtained by the solution of E.3.6, was used in the solution of E.3.7 to find Q_r.

$$Q_{s1} = Q_{sa1} - Q_i - Q_g - Q_r \qquad \text{E.3.7.}$$

where;

Q_{s1} Sensible heat of the gas stream burnt with the stoichiometric air requirement in the second stage.

Q_{sa1} Sensible heat of the oil gasified adiabatically.

Q_r Heat transferred from the fluidised bed to a water jacket surrounding it.

Typical values of $(Q_i + Q_g)$ and $(Q_i + Q_g + Q_r)$ are given in table 2, and a plot of heat transfer from the gas stream vs ϕ_1 is shown in Fig. 3.3.

TABLE 2 : TOTAL HEAT TRANSFER

ϕ_1 (-)	$(Q_i + Q_g)$ (kJ/kg)	T_{gp} (K)	$(Q_i + Q_g + Q_r)$ (kJ/kg)	T_r (K)
1.1	26,100	960	28,200	1010
1.25	22,500	800	25,000	1180
1.40	19,300	760	22,100	1340
1.55	16,150	725	19,300	1480

Q_i calculated by method in Appendix 2

Q_g, Q_r obtained by solution of E.3.6, E.3.7.

F_1 for all values in Table 2 , 3.5 g/s.

T_{gp} Temperature of gases in gas plenum chamber.

T_r Temperature reached by gases during stoichiometric combustion in combustor.

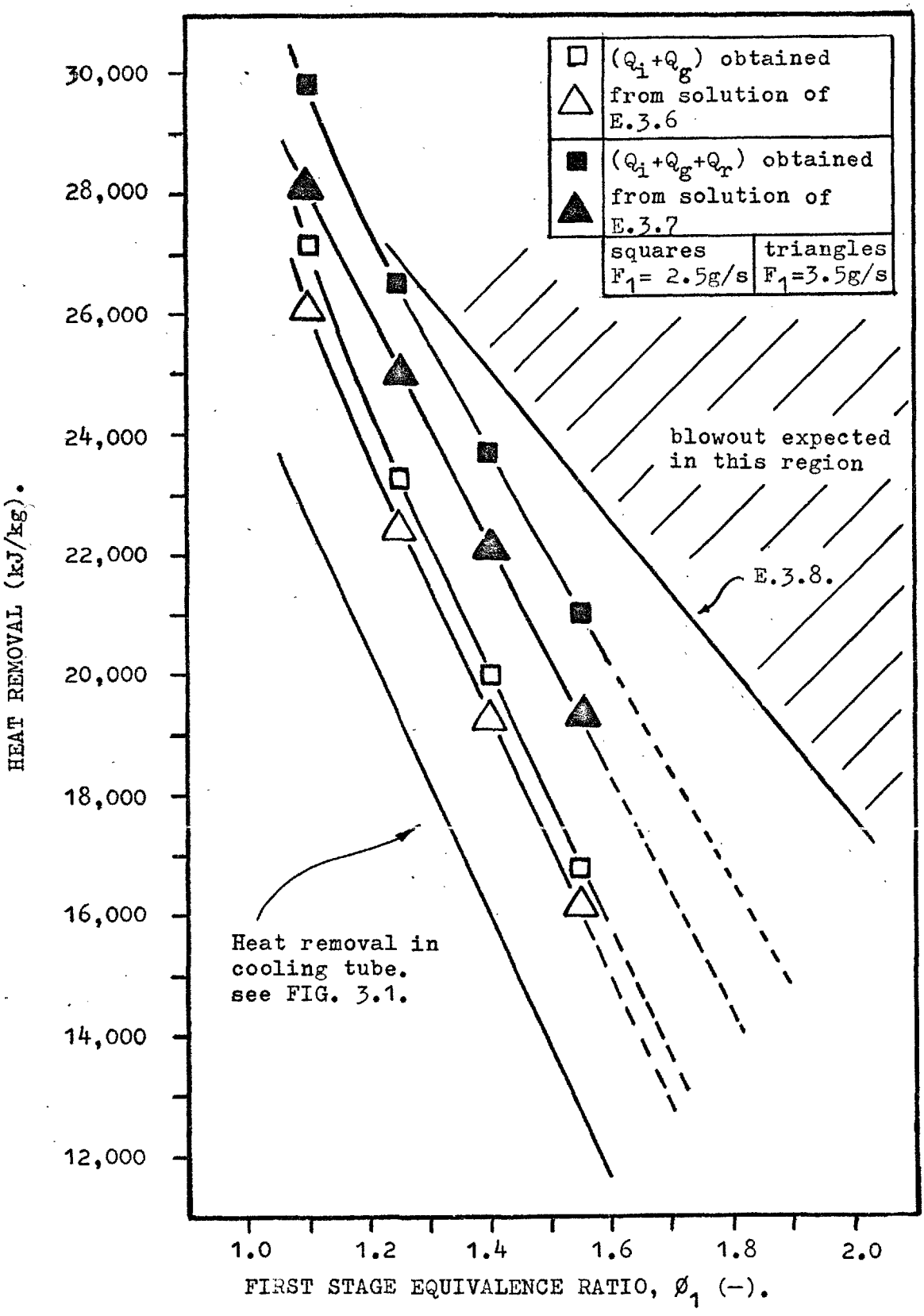

FIG. 3.3: HEAT REMOVAL FROM GASIFIED OIL AND SECOND STAGE STABILITY.

3.2.3. Stability. Archer et al. (42) studied the stability of a tunnel type burner firing the products of the H.D.C.C., and using steam as the atomising fluid it was found that the differences in measured and theoretical interstage heat removal at blowout could not be explained either by experimental errors or by errors in the rate constants used in the theoretical analysis. Modelling blowout therefore failed, and for this reason, a theoretical combustion stability analysis of the fluidised bed combustor has not been attempted. Values of direct interstage heat transfer at blowout obtained by employing a water spray to quench the combustion gases, were presented by Grout (8), p213. In reference (42) these were correlated by the equation:

$$Q_t = 42.46 - 12.5\phi_1 \qquad \text{E.3.8.}$$

The units of Q_t in E.3.8 are MJ per kg fuel burnt.

Interstage heat transfer at blowout given by E.3.8 has been compared with the heat, Q_t, removed from the gas stream between the point of gasification, and the top of the fluidised bed where;

$$Q_t = Q_i + Q_g + Q_r \qquad \text{E.3.9.}$$

Fig. 3.3 shows that the heat removal from the fluidised bed combustor is lower than a critical value given by E.3.8, and this suggests that the combustor could operate stably. However, because of the demonstrated dependance of combustor stability on design, the stability of the combustor to low temperature operation must be found experimentally.

3.2.4. Control of Heat Transfer. The heat transfer in the cooling tubes is gas side controlled and for a specified F_1, ϕ_1, Q_i can only be affected by changing the amount of surface area in the exchanger. This may be done by altering the length of the tube connecting the gasifier to the combustor, but because of the heavy construction of the plant this is not easy to do once a specified plant configuration has been chosen, and still does not allow Q_i to assume a continuous range of values at a given gasifier oil flow and equivalence ratio.

By surrounding the combustor with a zoned jacket suitable for an air or water coolant, some degree of control of the heat removed from the system can be achieved. Heat passing through the walls of the combustor and gas plenum may either be used to preheat the air supplied to the fluidised bed, or it can be removed from the system by a water flow in the jacket.

In section 3.5.2 it is pointed out that the mass flow of air to the fluidised bed is such that heat transfer to boost its volumetric flow, could be advantageous to the formation of air bubbles on the distributor and good flow distribution. This observation also encourages the provision of a facility in the combustor for air preheat, as both the quality of fluidisation and combustion efficiency are sensitive to flow maldistribution resulting from partial operation of the air orifices.

3.3. Gas Mixing in Fluidised Beds.

In all combustion processes, the fuel and oxidant must be brought into contact before combustion will proceed, and when air and gas

are injected separately into a fluidised bed, good gas-air mixing must be ensured for high combustion efficiency to be obtained.

Gas mixing in a bubbling bed of inert nonsorbent particles occurs by both convective and diffusional mechanisms. The contents of two bubbles that coalesce to form a single bubble are mixed when this occurs. Exchange between a bubble and the particulate phase takes place by diffusion, and also by the bulk flow of gas entering through the bottom and leaving through the top of the bubble.

The velocity of rise of a bubble in a fluidised bed, U_b, is approximately given by the expression for a gas bubble rising in a liquid:

$$U_b = 0.71 \, (g \, D_b)^{\frac{1}{2}} \qquad \text{E.3.10.}$$

where D_b is the bubble diameter.

When U_b exceeds the velocity of the fluid in the particulate phase, all the gas leaving the top of the bubble is swept downwards by the relative motion of the particles, and re-enters the bubble at the bottom (43). The region outside the bubble penetrated by the circulating gas is called the cloud, and the ratio of the radius of the penetration sphere, r_c, to the bubble radius, r_b, is given by E.3.11;

$$\frac{r_c}{r_b} = \left[\frac{U_b + 2\left(\frac{U_{mf}}{\epsilon_{mf}}\right)}{U_b - \left(\frac{U_{mf}}{\epsilon_{mf}}\right)} \right]^{\frac{1}{3}} \qquad \text{E.3.11.}$$

ϵ_{mf} is the bed voidage at incipient fluidisation.

Thus although there is a bulk gas flow into the particulate phase, there is no convective exchange across a cloud boundary.

3.3.1. Diffusion Across a Cloud Boundary. The gasified oil used in the combustor consists principally of nitrogen, and contains the combustible gases carbon monoxide and hydrogen. The composition of the stoichiometric combustion products is given in table 3, and typical gas compositions are shown in Fig. 3.4, as a function of ϕ_1.

An estimate of the amount of combustible that diffuses across a cloud boundary can be made by considering single bubbles containing carbon monoxide or hydrogen injected singly into a bed incipiently fluidised by nitrogen.

Assuming, for the purposes of this calculation that the concentration of combustible in the particulate phase is zero, and following an analysis similar to one by Davidson and Harrison (43), a material balance over a single bubble rising in a large bed gives the equation:

$$-\frac{dc_b}{dt} = k_{bp}\, c_b \qquad \text{E.3.12.}$$

where;

c_b concentration of combustible in the bubble.

k_{bp} volume of gas exchanged between bubble and particulate phase, per unit volume of bubble per unit time.

TABLE 3 : COMPOSITION OF STOICHIOMETRIC COMBUSTION PRODUCTS OF DIFFERENT FUELS

Fuel	Constituent in combustion products, % vol.		
	N_2	H_2O	CO_2
Town gas*+	69.1	20.8	10.1
Natural gas+	69.5	21.4	9.1
Residual fuel	74.6	11	14.4

* Solihull Town Gas

\+ Data taken from reference (51).

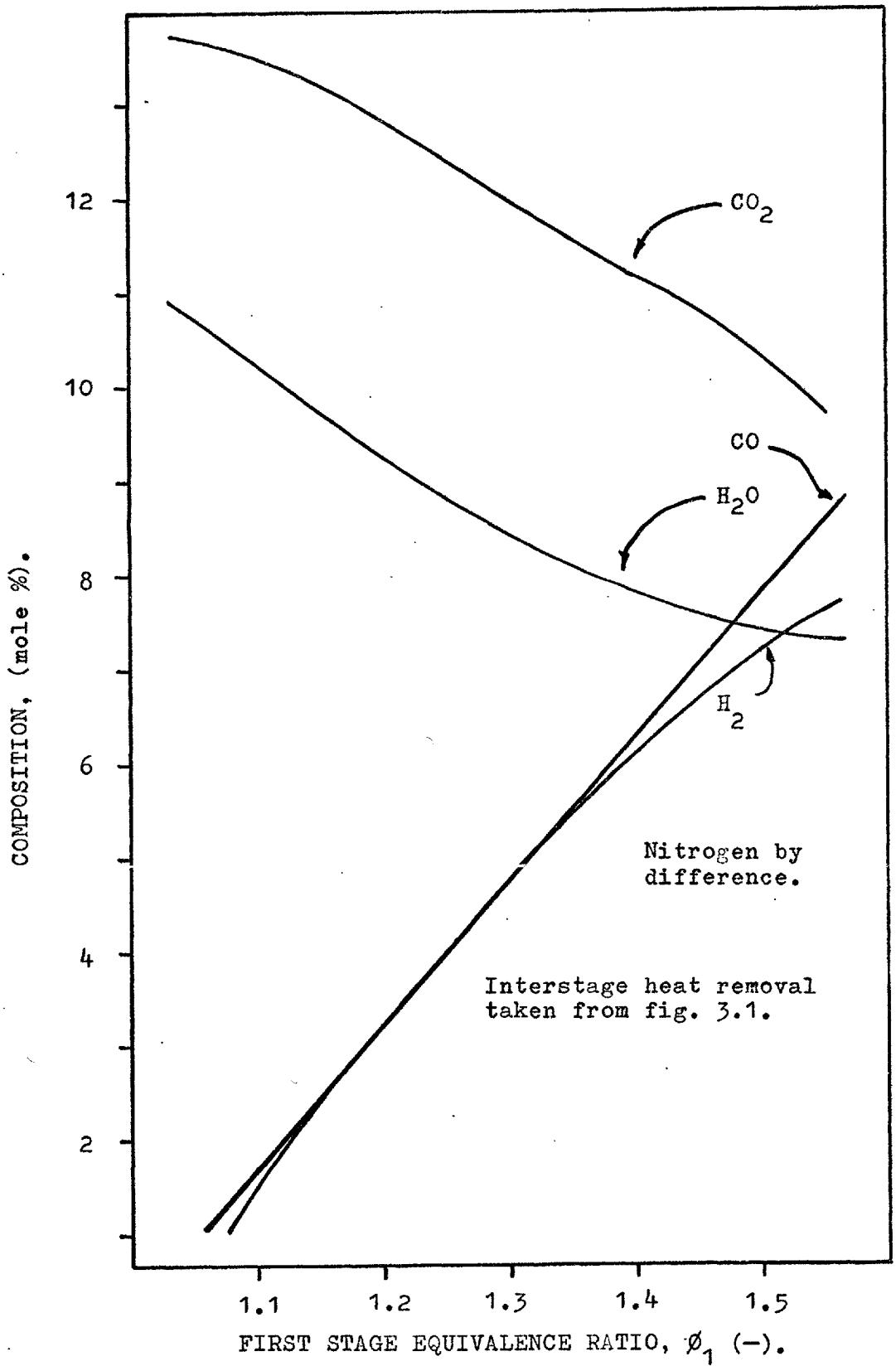

FIG. 3.4: PREDICTED GAS COMPOSITION.

Rewriting E.3.12;

$$-\frac{dc_b}{ds}\frac{ds}{dt} = k_{bp}\, c_b \qquad \text{E.3.13.}$$

and integrating with the boundary conditions;

$s = 0$, $c_b = c_{bo}$

c_b is found as a function of height in the bed, s, and the concentration of the combustible in the bubble, at the base of the bed, c_{bo}:

$$\frac{c_b}{c_{bo}} = \exp\left(-\frac{k_{bp}\, s}{U_b}\right) \qquad \text{E.3.14.}$$

Rearrangement of E.3.14 gives the height at which a known concentration is reached:

$$s = \frac{U_b}{k_{bp}} \ln\left(\frac{c_{bo}}{c_b}\right) \qquad \text{E.3.15.}$$

It is shown in the next chapter that mechanical and geometrical factors limit the distributor design, and hence the initial bubble diameters. Therefore, in this calculation, a diameter is used which is estimated for uncoalesced bubbles of gasified fuel oil forming in a bed of particles of the type chosen for the initial experimental trials. Thus, taking a diameter of 75 mm from table A.7.4 and a bed temperature of 1000 C, values of k_{bp} were calculated by the method described by Potter (44), as outlined in Appendix 3. U_b was obtained from E.3.10. Substitution of U_b and k_{bp} into E.3.15 gives results which show that the height of bed required to reduce c_b to 5% of its inlet value is 0.84 m in the case of carbon monoxide, and 0.48 m for

hydrogen in the bubble. Alternatively, at the surface of a bed 0.305 m deep, $\left(\frac{c_b}{c_{bo}}\right)$ is as high as 0.34 and 0.15 for carbon monoxide and hydrogen respectively.

It is apparent that when a large bubble containing a combustible gas rises through a shallow bed, there will be considerable bypassing of the combustible, and complete combustion in the bed will not be possible, unless some other form of gas-air contacting occurs.

3.3.2. Gas Mixing by Bubble Coalescence. The even distribution of air and gas over the base of a bed is represented schematically in Fig. 3.5 (b), by pairs of bubbles, one of which contains the portion of the gas supply to a small area at the base of the bed, and the other, the corresponding air supply. The distribution is even, and thus neglecting diffusional exchange between the bubble and particulate phases, when these bubbles coalesce the resulting bubble will contain air and gas in the same proportions as the ratio of the supplies.

When the air and gas supplies are not evenly distributed, or when supplies to small areas of the base of the bed are not in the same proportions as in the overall amounts of gas and air fed to the bed, the number of successive dual coalescences, N_{dc}, that most bubbles must undergo before a bubble is formed in which the air to gas ratio is the same as in the supply, increases. This is shown schematically in Fig. 3.5 (a) in which air is supplied to a smaller area than the gas, and in Fig. 3.5.(c) in which gas is supplied to the smaller area.

It can be inferred from this that in a shallow bed particularly, the distribution of air and gas at the bottom of the bed should be as even as possible, if complete mixing within the bed is to be achieved.

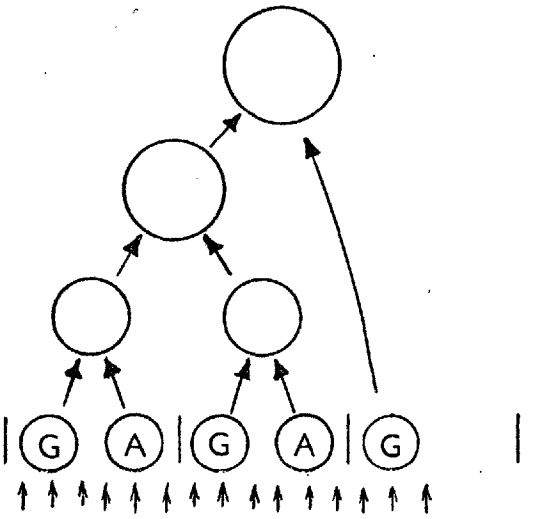

Air supplied to smaller area of plate than gas.

$N_{dc}=3$, before bubble is formed that has the same air/gas ratio as the overall supplies.

Fig. 3.5 (a).

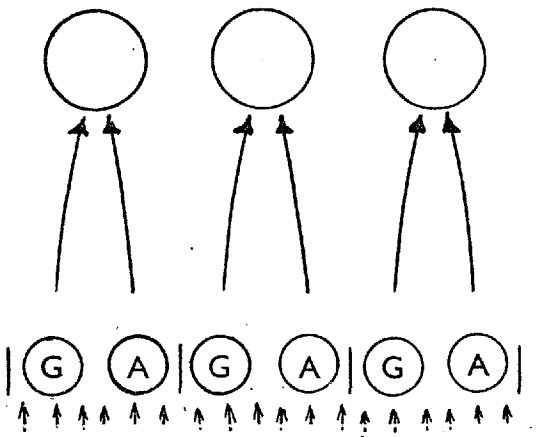

Air and gas supplied to equal areas of the plate.

$N_{dc}=1$, to form bubble that has the same air/gas ratio as the overall supplies.

Fig. 3.5 (b).

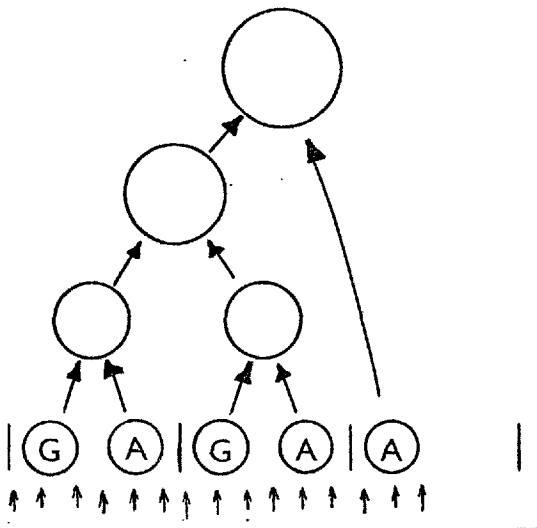

Gas supplied to smaller area of plate than air.

$N_{dc}=3$, before bubble is formed that has the same air/gas ratio as the overall supplies.

Fig. 3.5 (c).

FIG. 3.5: SCHEMATIC REPRESENTATION OF GAS MIXING BY BUBBLE COALESCENCE.

3.4. Gas Mixing and Combustion on the Distributor Plate.

The interaction and subsequent coalescence of two bubbles, i and j, forming on adjacent coplanar orifices on a distributor plate depends on several variables. The volumetric flow to each bubble, G_{bi} and G_{bj}, the spacing of the orifices, λ, and the length of time each orifice operates with respect to the other one, usually expressed as a delay time t_d, are all important.

When bubbles of gas and air coalesce and react, the composition of the resulting bubble is determined by the factors listed above, and also by the initial composition of the gas. A model was developed to study the effect of the parameters λ, G_b, ϕ_g and t_d, on bubble interaction and the composition of bubbles formed. The equivalence ratio of the gas, ϕ_g, defines an equilibrium composition for a specified fuel gasified under known thermal conditions. An array of gas and air orifices was considered, and bubbles whose perimeters touched were assumed to coalesce instantaneously. The model for reacting gases has already been published (45), and this paper which is for a twin orifice system is included in this thesis as Appendix 8.

A flow chart of the program used to model the growth of a bubble on an orifice, its coalescence with an adjacent bubble, chemical reaction that occurs on mixing with air when the gas temperature is high, and the detachment of the bubble from the plate, is given in Appendix 4.

What follows here is additional to what is already published.

When air and gas bubbles are formed on orifices that are part of large arrays fed from independent manifolds, the analysis of the bubble interaction is complicated by uncertainty in the flow through

each individual orifice. In practical applications, the metered fluid flow will be the total flow into the manifold. Although with some types of tuyere the total flow through each tuyere can be recorded, the net flow to a bubble is not directly measurable.

3.4.1. Bubble Equivalence Ratio. In the following analysis, a bubble of gasified fuel oil called the gas bubble, and a bubble of air called the air bubble are considered. These grow on adjacent orifices and coalesce to form a single bubble called the product bubble. The gas orifice is one of N_g gas orifices on a distributor plate, and these are fed from a single manifold by R_g kg/s gasified oil of equivalence ratio ϕ_g. The air orifice is one of N_a air orifices on the distributor plate. The air manifold is fed by R_a kg/s air. The gas orifice operates for t_g seconds, and the air orifice operates for t_a seconds, where $t_g \geq t_a$. The formation time of the product bubble is t_b, and is measured from the commencement of operation of the gas orifice; thus t_b is equal to t_g. At any time, a proportion p_g of the gas orifices and p_a of the air orifices are operative.

Some of the fluid supplied to the bed flows into the particulate phase, which according to the two phase theory of fluidisation is maintained in a state of incipient fluidisation, and the remainder forms the flow the the bubble phase. Thus, R_{gb}, the gas flow to the bubble phase is:

$$R_{gb} = R_g - R_{gp} \qquad \text{E.3.16.}$$

where R_{gp} is the gas flow into the particulate phase.

Assuming equal bubble flow through each similar operative orifice, R^*_{gb}, the flow to the bubble phase through each operating gas orifice is:

$$R^*_{gb} = \frac{R_g - R_{gp}}{p_g N_g} \qquad \text{E.3.17.}$$

Similarly for the air orifices:

$$R^*_{ab} = \frac{R_a - R_{ap}}{p_a N_a} \qquad \text{E.3.18.}$$

where;

R^*_{ab} Air mass flow through each operative air orifice to the bubble phase.

R_{ap} Air mass flow to the particulate phase.

If we consider the air and fuel that react to form the gas feed and the air that is supplied from the air orifices, the air to fuel ratio in a product bubble can be found by material balance using the relationships given on page A4-6 in Appendix 8. The fuel in the bubble, f_b, after t_b is:

$$f_b = \frac{R^*_{gb} \phi_g t_g}{(\phi_g + w)} \qquad \text{E.3.19.}$$

where w is the air to fuel mass ratio at an equivalence ratio of one. The corresponding total air flow during t_b is made up of the air flow

from the air orifice, and the air (now chemically combined with the fuel) in the gas feed. Thus;

$$a_b = \frac{R^*_{gb}\, w\, t_g}{(\phi_g + w)} + R^*_{ab}\, t_a \qquad \text{E.3.20.}$$

and,

$$\frac{a_b}{f_b} = \frac{\dfrac{R^*_{gb}\, w\, t_g}{(\phi_g + w)} + R^*_{ab}\, t_a}{\dfrac{R^*_{gb}\, \phi_g\, t_g}{(\phi_g + w)}} \qquad \text{E.3.21.}$$

When R_a air is the stoichiometric requirement for R_g gasified fuel oil;

$$\frac{R_a}{R_g} = \frac{\phi_g\, w\, (1 - \frac{1}{\phi_g})}{(\phi_g + w)} \qquad \text{E.3.22.}$$

The relative amounts of air and gas that flow into the particulate phase may be expressed in terms of an equivalence ratio, ϕ_p, and the relationship between R_{ap}, R_{gp}, ϕ_g and ϕ_p is given by E.3.23.

$$\frac{R_{ap}}{R_{gp}} = \frac{w\, \phi_g\, (1 - \frac{\phi_p}{\phi_g})}{\phi_p\, (\phi_g + w)} \qquad \text{E.3.23.}$$

If the particulate phase has an equivalence ratio of one, E.3.23 reduces to:

$$\frac{R_{ap}}{R_{gp}} = \frac{\phi_g \; w \; (1 - \frac{1}{\phi_g})}{(\phi_g + w)} \qquad \text{E.3.24.}$$

and it follows that,

$$R_a - R_{ap} = \frac{\phi_g \; w \; (1 - \frac{1}{\phi_g}) \; (R_g - R_{gp})}{(\phi_g + w)} \qquad \text{E.3.25.}$$

substituting E.3.25 into E.3.21, and rearranging the terms, the equivalence ratio, ϕ_b, of a product bubble is obtained:

$$\phi_b = \frac{\frac{\phi_g \; t_g}{p_g \; N_g}}{\frac{t_g}{p_g \; N_g} + \phi_g \; (1 - \frac{1}{\phi_g}) \; \frac{t_a}{p_a \; N_a}} \qquad \text{E.3.26.}$$

If $\bar{t}_d$ is now defined as the average time between the cessation and recommencement of operation of each orifice on a multi-orifice plate on which random movement of the defluidized zones (36) takes place, it may be found in terms of the proportion of the orifices, p, that are operating during a small interval Δt. For the purposes of

this analysis, it is assumed that p is constant.

Thus:

$$\bar{t}_d = \frac{\left[\begin{array}{l}\text{total accumulated non-operative time for all}\\ \text{orifices on a multi-orifice plate during an}\\ \text{extended period of plate operation.}\end{array}\right]}{\left[\begin{array}{l}\text{total number of bubbles formed on the plate}\\ \text{during the same period of operation.}\end{array}\right]} \qquad \text{E.3.27.}$$

In an extended period of plate operation τ, during which many bubbles are formed at each orifice in an array, the total maximum operative time, τ_m, for a plate having N_{or} orifices is given by E.3.28:

$$\tau_m = \sum_{t=0}^{t=\tau} (N_{or}\,\Delta t) = N_{or} \qquad \text{E.3.28.}$$

The actual operative time, τ_a, for the whole plate during the same period is:

$$\tau_a = \sum_{t=0}^{t=\tau} (N_{op}\,\Delta t) = N_{op} \qquad \text{E.3.29.}$$

where N_{op} is the average number of orifices operating during an interval Δt.

The average operative time for each orifice, $\bar{t}$, or the average bubble formation time, is given by E.3.30.

$$\bar{t} = \frac{\tau_a}{n_b} \qquad \text{E.3.30.}$$

where n_b is the number of bubbles formed on the plate during the extended period of operation, thus:

$$n_b = \frac{\tau_a}{\bar{t}} = \frac{N_{op}\tau}{\bar{t}} \qquad \text{E.3.31.}$$

and;

$$\bar{t}_d = \frac{N_{or} - N_{op}}{\frac{N_{op}}{\bar{t}}} \qquad \text{E.3.32.}$$

or,

$$\bar{t}_d = \left(\frac{1-p}{p}\right)\bar{t} \qquad \text{E.3.33.}$$

When two arrays produce bubbles that coalesce in the manner described at the beginning of this section, E.3.33 may be applied to each array independently when t_g, t_a and t_{da}, t_{dg}, the delay times at the air and gas orifices respectively, have average values:

$$\frac{\bar{t}_a}{p_a} = \frac{\bar{t}_{da}}{1-p_a} \qquad \text{E.3.34.}$$

and,

$$\frac{\bar{t}_g}{p_g} = \frac{\bar{t}_{dg}}{1-p_g} \qquad \text{E.3.35.}$$

where p_a, p_g are respectively the proportions of operative air and gas orifices.

Using the relationship:

$$\bar{t}_a = \bar{t}_g + \bar{t}_{dg} - \bar{t}_{da} \qquad \text{E.3.36.}$$

and substituting E.3.34 and E.3.35 into E.3.36, the result is that;

$$\frac{\bar{t}_a}{p_a} = \frac{\bar{t}_g}{p_g} \qquad \text{E.3.37.}$$

Fig. 3.6. depicts the independent recommencement of operation of adjacent air and gas orifices, following the detachment of a product bubble. The single bubbles that form when the orifices start to operate subsequently coalesce, and the process is repeated.

Assuming average values of t_a and t_g in E.3.26, which was found for the condition ϕ_p equal to one, and substituting for $\frac{\bar{t}_a}{p_a}$ from E.3.37:

$$\phi_b = \left[\frac{1}{\phi_g} + \frac{N_g}{N_a}\left(1 - \frac{1}{\phi_g}\right)\right]^{-1} \qquad \text{E.3.38}$$

This equation shows that the equivalence ratio of an average product bubble is independant of the delay time $\bar{t}_d$, and as expected reduces to

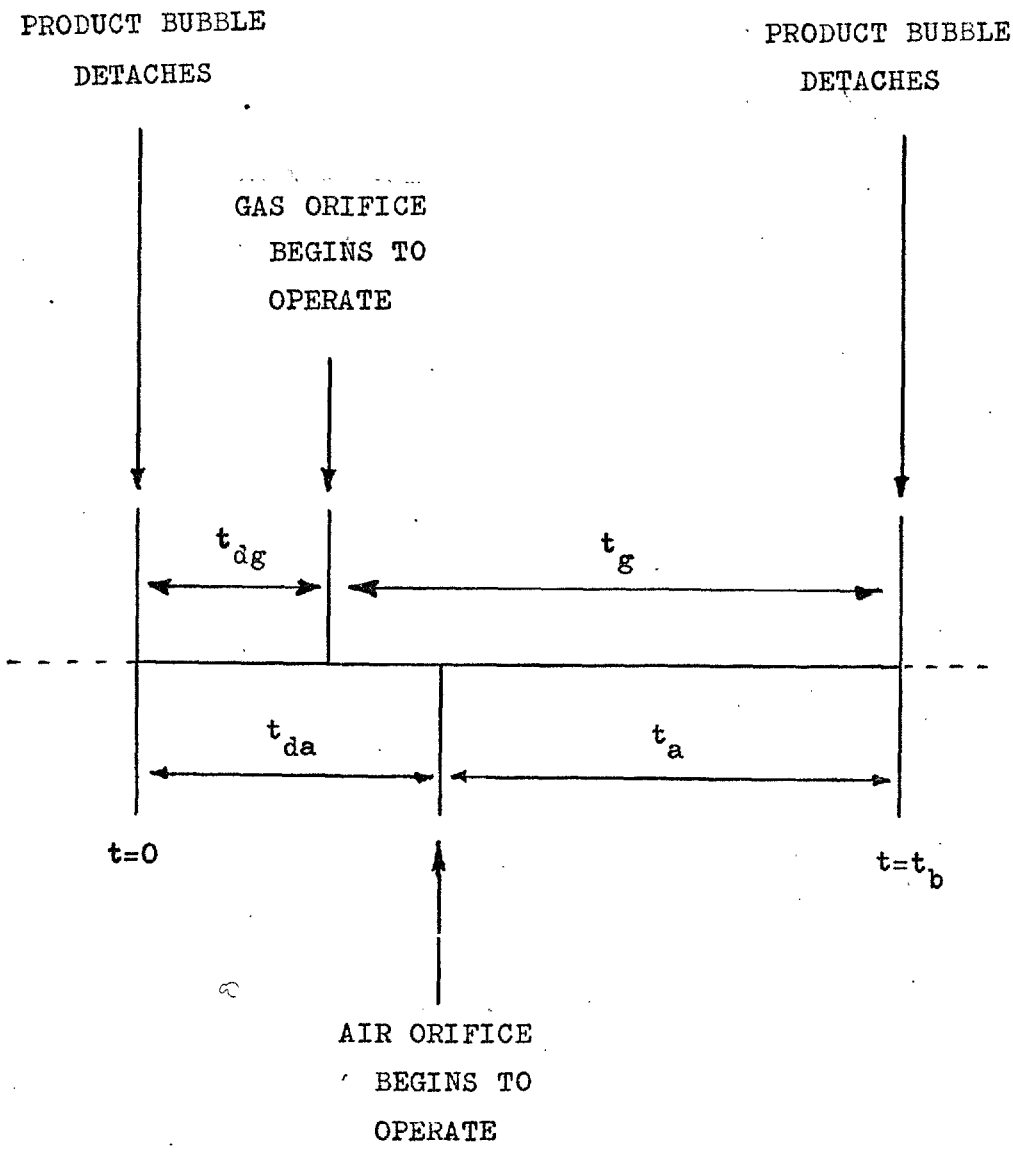

FIG. 3.6: SEQUENTIAL OPERATION OF AIR AND GAS ORIFICES FORMING PRODUCT BUBBLE.

ϕ_b equal to one when equal numbers of air and gas orifices are used on the plate.

3.4.2. Combustion efficiency. E.3.38 shows that when N_g is equal to N_a, and some maldistribution is taking place, i.e. $\bar{t}_d > 0$, combustion inefficiency on the plate does not necessarily result. However, it is unlikely that t_d will always take the average value, and E.3.26 has been rewritten to show the effect of variations in t_{da} on ϕ_b. Taking the case of t_{dg} equal to zero, and considering a constant value of t_g,

$$t_a = t_g - t_{da} \qquad \text{E.3.39.}$$

and substituting for t_a in E.3.26;

$$\phi_b = \frac{k_1}{k_2 - k_3\, t_{da}} \qquad \text{E.3.40.}$$

E.3.40 shows that as t_{da} falls, so does ϕ_b, and that ϕ_b rises with increasing t_{da}. When ϕ_b is greater than one, fuel rich combustion occurs in the bubble and ϕ_b less than one indicates the presence of unreacted oxygen.

The effect of variations in delay time on the combustion efficiency in a bubble formed by the coalescence of air and gas bubbles respectively fed at constant mass flow rates, has been investigated in Appendix 8. It is shown in Fig. 4, page A4-8 that at a constant orifice separation, the combustion efficiency in a bubble falls as t_{da} increases.

The combustion efficiency of a whole plate is defined as the ratio of the actual heat release on the plate during a prolonged interval of plate operation, τ, to the maximum possible heat release.

$$E_p = \frac{\Delta H_p \; F_p \; \tau \; + \sum_{i=1}^{i=n_b} \left(\Delta H_{bi} \; f_{bi} \right)}{\Delta H_{ov} \left(F_p \; \tau \; + \sum_{i=1}^{i=n_b} f_{bi} \right)} \; 100\% \qquad \text{E.3.40.}$$

where;

F_p Flowrate of fuel into the particulate phase (cf. E.3.19 for fuel in a bubble, f_b).

ΔH_{bi} Heat release in a bubble per unit mass of fuel.

ΔH_{ov} Heat release at an equivalence ratio of one per unit mass of fuel.

ΔH_p Heat release in the particulate phase per unit mass of fuel.

τ is large and many bubbles are formed, thus for specified operating conditions;

$$\frac{\sum_{i=1}^{i=n_b} \left(\Delta H_{bi} \; f_{bi} \right)}{\bar{n}_b} = \text{constant} \qquad \text{E.3.41.}$$

and;

$$\frac{\sum_{i=1}^{i=n_b} f_{bi}}{n_b} = \text{constant} \qquad \text{E.3.42.}$$

Considering E.3.41 and E.3.42 in conjunction with E.3.31, it is seen that

$$E_p \neq E_p(\tau) \qquad \text{E.3.43.}$$

The distribution of t_{da} about the mean value $\bar{t}_{da}$ is not known, but the way in which combustion inefficiency may arise can be shown by considering the following extreme case.

During a short sequence of bubble formation in which bubbles form simultaneouslyat all the gas orifices, the number of air orifices that operate is less than the number of gas orifices on the plate. At time $t = 0$, a gas bubble begins to form at each gas orifice, and at $t = \bar{t}_{da}$, bubbles begin to form on the air orifices, and these subsequently coalesce with a corresponding number of gas bubbles. The product bubbles detach, and the gas bubbles that do not coalesce with air bubbles grow until they too detach without any combustion taking place in them. A mean combustion efficiency has thus been defined in terms of the average number of product bubbles, N_c, that would be present on the plate in an extreme case such as described above.

$$\bar{E}_p = \frac{\Delta H_p F_p t_b + N_c \Delta H_b f_b}{\Delta H_{ov} (F_p t_b + N_g f_b)} \quad 100\% \qquad \text{E.3.44}$$

where f_b is the mass of fuel in a product bubble of formation time t_b.

For a plate on which the numbers of air and gas orifices are the same, $\bar{E}_p$ is the same as the combustion efficiency that would result if there were no random movement of the defluidised zones, and those air orifices that did operate, bubbled continuously.

3.5. Bubbling mode of distributor.

Equation E.2.4 has been used to provide an indication of the bubbling

mode of the gas and air orifices in the distributor plate, and because the temperature of the gases in the plenum chambers will be different from that of the gases in the bed, the values of the flow parameters were calculated from the upstream gas properties.

3.5.1. Gas orifices. The gasification model was used to provide temperature and density data required in the estimation of the parameters in E.2.4 which was used to indicate the expected bubbling mode of the tuyeres in the distributor. The particledensity and bed depth were respectively 3.1×10^3 kg/m^3, and 0.305 m.

Fig. 3.7 was prepared for the condition;

$$Q_t = Q_i + Q_g \qquad \text{E.3.45.}$$

and Fig. 3.8 for the case of;

$$Q_t = Q_i \qquad \text{E.3.46.}$$

The values of Q_t given by E.3.45 and E.3.46, respectively represent the upper and lower limits of heat removal from the gas stream.

The pressure drop across the distributor was found from E.3.47.

$$\Delta p_d = \frac{\rho_o U_{or}^2}{2 c_d^2} \qquad \text{E.3.47.}$$

where;

c_d Discharge coefficient.

U_{or} Fluid velocity at an orifice.

ρ_o Fluid density at the orifice.

A value of c_d equal to 0.6 was used in all calculations (29).

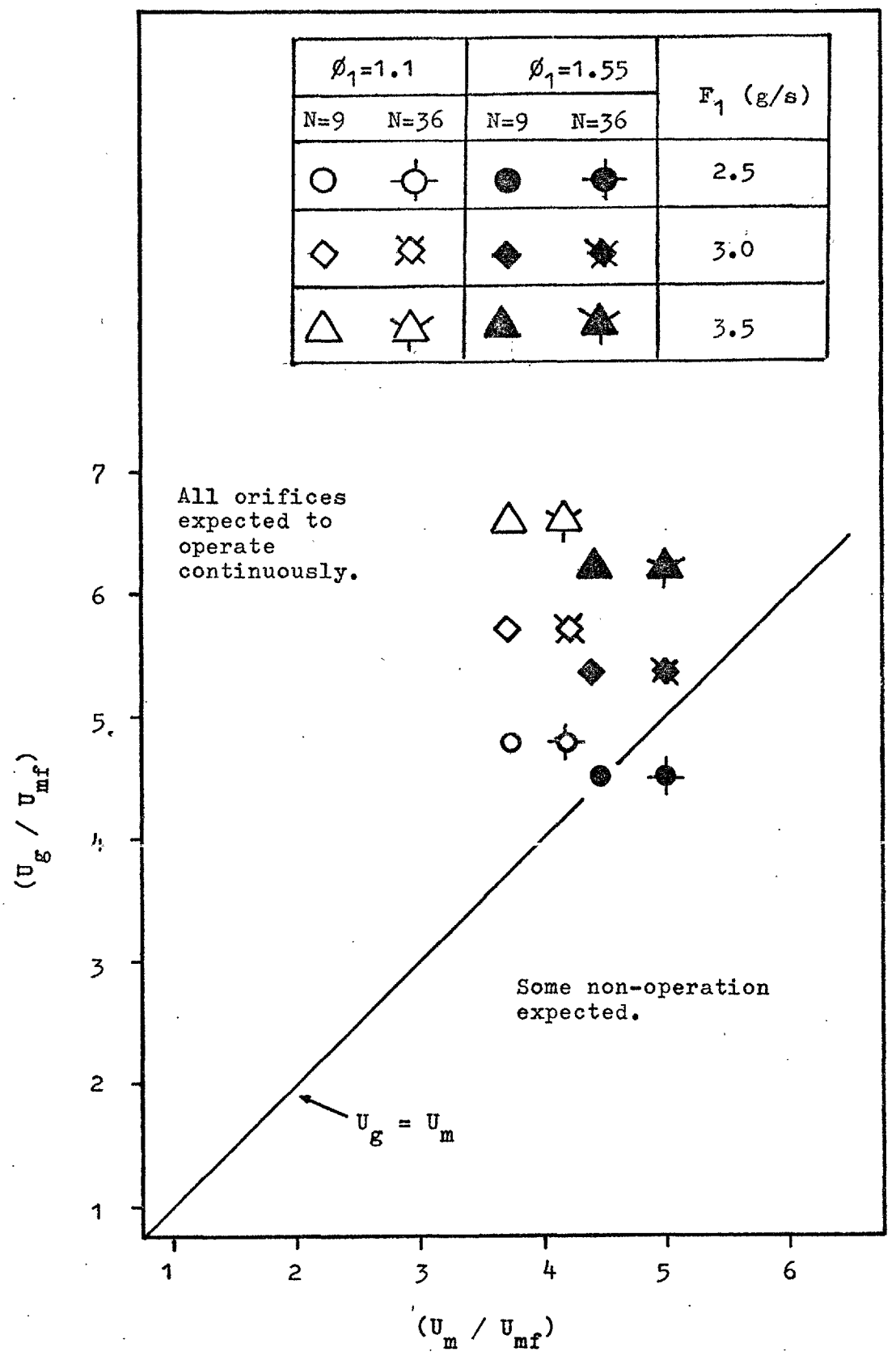

FIG. 3.7: OPERATIVE MODE OF GAS ORIFICES. (Interstage heat removal by cooling tube only).

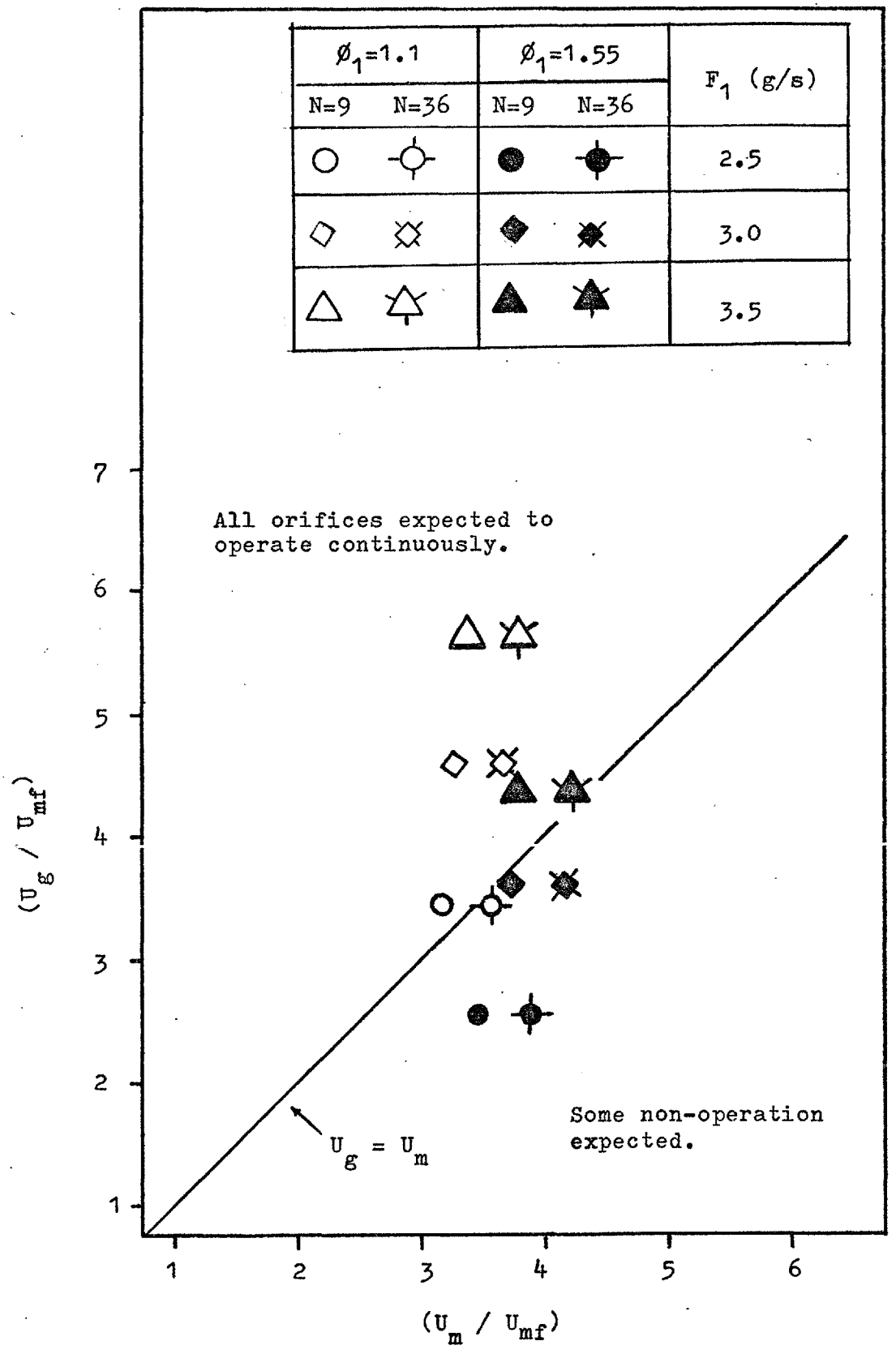

FIG. 3.8: OPERATIVE MODE OF GAS ORIFICES. (Interstage heat removal by cooling tube and gas plenum chamber).

Fig. 3.7 and Fig. 3.8 show that as the heat removed from the gas entering the bed increases, with a consequent decrease in the volumetric throughput, there could be some nonoperation of the tuyeres in the plate. At higher flowrates, all orifices should bubble continuously.

Nine tuyeres each having four orifices serve to inject the gas and air to the fluidised bed combustor and a gas and air tuyere are shown in Fig. 4.3. The predictions of E.2.4, which was derived for tuyeres of the bubble cap type, (see section 2.6.4), are not a strong function of the number of tuyeres in an array, and this is illustrated by the similarity in the values of $(\frac{U_m}{U_{mf}})$ found separately with N equal to 9, the number of tuyeres, and N equal to 36, the number of gas orifices in the plate.

3.5.2. Air Orifices. Bubbles will form in the region of the gas nozzles as:

$$U_g \gg U_{mf}$$

where U_g is the superficial velocity in the bed, based on the velocity of the unreacted gas stream, but the formation of bubbles in the region of the air nozzles will not necessarily occur, since the volumetric flow of air, supplied to the air plenum chamber at room temperature, is below the volumetric rate required to cause incipient fluidisation. The mass flow rate of air to the fluidised bed is given by E.3.48 for overall stoichiometric conditions:

$$R_a = F_1 \; w(1 - \frac{1}{\phi_1}) \qquad \text{E.3.48.}$$

At ϕ_1 equal to 1.55 and F_1 equal to 3.5 g/s, the superficial velocity of the air in the air plenum calculated at 25C and on the basis of the bed diameter of 610mm is 0.06 m/s and this is below U_{mf} in the bed ($\sim$ 0.07 m/s). Whether or not bubbles form at the air orifices will therefore depend on the amount of fluid flow in the particulate phase in the region of the air nozzles that results from the efflux from the gas tuyeres, the local volumetric flow due to the air from the air nozzles, and any local flow that results from reaction between air and gas. At specified gasifier conditions, the local volumetric flow of air will depend on heat transfer to it before and during its entry into the bed, and also on whether the flow is evenly distributed at the base of the bed. E.2.5 predicts that as U is raised, the proportion of operative orifices in an array increases, and this suggests that preheat of the air to increase its volumetric flow could be advantageous to the formation of air bubbles and at the same time, discourage flow maldistribution.

3.5.3. Bubble Formation Bewteen Tuyeres. The formation of bubbles at the point of contact of opposing jets from tuyeres set in a distributor plate, has been noted by Kozin and Baskakov (46), and Zenz (47) has included data also by these authors in a graphical presentation of data on jet penetration into fluidised beds. Typical jet lengths found from this correlation were 0.01 m at the gas nozzles and 0.008 m at the air nozzles. Merry (48) has derived a semiempirical equation for the penetration of a horizontal gas jet into a bed fluidised from below:

$$\left(\frac{L}{d_{or}}\right) + 4.5 = 5.25 \left[\frac{\rho_o U^2_{or}}{(1-\epsilon)\,\rho_p\, g\, d_p}\right]^{0.4} \left[\frac{\rho_f}{\rho_p}\right]^{0.2} \left[\frac{d_p}{d_{or}}\right]^{0.2} \qquad \text{E.3.49.}$$

where;

d_p Particle diameter.

d_{or} Orifice diameter.

L Jet length.

The jet length predicted by this equation is 0.0005 m at the air orifices. A negative result is obtained when E.3.49 is used with typical parameter values at the gas orifices. See table 4.

The lengths of jets forming at both the air and gas orifices are short, and in applying the bubble coalescence model to the bubbles on the orifices of horizontally blowing tuyeres, bubble growth and detachment was considered to take place as shown in Fig. 3.9. This is similar to the growth and detachment of a bubble at an orifice blowing vertically upwards, shown schematically in Fig.1, page A4-8, in Appendix 8. The coalescence of bubbles growing on opposing tuyeres is shown schematically in Fig. 3.10.

3.6. Estimation of Incipient Fluidising Veolcity at Elevated Temperatures.

A series of cold experiments was conducted to examine the fluidising behaviour of fused mullite. This material was found to fluidise satisfactorily, and U_{mf} of the sample selected for the first experimental trials was found to be 0.18 m/s. The particle properties are given in Appendix 5.

Values of U_{mf} at 25C were obtained for samples of different surface mean diameter d_p, and a plot was made of $\ln(U_{mf})$ vs $\ln(d_p)$. All points were well described by a line fitted by eye to the data in order to estimate the exponent on d_p, and it was found that;

TABLE 4. PENETRATION OF JET INTO FLUIDISED BED.

	ρ_o (kg/m^3)	d_{or} (mm)	U_{or} (m/s)	Jet length (mm)	
				Merry (48)	Zenz (47)
AIR	1.184	3.2	38	2	8
GAS	0.31	12.7	24	-	10

conditions:

F_1 3.5 g/s

ϕ_1 1.55

ρ_f 0.22 kg/m^3

ρ_p 3.1 x 10^3 kg/m^3

d_p 402 m

ϵ 0.55

p_a 1

Interstage heat removal taken from Fig. 3.1.

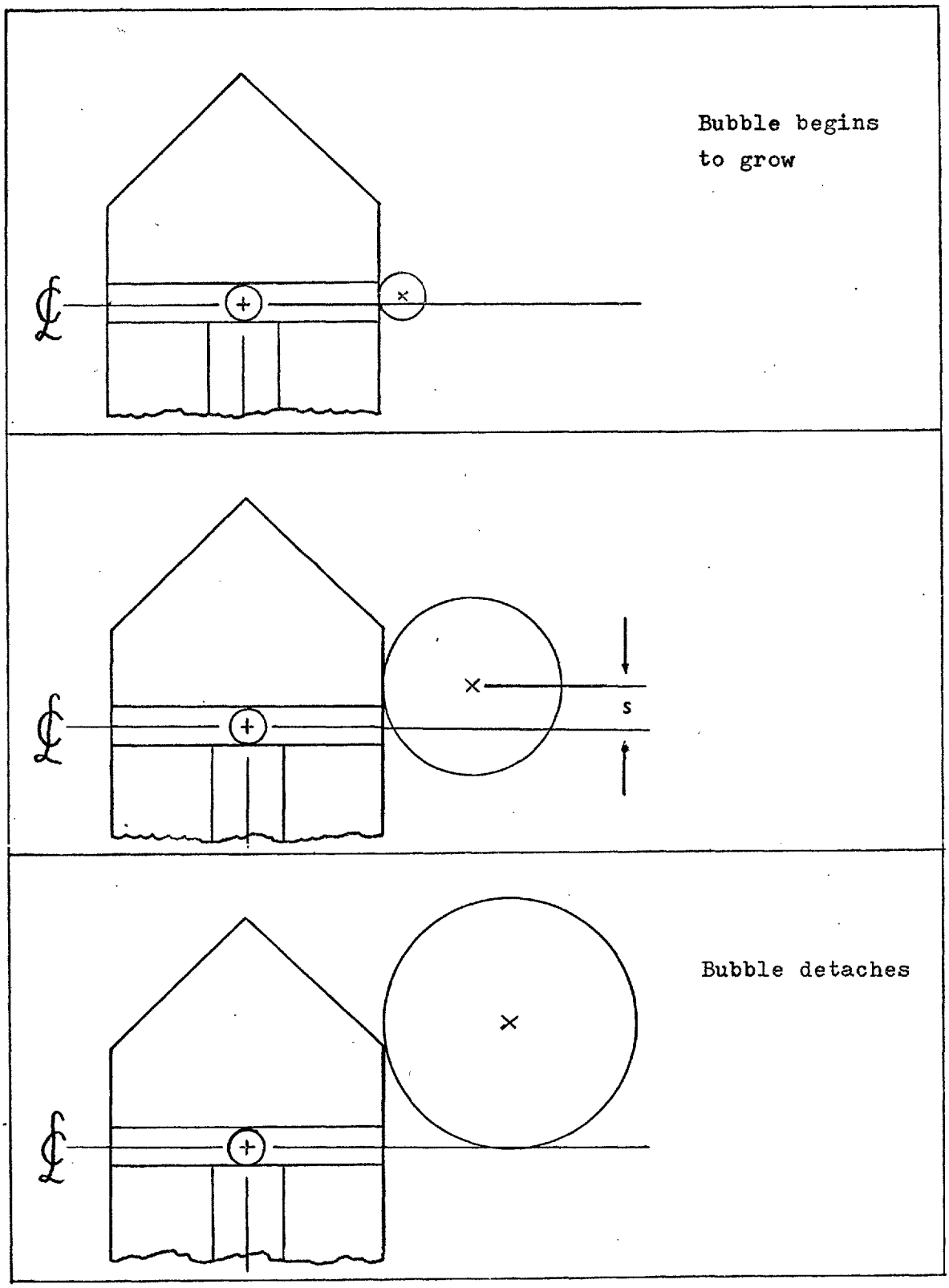

FIG. 3.9: GROWTH OF BUBBLE ON SINGLE ORIFICE OF TUYERE

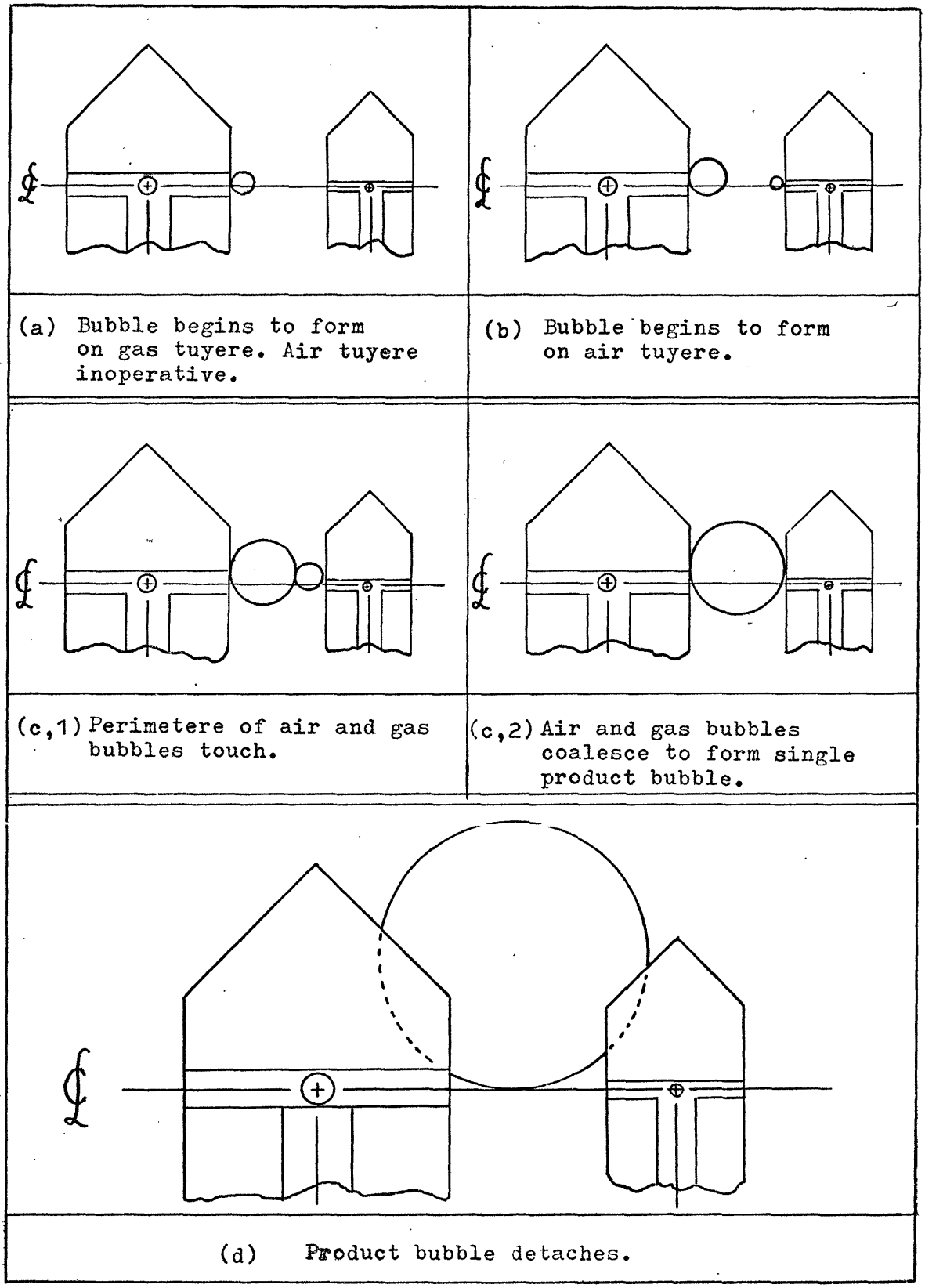

FIG. 3.10: COALESCENCE OF BUBBLES FORMING ON OPPOSING GAS AND AIR ORIFICES.

$$U_{mf} = 0.00001506\ d_p^{1.57},\quad 240\ \mu m < d_p < 500\ \mu m \qquad \text{E.3.50.}$$

where d_p is in microns.

This equation does not show the relationship between U_{mf} and the fluid viscosity μ_f, but it does indicate a power of d_p less than two, and this suggests that E.3.51 recommended for Re_{mf} less than 20 by ref. (29) is not applicable. Re_{mf} is the Reynolds number based on the particle diameter and U_{mf}, and in the cold experiments varied from 1.3 to 9.

$$U_{mf} = \frac{d_p^2\ (\rho_p - \rho_f)\ g}{1650\ \mu_f} \qquad \text{E.3.51.}$$

The difference between the value of 0.18 m/s measured at 25C and U_{mf} predicted by E.3.51 is only -11%, and all values at elevated temperatures were estimated using;

$$U_{mf}\ \mu_f = \text{constant} \qquad \text{E.3.52.}$$

E.3.52 has been verified experimentally by Singh et al. (49) for particles 200 μm wt. mean diameter, and temperatures up to 700C.

3.6.1. Viscosity of Combustion Gases. Although sophisticated techniques are available for the calculation from first principles of the viscosity of mixtures containing polar gases, proven expressions are complex (50), and a simple method of estimating the viscosity of the products of combustion of residual fuel oil was sought.

Town gas and natural gas have different constituents, but the

compositions of the stoichiometric combustion products of both gases are similar, and the viscosities identical over a wide range of temperature (51). The stoichiometric combustion products of residual fuel oil are similar in composition to those of town gas and natural gas, the main constituent in each case being nitrogen (see table 3), and in finding U_{mf} at elevated temperatures, it was assumed that the viscosity of the gases in the particulate phase was the same as that of town gas or natural gas combustion products at the same temperature. E.3.52 expresses viscosity as a function of temperature, and was obtained by regression of data taken from curves in reference (52). The equation is valid between 800K and 2300K, and T is in degrees Kelvin.

$$\mu_f^T = 10^{-6} \left[2.6113 + 5.1581.10^{-2}T - 1.5688.10^{-5}\, T^2 + 2.15.10^{-9}\, T^3 \right] \qquad \text{E.3.52.}$$

The units of μ_f are $(N\ s/m^2)$.

3.7. Combustion on a Distributor Plate.

The equations developed in section 3.4 enable the calculation of equivalence ratio of a product bubble formed by the coalescence of bubbles of air and gas when these both begin to grow on their respective orifices after delay times equal to mean values. Since heat release per unit mass of fuel at known thermal conditions is a function of the initial gas composition, ϕ_g, and the final gas composition, ϕ_b, efficiency $\bar{E}_p$ may also be found without recourse

to a dynamic bubbling model.

When information on the diameter of bubbles is required, and in cases where there are variations in t_d or the air or gas mass flows, a dynamic model is needed, and the model described in Appendix 8 has been applied to the distributor which was designed as outlined in Chapter 4. Results have been found in terms of the controllable variables ϕ_1, F_1, and the parameter p_a. The separation of the opposing air and gas orifices is always 0.054 m. All results are for the case of $t_{da} = \bar{t}_{da}$, and $t_{dg} = 0$. Thus the plate efficiency was in all cases found from E.3.44.

The combustion of the carbon in the gas feed was not considered, although the air requirement for it was included in the total air supply. The air supply was calculated as the overall stoichiometric requirement for Vanilla fuel oil, using in E.3.48 a value of w equal to 13.89.

The air and gas supplies were considered to divide between the bubble and particulate phases in such a way that ϕ_p was 1, and R^*_{gb} and R^*_{ab} were found from E.3.17 and E.3.18, with R_a, R_g given by E.3.48 and E.3.22, and R_{ap}, R_{gp} by E.3.23 and by;

$$(R_{ap} + R_{gp}) = \frac{\pi}{4} D_r^2 \ (\rho_f U_{mf}) \qquad \text{E.3.53.}$$

where D_r is the diameter of the fluidised bed.

In all cases, U_{mf} was found from E.3.52; for the particles that were selected for the initial trials, U_{mf} at 25C is equal to 0.18 m/s.

No preheat to the air was used, and all air volumes were computed at 25C. The density of the gasified oil, and all densities

used in the numerical integration of equation 9 in Appendix 8 (see also page A4-6 Appendix 8) were calculated for values of inter-stage heat removal taken from Fig. 3.1. The number of air orifices is greater than the number of gas orifices, and the average number of product bubbles, N_c, used in finding $\bar{E}_p$ was always considered to be the maximum. There were 48 air orifices and 36 gas orifices, thus;

$$N_c = N_g \quad , \qquad N_{op} > N_g \qquad \text{E.3.54.}$$

$$N_c = N_{op} \quad , \qquad N_{op} < N_g \qquad \text{E.3.55.}$$

$$N_{op} = \text{INT}\,(p_a N_a) \qquad \text{E.3.56.}$$

INT (x) signifies the nearest integer value of the variable x. Computed results are tabulated in Appendix 7.

3.7.1. Equivalence Ratio. In section 3.4.2 the qualitative effect of changes in t_{da} on ϕ_b was discussed, and in applying the coalescence model to the combustion of gases containing solid carbon, the effect of maldistribution on the availability of oxygen in a product bubble after the gas phase reactions are completed, has been examined.

E.3.38 is applicable to the case of the overall gas and air supplies R_g, R_a, being in stoichiometric ratio, and consideration of E.3.21 shows that where R^*_{ab} is greater than the stoichiometric requirement, the air to fuel ratio in the product bubble will rise. Equivalence ratio is inversely proportional to the air to fuel ratio, thus in this

case, ϕ_b is always expected to be smaller than the value predicted by E.3.38. Table A.7.1 lists both the computed values of ϕ_b, and those given by E.3.38 for the case of F_1 = 3.5 g/s and these are plotted in Fig. 3.11. At all ϕ_1, the computed values of ϕ_b are lower than those given by E.3.38; for instance, at ϕ_1 = 1.55, ϕ_b is 1.024, whereas E.3.38 gives ϕ_b = 1.097.

Values of $\phi_b > 1$ indicate that the product bubbles contain no oxygen, and by implication and consideration of E.3.40, all values of $t_{da} > \bar{t}_{da}$, and some values of $t_{da} < \bar{t}_{da}$ will result in fuel rich product bubbles. Under these conditions and considering the gas phase reactions to be instantaneous, the solid carbon in the bubble would not be able to burn.

3.7.2. Combustion Efficiency and Heat Release. The results for these are in tables A.7.2 and A.7.3.

Fig. 3.12 for the case of F_1 = 3.5 g/s, shows the strong effect of orifice non operation on $\bar{E}_p$, and the shape of the curves, falling from a high value of $\bar{E}_p$ at lower gasifier equivalence ratios to a smaller value as ϕ_1 is increased, is consistent with the assumption of a particulate phase in which stoichiometric combustion is completed. The temperature of the particulate phase increases as ϕ_1 increases (see Fig. 3.13) and U_{mf} falls with increasing temperature. Thus the fraction of the total flow into the bed that is diverted to the bubble phase rises as ϕ_1 increases. Typical results are illustrated by an example. When F_1 = 3.5 g/s, and p_a = 1, $\bar{E}_p$ at ϕ_1 = 1.1 is 96.2%; when ϕ_1 = 1.55, $\bar{E}_p$ falls to 92.3%. The corresponding values of $\bar{P}$, the heat release rate

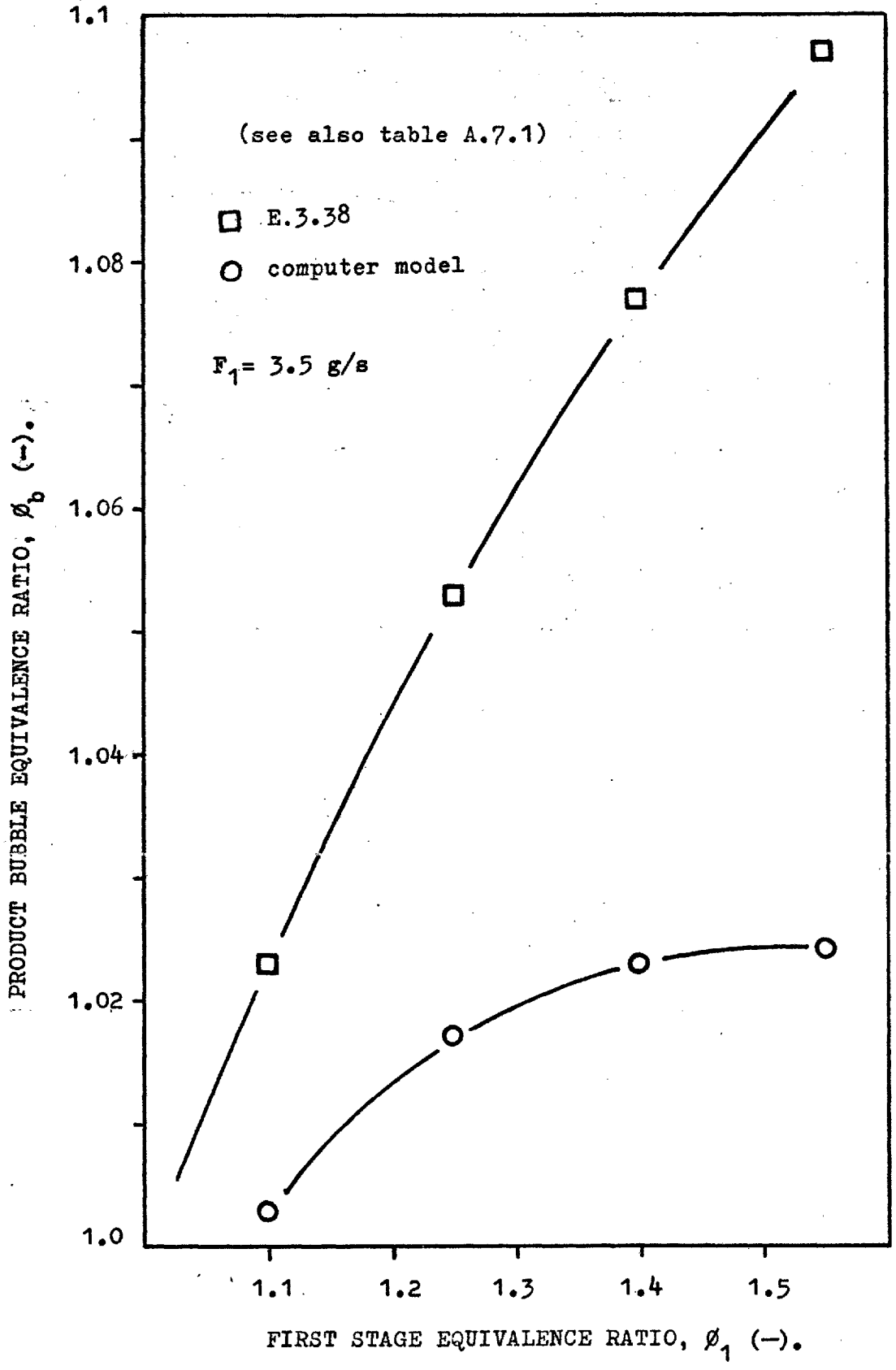

FIG. 3.11: PRODUCT BUBBLE EQUIVALENCE RATIO AT DIFFERENT FIRST STAGE EQUIVALENCE RATIOS.

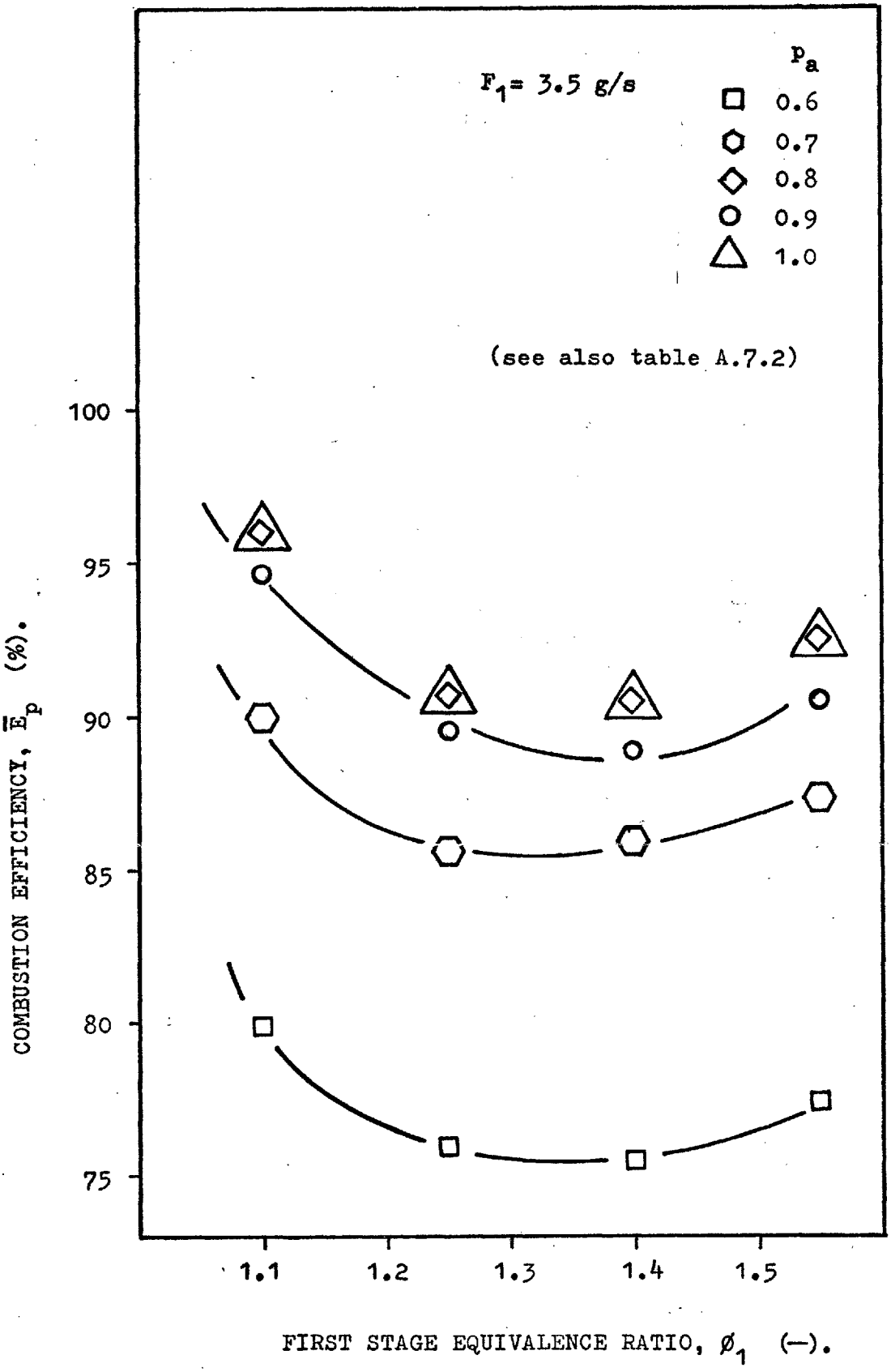

FIG. 3.12: COMBUSTION EFFICIENCY OF DISTRIBUTOR PLATE.

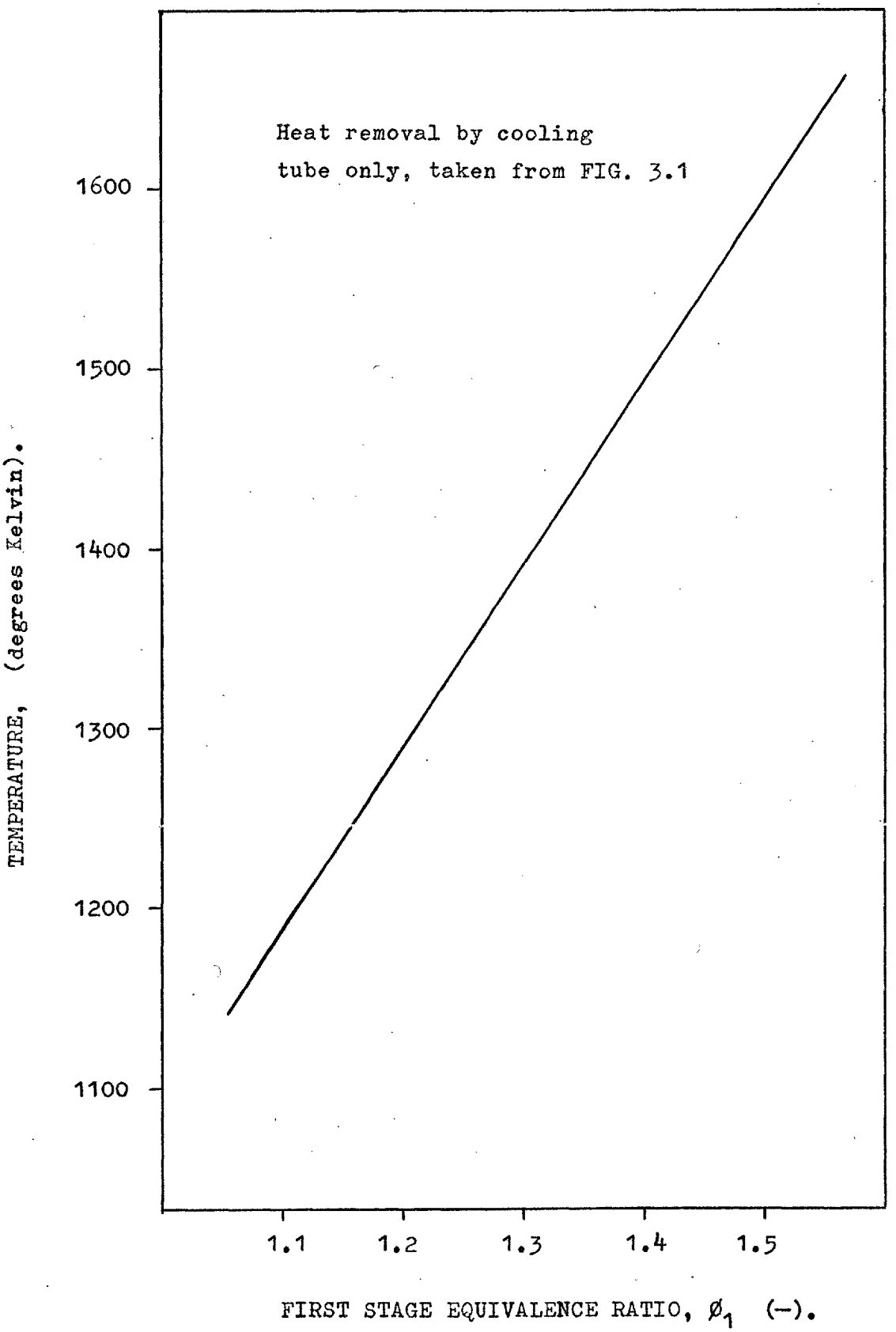

FIG. 3.13: GAS TEMPERATURE AFTER STOICHIOMETRIC COMBUSTION IN SECOND STAGE.

are 2.93 kw and 11.13 kw. The equation for $\bar{P}$ is given below, and values of $\bar{P}$ are listed in table A.7.3.

$$\bar{P} = \frac{\bar{E}_p \quad \Delta H_{ov} (F_p t_b + N_g f_b)}{100} \qquad \text{E.3.57.}$$

3.7.3. Bubble Diameter. The diameters of bubbles forming on the distributor plate have been estimated both from E.2.3 for the unreacted gas feed, and using the coalescence model. Results are listed in tables A.7.4, A.7.5 and these are plotted in Fig. 3.14 and Fig. 3.15.

The effect of chemical reaction after the coalescence of an air and gas bubble, and the subsequent growth of the product bubble fed by both air and gas until detachment, is seen to be considerable. When F_1 = 3.5 g/s and ϕ_1 = 1.55, D_b for the unreacted gas feed as given by E.2.3 is 78 mm, while the value of D_b for a product bubble fed at the same gas rate is 103 mm. Increased interstage heat removal will decrease the diameter of bubbles formed at the distributor , and table A.7.4(ii) is for the case of interstage heat removal, equal to $(Q_i + Q_g)$, for single gas bubbles. The computed bubble diameters, are large for the shallow depth of the bed (0.3 m) which is necessary to cope with the low delivery pressure of the feed gas. This fact could lead to unsatisfactory fluidisation.

3.7.4. Implications of Results. The computed results taken in conjunction with Fig. 3.3, Fig. 3.7 and Fig. 3.8, suggest that throughout the range of gasifier oil flows 2.5 - 3.5 g/s, the operation of the combustor will be satisfactory, although the higher flowrates and equivalence ratios should favour good gas distribution and second stage stability. The possibility of carbon bypassing the bed unburnt illustrates the importance of a mechanism for capture of carbon by the particulate phase. More work

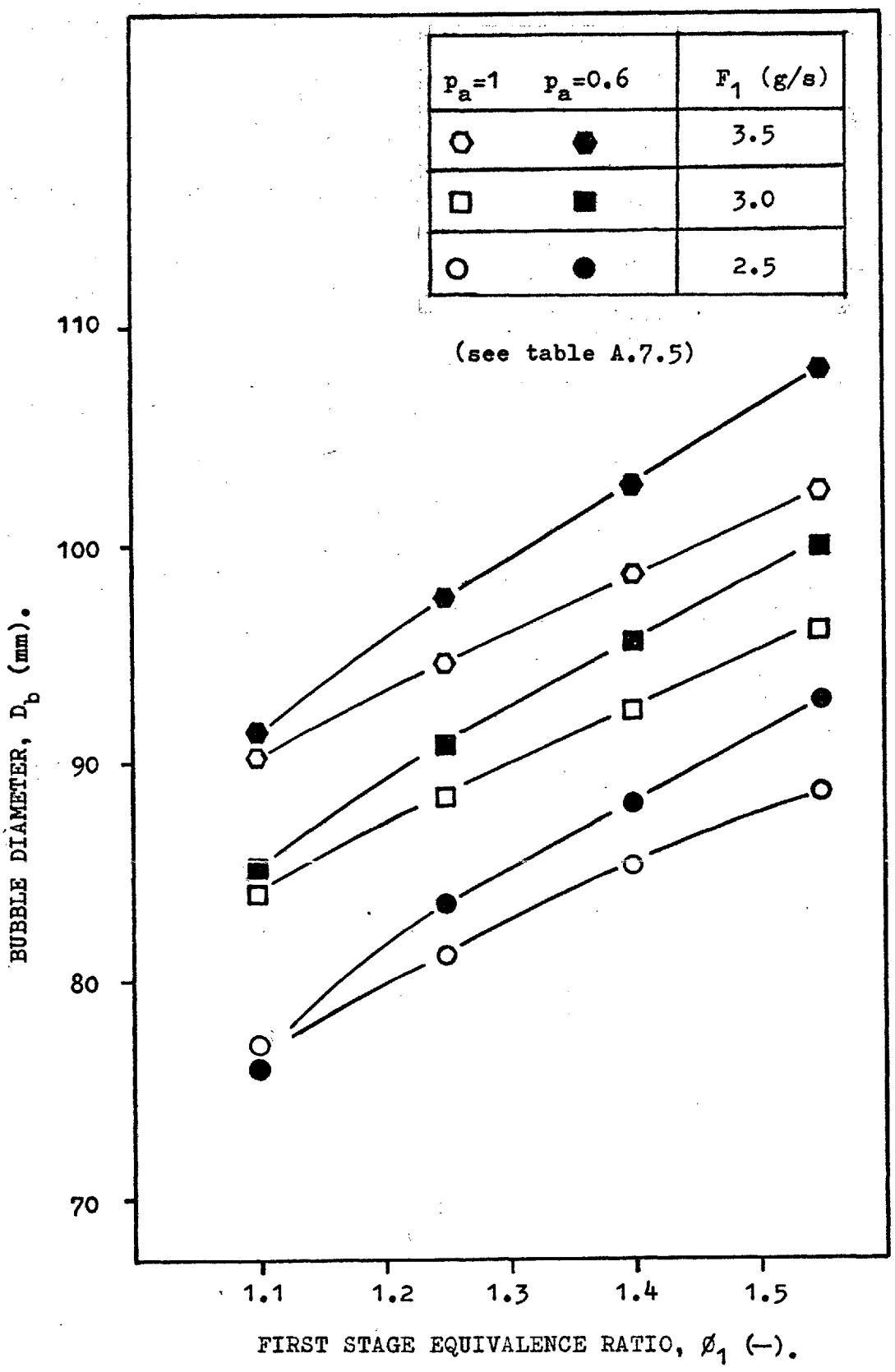

FIG. 3.14: DIAMETERS OF PRODUCT BUBBLES OBTAINED FROM COMPUTER MODEL.

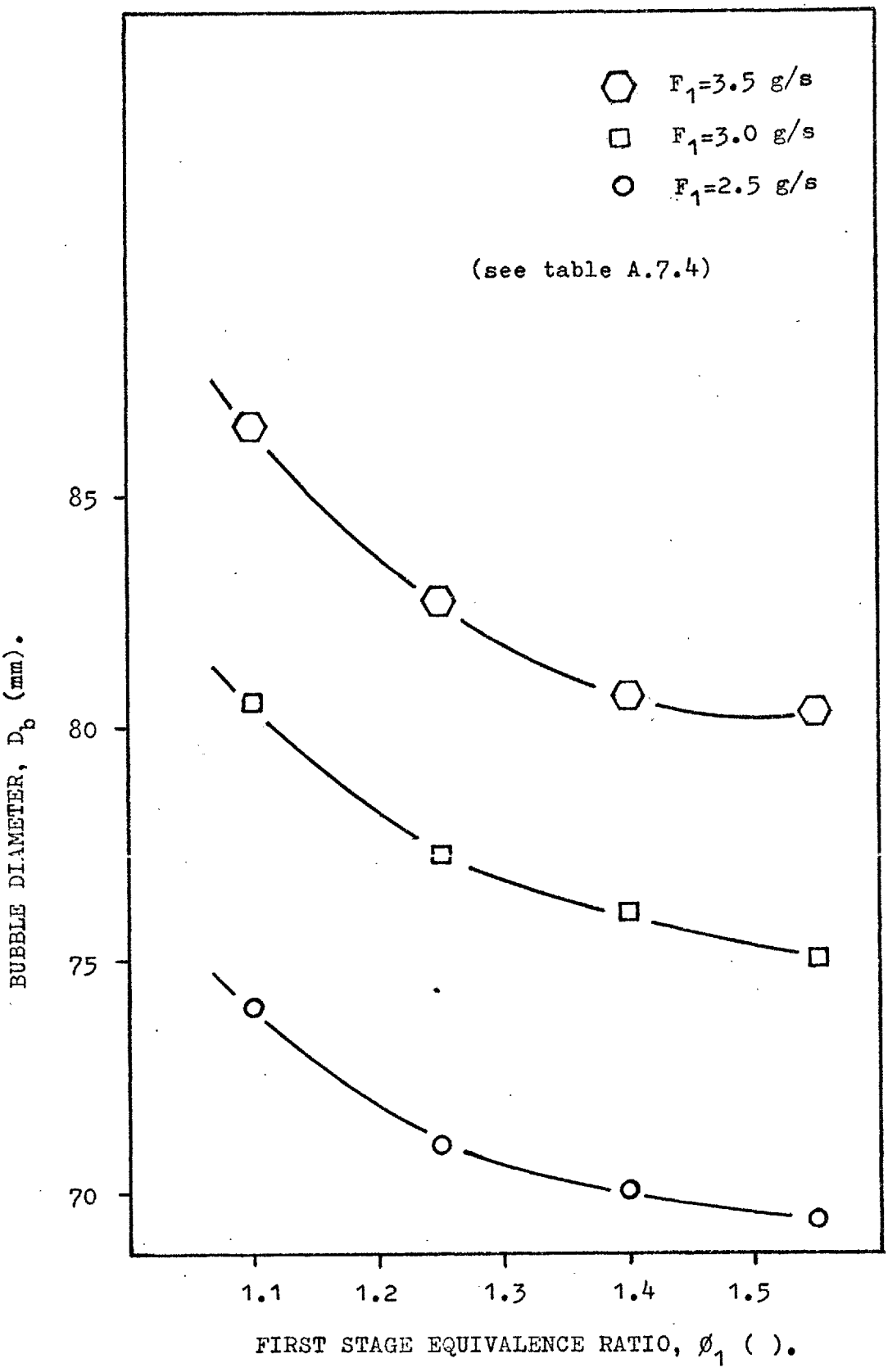

FIG. 3.15: DIAMETERS OF GAS BUBBLES OBTAINED FROM E.2.3.

on this aspect is at present being undertaken in the laboratory.

It is apparent that particle diameter is an important parameter in the system under consideration, as it could be used advantageously to control bubble diameter, though the raising of d_p with subsequent increase is U_{mf} could adversely affect flow distribution at the distributor plate.

There are of course many intriguing interactions occurring between most operating parameters, and it is hoped that the preceeding part of this work has made this observation very clear.

CHAPTER FOUR

DESIGN

4.1. Constraints.

The design of the fluidised bed was governed by the following mechanical and system constraints:

(i) The combustor had to fit into a laboratory with a 3 m (10 ft) ceiling.

(ii) The blower supplying secondary air to the gasifier delivers at 7.5 kN/m^2 (30 in w.g.) and under normal operating conditions, the pressure drop across the nozzles in the forward and reverse casings of the gasifier (see Fig. 1.1) is 2 - 2.5 kN/m^2 (8-10 in w.g). This means that the fluidised bed will have to be shallow, and the distributor plate pressure drop will, in absolute terms, be very low.

(iii) In view of the large physical size and weight of each sub-unit of the combustor and the noted difficulties associated with the use of a reducing gas containing suspended solid carbon, the distributor should be simple in design and allow the plate parameters to be changed easily, apart from being accessible to inspection.

(iv) The hot gas stream must be mixed with air inside the bed, and it is desirable that the combustion of the gasified oil should proceed to completion within the bed if full advantage is to be taken of the benefits offered by the use of a fluidised system.

(v) The flow of solids out of the bed into fluid distributing manifolds is not tolerable either during operation or during periods of shut down. The accumulation of particles inside a plenum chamber during

times when the bed is not fluidised could cause operating problems, particularly as experimental research involves repeated start up and shut down of the plant. In addition, re-entrainment of abrasive material into the bed should be minimised because it causes wear at the distributor.

4.2. Combustor Configuration.

A combustor having a configuration such as that shown in Fig. 4.1 and a low pressure drop at the gas tuyeres is compatible with all the constraints mentioned above. The gas and air both enter the bed through horizontally blowing ceramic tuyeres. Johnson and Davison (30) have noted that carbonaceous solids do not build up as readily on ceramic materials as they do on cooled metal surfaces and Lever (53) has made a similar finding when sampling the gases produced from oil in a chamber similar to the H.D.C.C.. This observation is confirmed by experimental experience gained by this laboratory over the past ten years. Flowback of solids is eliminated, and the tuyeres are removable for inspection alteration or change, without the dissembly of the heavy sub-units for using the combustor. In section 3.2.4 it was pointed out that the volumetric flow of the air entering the bed is low, with the accompanying possibility of orifice nonoperation. However, designs encouraging high heat transfer from the hot surfaces in the air plenum chamber were not compatible with the need for simplicity in construction.

The possibility of preheating the air by partial combustion with some of the gas feed was considered. This was not a practicable solution

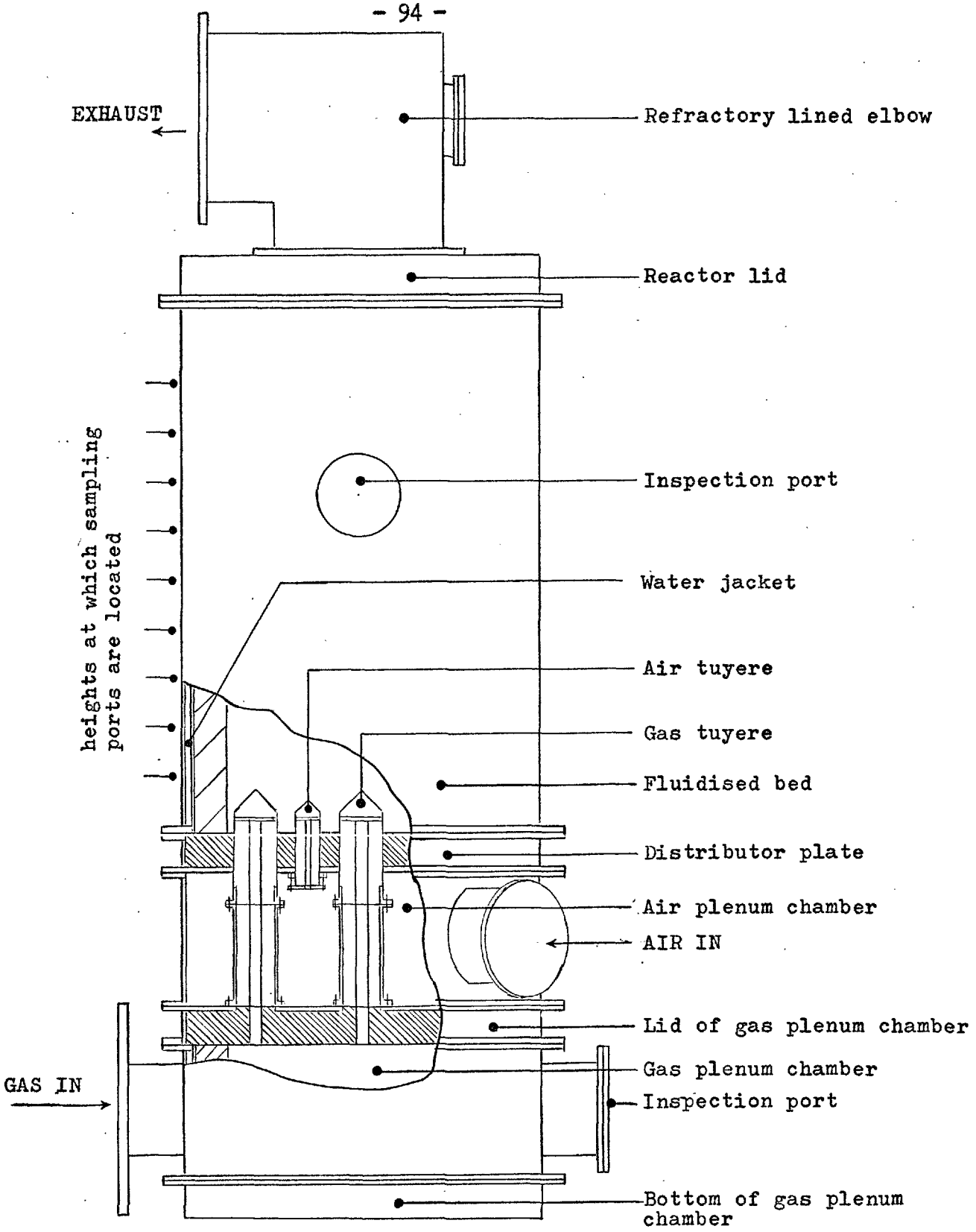

FIG. 4.1: ASSEMBLY OF FLUIDISED BED COMBUSTOR.

to the problem of ensuring good air distribution at low air flow rates.

4.3. Distributor Plate and Tuyere Design.

The relative disposition of the air and gas tuyeres, and the numbers of tuyeres on the plate were fixed by the external diameter, d_t, of the tuyeres. This in turn was fixed by the interaction of the following conditions;

(i) The tuyere should not allow any flowback of solids into a plenum chamber.

(ii) The tuyere should be strong and not liable to fracture during fabrication or operation.

(iii) The air and gas should both be distributed evenly over the base of the bed, and gas and air mixing at the plate level should be encouraged.

(iv) The total pressure drop across a gas tuyere and the fluidised bed should be approximately 4 - 5 kN/m^2 (16 - 20 in w.g.), with $\Delta P_d \doteqdot 0.2\,\Delta P_b$. Thus ΔP_d should be $\sim$1 - 2 in w.g..

(v) The gas orifices should not under any circumstances become blocked by the carbonaceous matter in the gas feed.

The gases used in the combustor contain less solid carbon than the gas feed used by Johnson and Davison (30). Their feed had a solid burden of 17 g/m^3 whereas at $F_1 = 3.5$ g/s and $\phi_1 = 1.55$, the solid loading is one tenth of the above figure. However, at $\phi_1 = 2$, the solid loading rises to one third of the above figure. Thus it was decided that the gas orifices should have a diameter, d_{org}, larger than the smallest used in

reference (30), viz.,

$$d_{org} \geq 6.4 \text{ mm } (\tfrac{1}{4}\text{in}) \qquad \text{E .4.1.}$$

The back flow of solids into the plenum chambers was discouraged by choosing the length l_t (see Fig. 4.2) so that:

$$\tan^{-1}\left[\frac{d_{or}}{l_t}\right] < \beta \qquad \text{E.4.2.}$$

where β is the angle of repose of the bed material. Various values are listed by Leva (54). The bounding values of β for inorganic matter in this list are 22° and 45°. Hence it is considered that;

$$\frac{l_t}{d_{or}} \geq 2.47 \qquad \text{E.4.3.}$$

will stop the backflow of material when the bed is defluidised. The angle of repose of the fused mullite chosen as the particulate filler was found to be 35°.

The upper ends of the tuyeres were conically shaped to discourage the accumulation of solids there, and a cone half angle, θ , of 45° was chosen using the equation:

$$\theta \leq \left(\frac{\pi}{2} - \beta_{max}\right) \qquad \text{E.4.4.}$$

where β_{max} is the maximum angle of repose of any material likely to be used in the combustor.

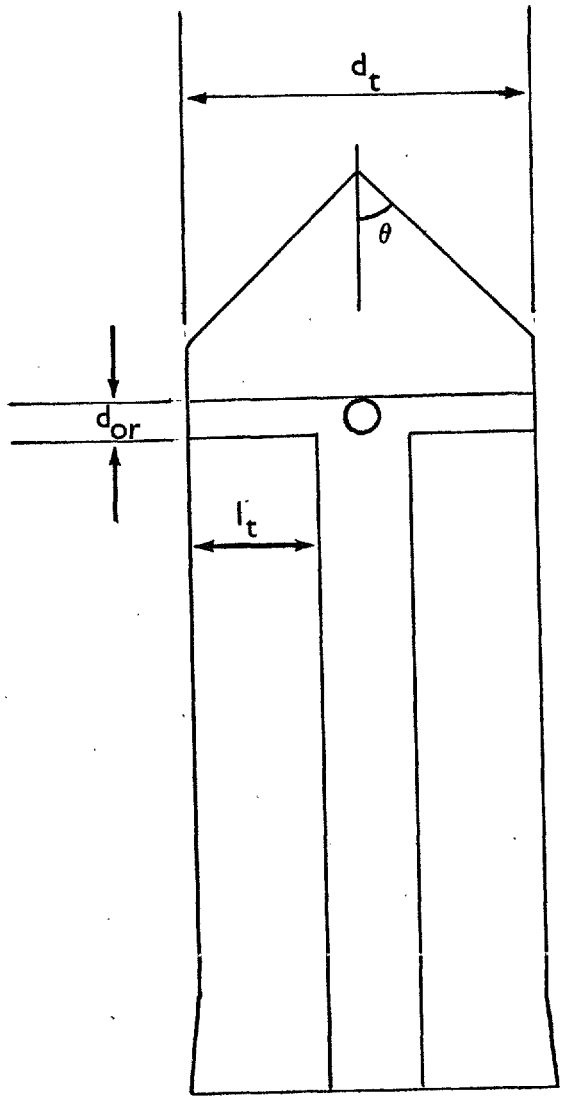

FIG. 4.2: TYPICAL TUYERE.

4.3.1. Experimental Tests. Some cold experimental trials were carried out in a 114 mm (4½ in) diameter bed with one of the smaller (air) tuyeres. A tuyere having 6.4 mm (¼ in) orifices, and $\left(\frac{l_t}{d_{or}}\right) = 2.5$, was set in the centre of a multiorifice plate. The volume of air supplied to the bed was slowly raised until the bed was vigorously fluidised andthen U was decreased. Visual observation showed that no particles fell back into the perspex plenum chamber.

In another series of tests, breakage of the tuyere was simulated by removing its top while the bed was fluidised. The air flow to the bed was gradually reduced until weepage through the unobstructed vertical conduit left by the removal of the covering dome of the tuyere was observed. This flowback did not take place until the air flow was below U_{mf} and too small to measure accurately. Once weepage had started, it did not stop until the air flow had been raised considerably. This constitutes a serious operating hazard if breakage were to occur.

These experiments showed that condition (i) in section 4.3 was satisfied when l_t was chosen according to E.4.3. The gas tuyeres had 12.7 mm (½ in) diameter orifices, with $l_t = 2.5\ d_{or}$, and the air tuyeres had the same external dimensions as the tuyere used in the cold trial, i.e. $l_t = 2.5 \times 6.4$ mm, but the diameter of the orifices was reduced to 3.2 mm (⅛ in).

4.3.2. Attachment of Tuyere to Plate. A typical tuyere is shown in Fig. 4.2,and has four horizontally blowing orifices all in the same plane and equi-spaced round its perimeter. The cross-sectional area

of the central duct was made to be the same as the combined cross-sectional area of the four orifices when their diameter was the upper value given by E.4.3, viz, $d_{or} = \frac{l_t}{2.5}$.

The way in which the gas and air are separately passed into the bed is shown in Fig. 4.1, and Fig. 4.3 is a detail of the air plenum chamber showing an air and gas tuyere fixed in position in the distributor plate. The removal of an air tuyere is easily accomplished by unbolting the flange of the holding collar from studs on the bottom of the distributor plate (these studs are not shown in Fig. 4.3; there are four for each tuyere). The distributor was designed so that the air tuyeres could be removed without taking out the gas tuyeres first.

A gas tuyere can be removed from the distributor by unbolting the flange connecting it to the cylindrical gas duct and gas plenum, unbolting the duct at the gas plenum, removing the duct and then lowering and withdrawing the tuyere. On reinstallation, a seal should be made inside the air plenum at the point where the tuyere passes through the distributor.

4.4. Combustor Dimensions.

The diameter of the fluidised bed, and the disposition of the tuyeres on the distributor plate were jointly decided. Using the techniques described in chapter 3, the effect of changes in ϕ_1, F_1, on;

(a) the velocity of the gases approaching the distributor in beds of different diameter and hence the bubbling mode of the distributor;

(b) the expected stability of the combustor,

was examined.

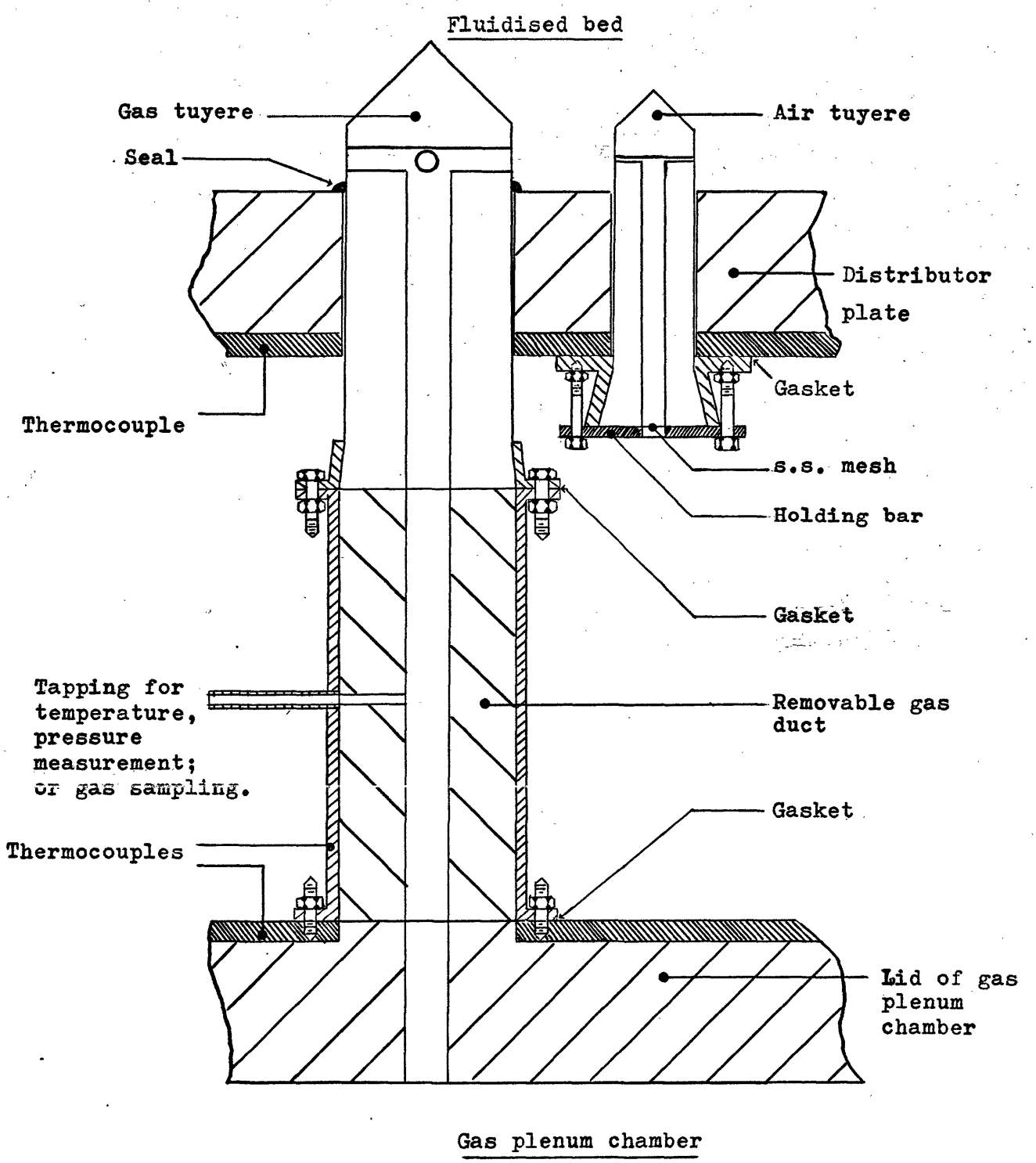

FIG. 4.3: LOCATION OF GAS AND AIR TUYERE IN DISTRIBUTOR PLATE (detail of Fig. 4.1).

Distributors were designed to fulfil the requirements listed in section 4.3, and it was found that a diameter of 610 mm (2 ft) was particularly suitable. Refractory bricks 76 mm (3 in) thick having a 305 mm (1 ft) radius of curvature profile were obtainable for the combustor lining, and Fig. 4.4 shows a plan view of the tuyere arrangement on the distributor plate finally adopted. The gas and air tuyeres are each centred on interlocking 241 mm ($9\frac{1}{2}$ in) square pitch arrays as shown. The separation of the centres of the tuyeres is thus 120 mm ($4\frac{3}{4}$ in), and the separation of the opposing orifices is 54 mm. Fig. 4.5 shows the effect of changes in gasifier flowrate on the pressure drop across the gas orifices (12.7 mm dia.); it is obtained using E.3.47.

The voids created in the refractory covered metal distributor plate to allow for the location of the tuyeres in the bed were not large enough to unduly weaken the plate, and sufficient area remained for the attachment of cooling water pipes. These can be seen in Fig. 4.6.

The dimensions of the casing of the fluidised bed and gas plenum chamber were thus chosen so that they each had a 610 mm (2 ft) internal diameter after the installation of a 76 mm (3 in) refractory lining.

Constraint (i) in section 4.1 imposed a severe limitation on the design of the height of each sub-unit, and dimensions were selected so that the freeboard of the fluidised bed was as high as possible. The air plenum had to be at least 0.3 m (1 ft) high to allow the removal of the air and gas tuyeres, and the standardised elbows used in the assembly of the plant were 0.57 m ($22\frac{1}{2}$ in) high. Thus the available space was allocated as follows:

(a) The fluidised bed measured from the distributor plate to the lid at the top was 1.22 m (4 ft).

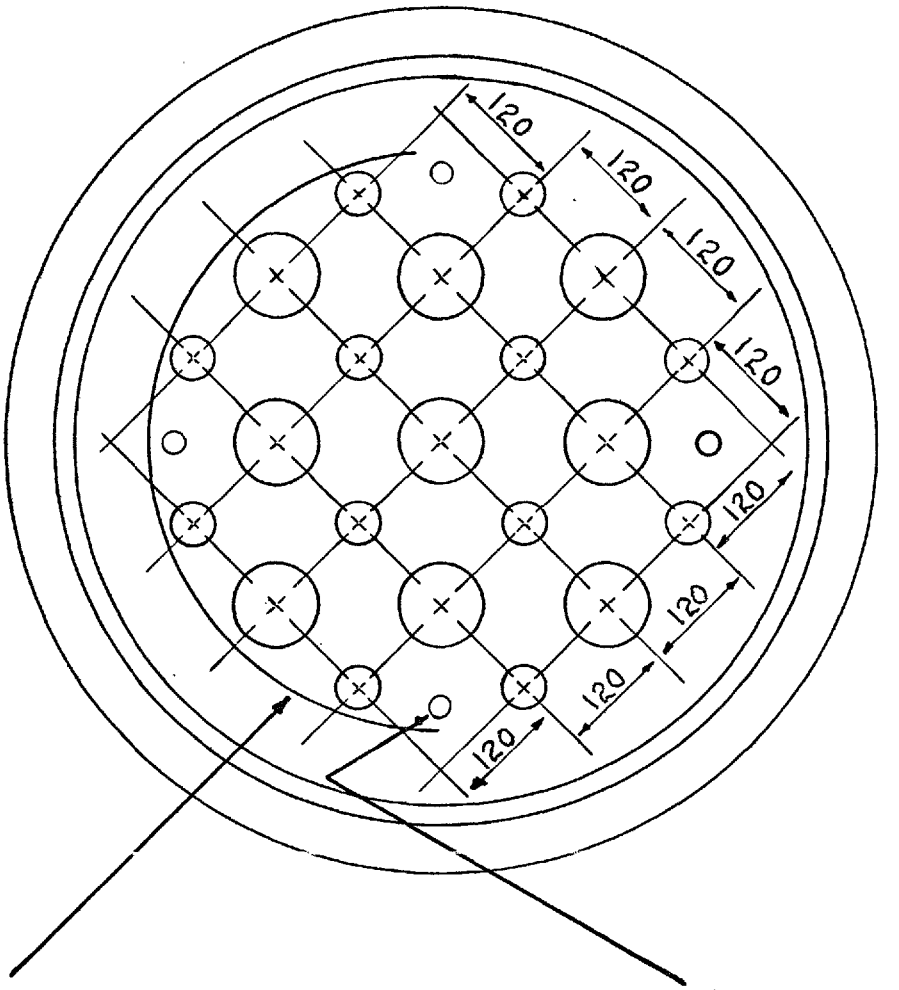

Position of wall
of fluidised bed

Tapping for pressure,
temperature measurement;
or gas sampling probe;
or cooling pipe.

1/8 scale
dimensions in mm

FIG. 4.4: PLAN VIEW OF DISTRIBUTOR PLATE.

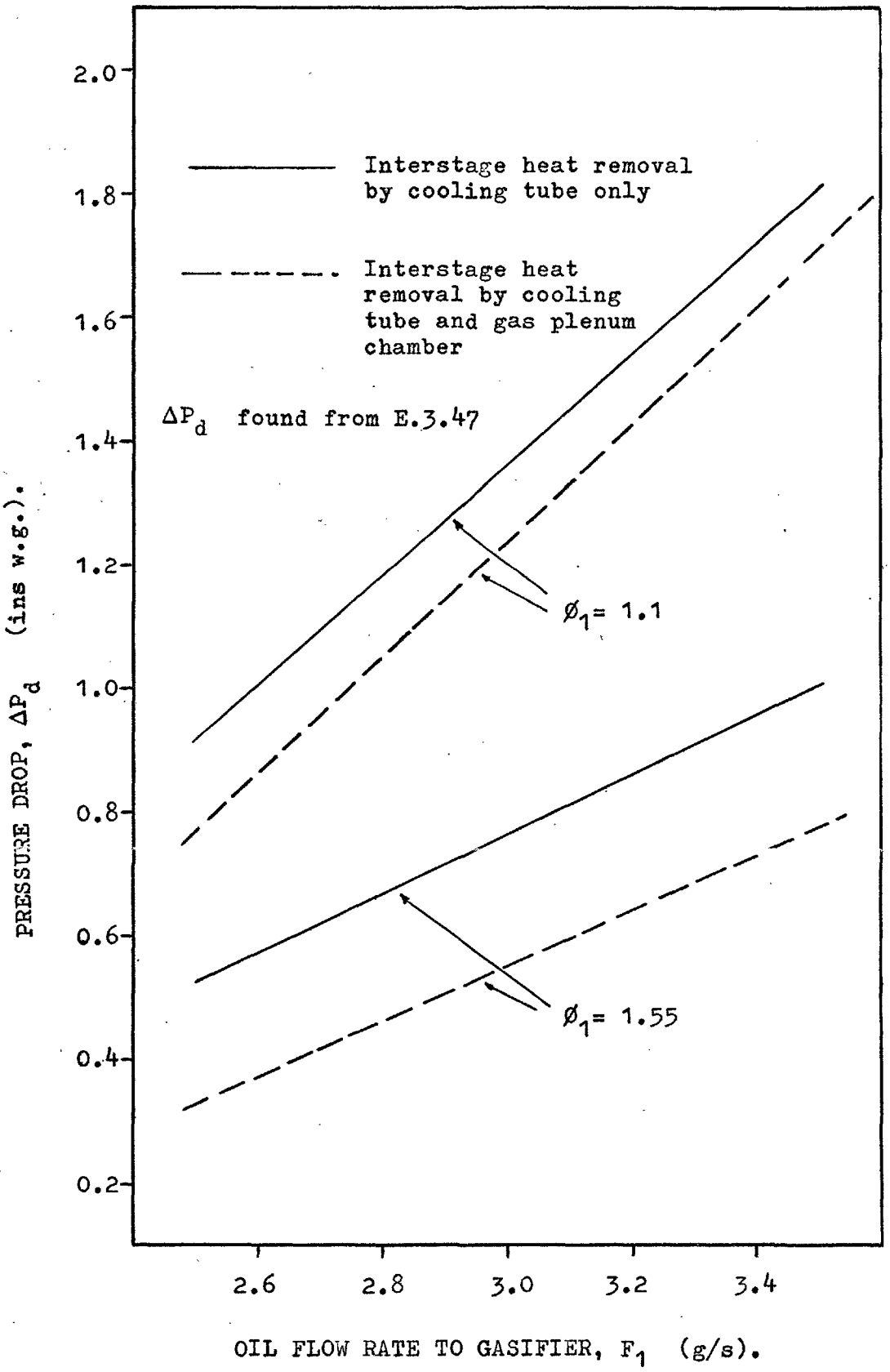

FIG. 4.5: PRESSURE DROP ACROSS GAS TUYERES.

(b) The gas plenum was 0.3 m (1 ft).

(c) The distributor plate, the gas plenum, and each of the end plates of the combustor were allocated 0.1 m (4 in).

The combustor was jacketed for reasons fully described in Chapter 3, section 3.2.4.

An exploded view of the combustor is shown in Fig. 4.6.

4.4.1. Sampling and Instrumentation. Nine sampling points were located at 0.11 m (4½ in) intervals up the height of the fluidised bed, the first one being 0.11 m (4½ in) above the distributor. These were designed to accommodate a gas sampling probe, and also to be used for pressure or temperature measurements (see Fig. 4.1). A tapping for the withdrawal of gas samples and for pressure or temperature readings was located in each of the refractory lined stainless steel ducts connecting the gas plenum chamber to the gas tuyeres. The tappings were positioned so that the properties of the gases entering the bed could be measured, and also allow the effect of any build up of carbon inside the tuyere on the pressure drop across the tuyere to be observed. Thermocouples were located in the metal casings of these ducts, and also in the metal plate of the distributor and gas plenum lid, (see Fig. 4.3). A pressure tapping was placed in the distributor plate so that the pressure at the base of the bed could be measured, (see Fig. 4.4).

The flow meters and also the location of the temperature and pressure tappings that are used to provide measurements for both experimental and control purposes are shown in the schematic flow diagram of the plant, Fig. 5.2.

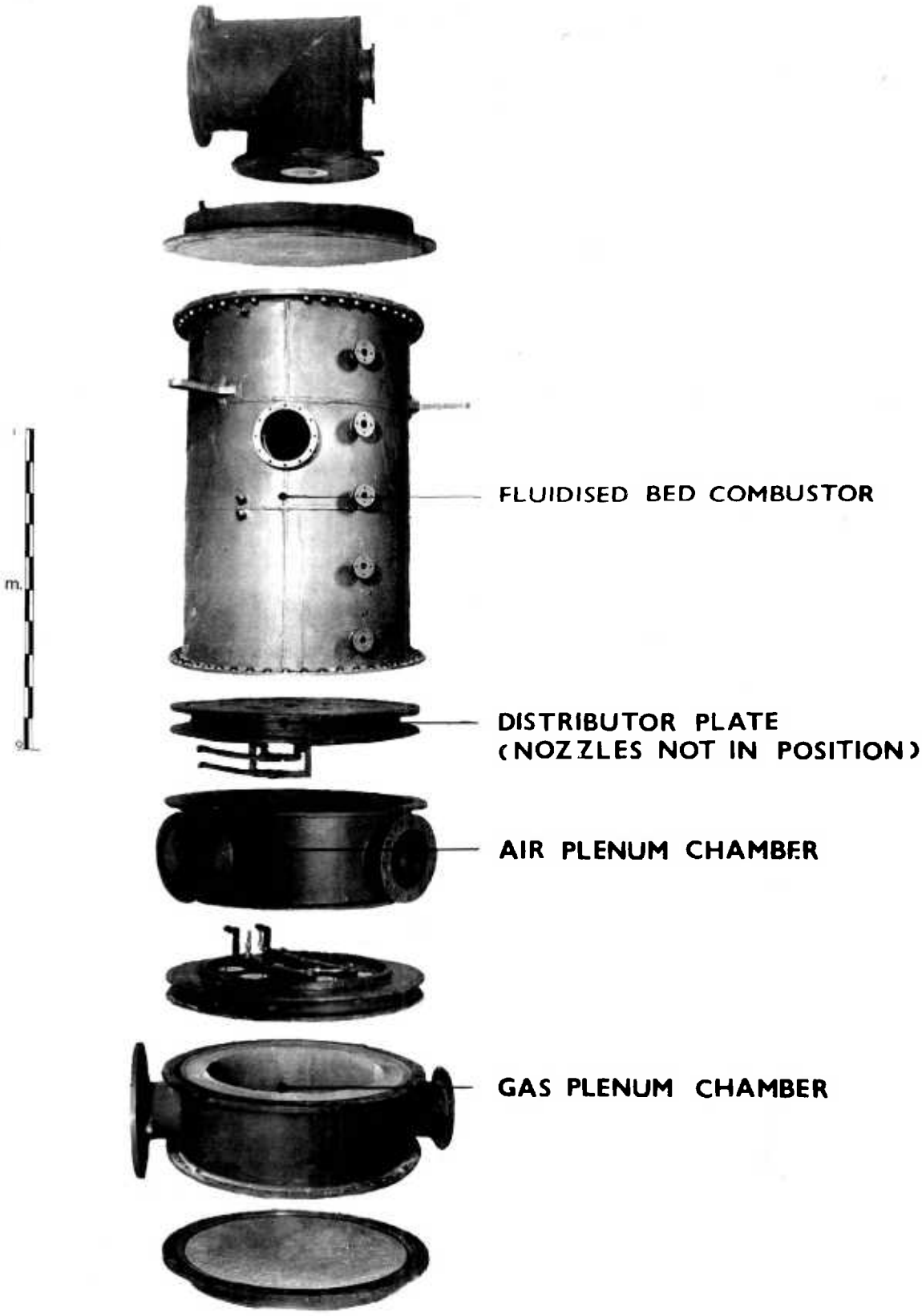

FIG. 4.6: **EXPLODED VIEW OF FLUIDISED BED COMBUSTOR**

4.5. Cyclone and Elbows.

A high efficiency cyclone required for removing ash, unburned carbon and fines from the combustor exhaust was designed according to the I.C.I. method due to Stairmand (55). Tangential gas entry was achieved by contra-posing two semicircular sections as shown in Fig. 4.7 so that a smooth pattern for the refractory lining could be simply and accurately made. The cyclone was surrounded by a water jacket to cool the refractory. It was designed to be a monolithic casting without expansion gaps, as imperfections in the refractory surface were undesirable and would be aggravated by any abrasive material in the process gas. The cyclone is depicted in Fig. 4.8.

The design of the elbows was adapted from a water cooled sampling tee-piece designed by Johns (3) for his experiments, which gave satisfactory operation at high temperatures over many years. For convenience the five elbows were built to the same standardised dimensions.

4.6. Particulate Material for Fluidised Bed.

Inert particles were selected for the initial trials, and had to meet several specifications. The material used had to be highly refractory and available in large quantities having a range of particle sizes so the mean diameter of a batch could be altered by the selective addition or removal of known size fractions. The material had to fluidise well. Fused mullite* met these specifications, and had previously been found

---

* manufactured by Cawoods Refractories Ltd., Belvedere, Kent.

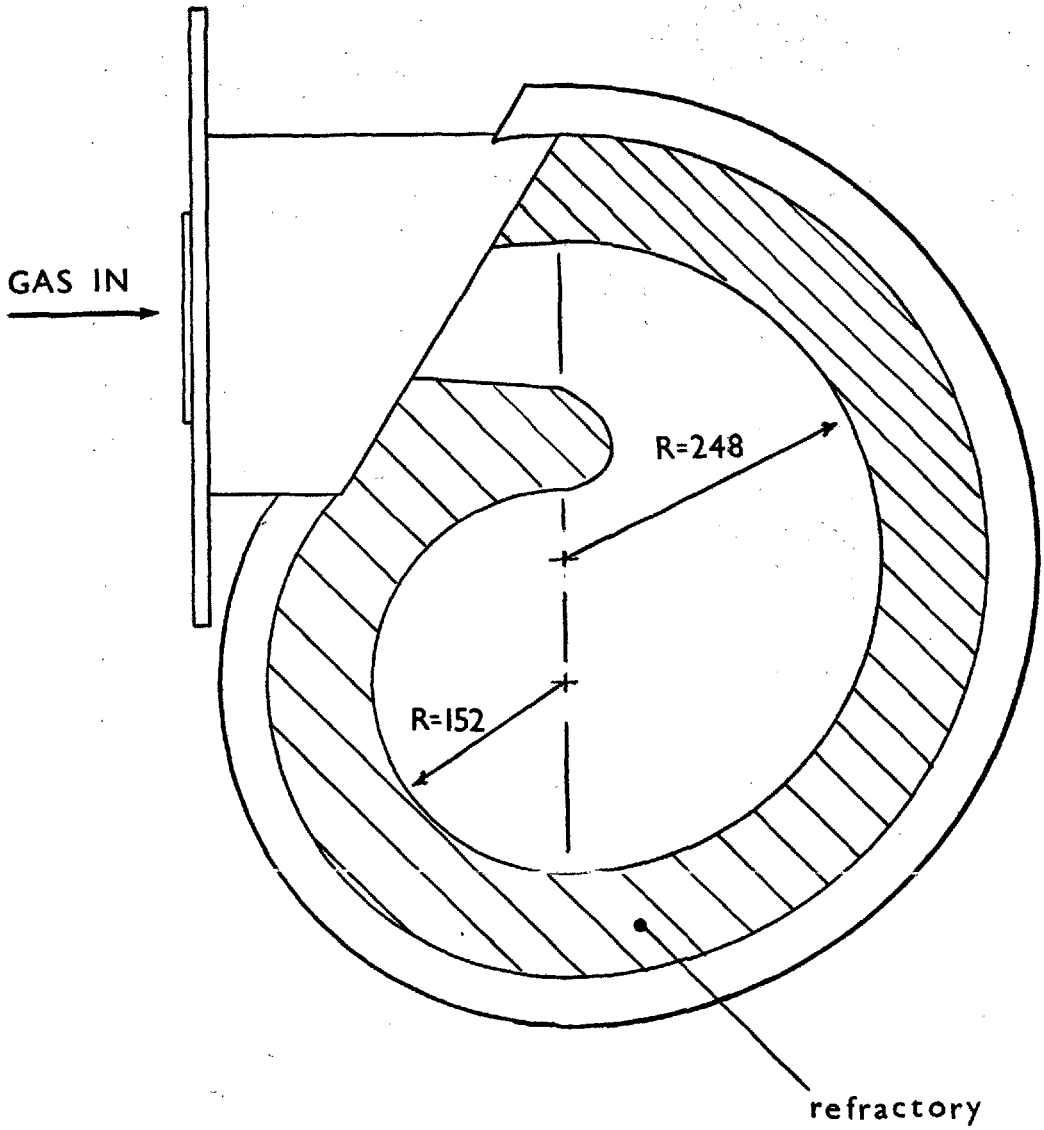

FIG. 4.7: PLAN VIEW OF CYCLONE GAS ENTRY SECTION.

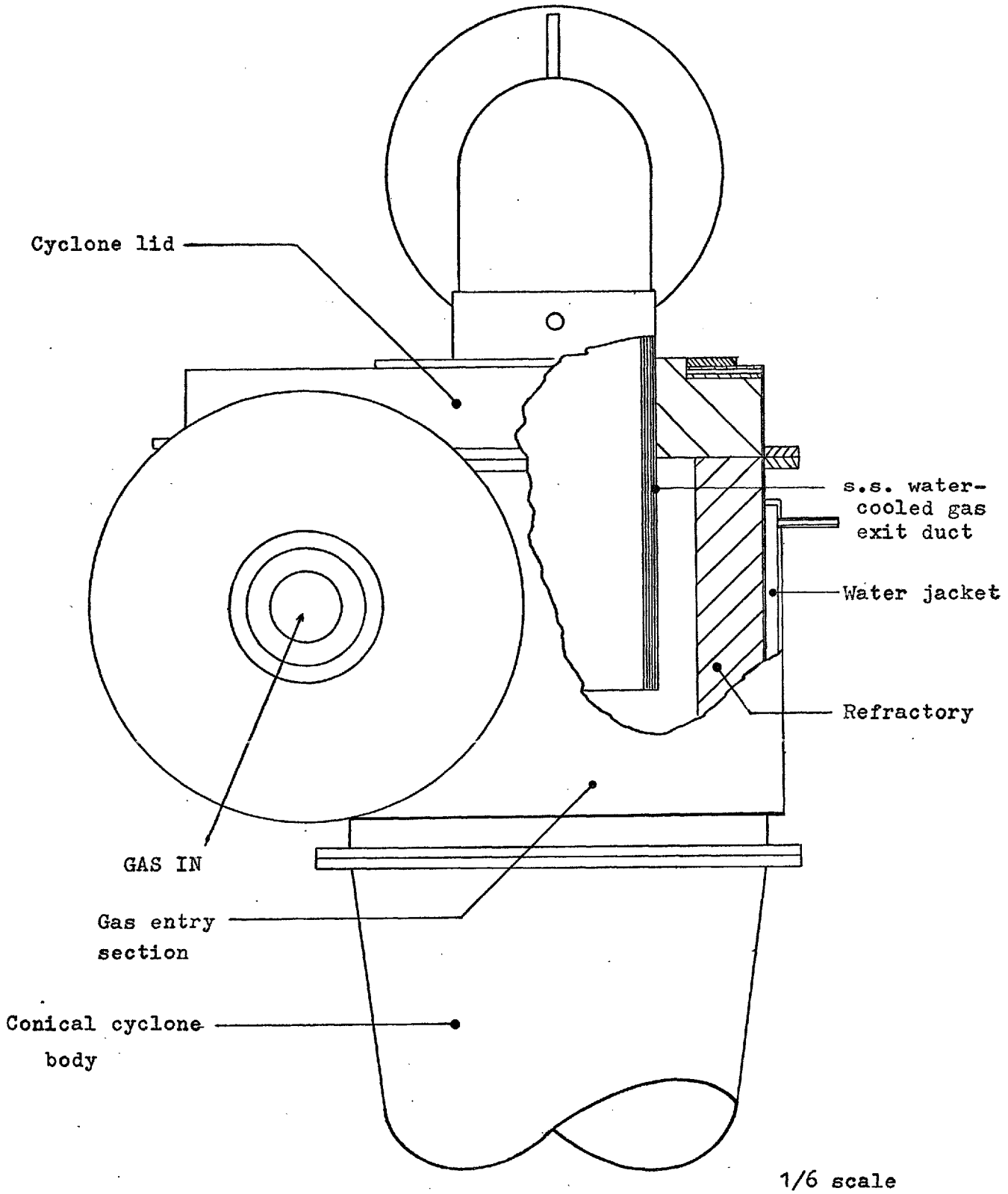

FIG. 4.8: ASSEMBLY OF CYCLONE.

satisfactory for use in fluidised bed combustors by other workers (56). Its relatively low density of 3.1×10^3 kg/m^3 rendered it attractive, as greater bed depths were permitted at any given bed pressure drop than for the more dense zirconia or alumina which were also suitable.

In view of the extremely shallow free board above the fluidised bed, steps were taken to minimise entrainment by choosing the minimum particle diameter of a batch so the terminal veolcity of a particle having this diameter was much greater than the superficial velocities expected in the bed, (maximum U $\sim$0.9 m/s).

A commercial batch of - 22 + 0 B.S. sieved mullite was tailed by a No. 85 B.S. sieve, and the resulting material had a surface mean diameter of 401 μm, with a minimum diameter of 178 μm. The particle specifications are listed in Appendix 5.

It was observed in the cold experiments carried out in a 114 mm ($4\frac{1}{2}$ in) diameter bed having a multi-orifice type of distributor that at high superficial velocities the mullite fluidised well, but when U was close to U_{mf} there was a tendency for the larger particles to sink to the bottom of the bed. Hot experiments were conducted with a small quartz tube 45 mm in diameter having a sintered glass distributor and fired at 730 C with premixed air and methane. The bahaviour of the mullite during fluidised bed combustion was seen to be perfectly adequate, with no particle stratification.

CHAPTER FIVE

CONSTRUCTION AND COMMISSIONING

5.1. Construction of Fluidised Bed Combustor Elbows and Cyclone.

Dimensions and specifications for the manufacturers* of the unlined steel shells of the elbows and each item of the combustor and cyclone, were detailed in numbered drawings (57). The material used was mild steel except in the casing of the conduits connecting the gas plenum to the gas tuyeres, the collars for holding the air and gas tuyeres in position, and the water cooled gas exhaust leg of the cyclone. These were fabricated in 18:8 chrome nickel steel. The vertical walls of the fluidised bed and gas plenum chamber could be lined either with bricks or with cast refractory. Bricks have the advantage of being pre-fired, but are expensive. The technique for moulding a vertical wall was simpler than that required for laying refractory bricks, and since the elbows, the gas plenum lid, distributor plate, and cyclone all required cast refractory, it was decided that cast linings would be used throughout the combustor. Steel anchors+ for securing the linings were therefore specified for the wall and hanging refractory ceiling of the fluidised bed, and wall and ceiling of the gas plenum chamber.

---

* Ellard Engineering Limited.

+ Manufactured by George Clark (Sheffield) Limited.

The monolithic casting of the gas entry section of the cyclone was firmly held by V- anchors located on the shell wall as was the refractory in the cyclone lid.

The refractory selected was a high alumina hight duty concrete* chosen to ensure the continued viability of the combustor in the event of diminution of the interstage heat transfer below the level previously achieved by the use of a 2.13 m cooling tube.

Advice on the design and installation of the refractory linings was received from the manufacturers (58).

Hardwood patterns were made for the bore of the elbows, the tuyere holes in the distributor plate, and the entry and exit ducts and inspection holes of the gas plenum and fluidised bed.

A mild steel sheet 0.46 x 0.69 m (1 ft 6 in x 2 ft 3 in) rolled to a 0.305 m (1 ft) radius of curvature was used as a pattern for the walls of the gas plenum and fluidised bed.

The gas plenum walls were cast in four sections, with expansion gaps between each quadrant. The fluidised bed was likewise lined by eight equal castings in two layers of four each. The quadrants were 0.61 m (2 ft) high and the vertical edges of the upper ones were orientated at 45° to the lower ones.

The refractory in the elbows, the distributor plate and the combustor end plates and cyclone lid was installed in a single operation in each case.

A pattern in mild steel sheet was designed for each of the monolithic castings of the gas inlet section and conical body of the cyclone,

---

* Durax 1700 manufactured by G.R. Stein Refractories Ltd., Deepcar, Sheffield.

both of which were completed in a single casting. Special care was taken to ensure that all joins in the patterns were smooth so that imperfections in the refractory surface were avoided. The refractory was bonded by a high alumina cement, and the quantity of water used when mixing the concrete was kept at a minimum to get maximum strength.

5.2. The Construction of a Tuyere.

Longitudinally splitting steel casings were used for moulding the tuyeres. Several different types of refractory were tried, and a silicon carbide* based material was selected. It was found that tuyeres were more difficult to make from phosphate bonded silicon carbide than alumina based aggregates, but when fabricated from the latter material, tended to crumble at all edges, and nozzle definition was poor. Silicon carbide tuyeres were also less liable to fracture by mechanical or thermal shock, and were more resistant to abrasion. Each tuyere was individually heat cured in a furnace in which the temperature was slowly raised to 400 C. The furnace temperature was then increased to 1200 C and held for six hours.

5.3. Assembly.

The fluidised bed combustor was assembled piece by piece in situ and bolted to the base plate which was designed to spread the load of the

---

* CFR 120 Manufactured by The Carborundum Company Limited, St. Helens Lancashire.

plant over the laboratory floor (59). The combustor was then connected to the gasifier via the three cooling tubes and two elbows. Three elbows were then located to convey the combustor exhaust to the cyclone. The cyclone lid, gas inlet section, and gas exhaust leg were assembled and positioned, and then the conical body was added. The spray system used for quenching the exhaust gases and then scrubbing and collecting the carbon suspended in them has been described previously by Archer (60). This was then connected to the cyclone gas outlet.

All flanges were sealed with gaskets cut from a high temperature felt* and a refractory paste+.

Fig. 5.1 is a view of the combustor and cyclone, and a schematic flow diagram of the complete plant is shown in Fig. 5.2.

The air and water lines required by the combustor and cyclone were plumbed in, and pressure gauges and thermocouples for both control and experimental pruposes were connected to the tappings located as shown in Fig. 5.2.

The specifications of the air blowers used in the plant are listed in Table 5.

---

* Fibrefrax H felt.

+ L.D.S. mouldable.

Both manufactured by The Carborundum Company Limited, St. Helens Lancashire.

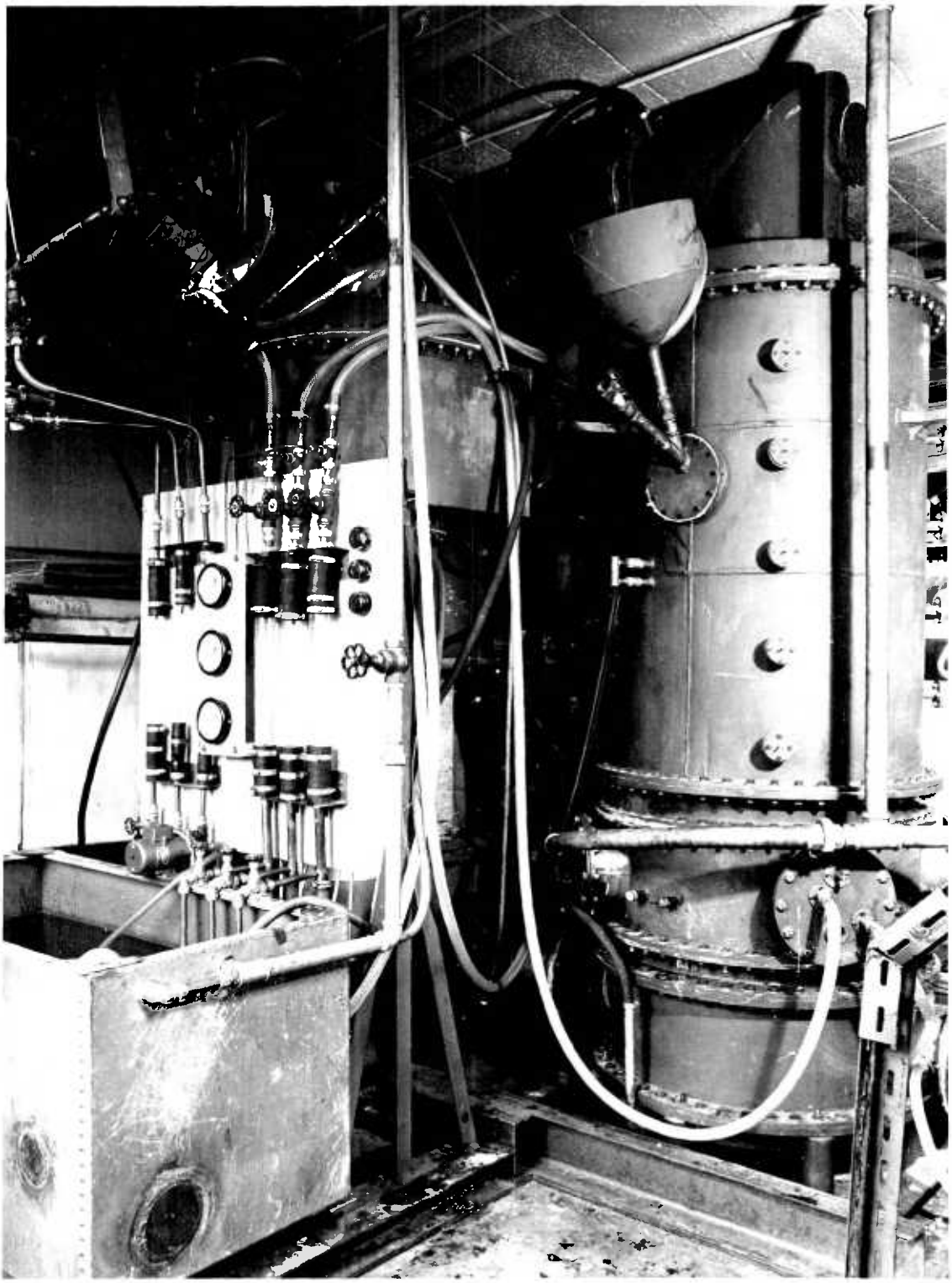

FIG. 5.1: FLUIDISED BED COMBUSTOR AND CYCLONE.

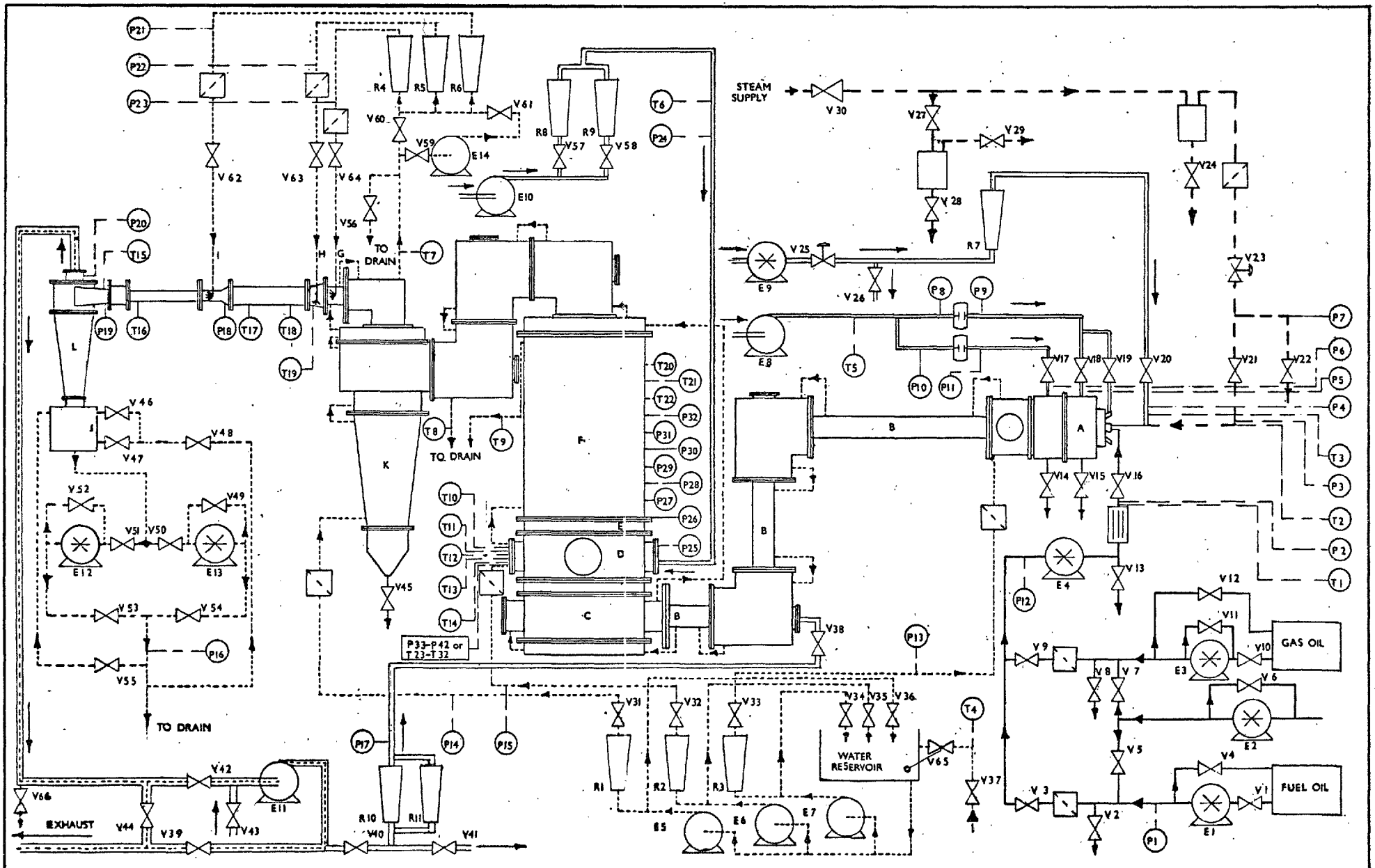

A	HIGH INTENSITY COMBUSTOR	E	DISTRIBUTOR PLATE	I	SCRUBBING SPRAYS	OIL	QUENCHED COMBUSTION
B	COOLING TUBE	F	FLUIDISED BED COMBUSTOR	J	LIQUID COLLECTING TANK	WATER	PRODUCTS
C	GAS PLENUM CHAMBER	G	QUENCH SPRAYS	K	SOLID SEPARATING CYCLONE	AIR	E pump R rotameter V valve
D	AIR PLENUM CHAMBER	H	WALL SPRAYS	L	LIQUID SEPARATING CYCLONE	STEAM	P, T. pressure/temperature tappings

SCHEMATIC FLOW DIAGRAM OF PLANT

FIG 5.2

TABLE 5: SPECIFICATIONS OF AIR BLOWERS AND COMPRESSOR.

Blower or Compressor	Number on Fig. 5.2.	Designated name	Air delivered	Pressure
Bullows hydrovane compressor	E9	Primary air (to atomiser)	4.5 g/s	to 100 p.s.i.g.
Blackman centrifugal fan	E8	Secondary air (to H.D.C.C.)	38 g/s 44 g/s	30 in w.g. 25 in w.g.
Osmond centrifugal fan	E10	Tertiary air (to fluidised bed)	21 g/s	30 in w.g.
Sturtevant Turbo Blower/exhauster	E11	Auxiliary air	138 g/s	42 in w.g.

5.4. Commissioning.

Before the fluidised bed combustor was built, plant incorporating the H.D.C.C. gasifier and a tunnel type second stage was recommissioned. The fuel metering pump and the venturimeters in the secondary air lines (see Fig. 5.2) were calibrated, and several runs were made to obtain operating experience.

The commissioning of the fluidised bed pilot plant was conducted in three stages:

(i) The fluidised bed was prepared for a cold run with no particles in the bed.

(ii) Hot trials were made with the empty combustor.

(iii) The combustor was charged with mullite, and trials were carried out to fully establish an operating routine.

5.4.1. Preparation of the Plant. The following steps were taken to set the system in working order:

The bolting of the flanges was checked and secured. All water jackets were pressure tested, and a pinhole leak in the cyclone exhaust leg was closed. The pumps and blowers were serviced, and all new lines cleared by running freely to remove metal swarf and other debris. All plumbing and flanges were leak tested, and bursting discs were installed on three of the elbows. The sprays were examined and cleaned.

A provisional startup and shutdown sequence was drawn up following the routine used by Archer (60) in previous work with the H.D.C.C. and a tunnel type second stage.

5.4.2. Cold Trial: Observations and Recommendations. It was observed that there was some water backflow from the sprays into the solid separating cyclone when the auxiliary air used to simulate the high volume flows of hot operation was reduced at shut down. The scrubbing sprays quickly blocked. Extensive maintenance to the spray system has been recommended (61, and Appendix 6B), but this was not deemed obligatory for the subsequent hot trials.

5.4.3. Hot Trials: Combustor Empty. Three runs were made. The first two were primarily to cure the refractory lining of the combustor, elbows, and cyclone, and the maximum temperature reached in the combustor was 500 C. In the third test, temperatures in excess of 700 C were recorded. In all of the hot tests carried out during the commissioning, gas oil was used as the fuel.

When curing the refractory lining the temperature of the process gas was slowly raised at 75 C per hour according to the instructions of the refractory manufacturers. The gasifier was fired stoichiometrically and the auxiliary air was admitted to cool the gasifier exhaust. The curing operation began with temperatures of 100 C in the combustor, and this was controlled by regulating the auxiliary air and observing the response on an iron constantan thermocouple T22 located in the gas stream (see Fig. 5.2).

The third run was conducted to test for ignition in the combustor. The temperature was slowly raised, and when that of the gas entering the gas tuyeres (T23) had exceeded 500 C, prebed combustion was established by raising the first stage equivalence ratio and adjusting the auxiliary air. Temperature in the bed was again controlled by noting the response of T22 to changes in oil flowrate and auxiliary air.

The high temperatures of the gases in this second burn were used to heat up the lining of the combustor, and when the auxiliary air was shut off, quenching was avoided and sustained combustion of the fuel rich gasified oil resulted. The thermocouples available were only calibrated to 700 C and ignition was inferred from observation of an increase in E.M.F. of the thermocouple as the air added to the combustor was raised gradually to the stoichiometric requirement.

5.4.4. Hot Trials: Sequential Action and Conclusions. All flanges were tightened. The refractory in the combustor was inspected and found to be in good condition.

Since the controlled temperature rise of the gases passing through the combustor had been followed as advised by the refractory manufacturers, it was concluded that the refractory had been cured.

A simple technique of preigniting the gas feed to raise the combustor temperature and thus avoid initial quenching was successfully used, and it was established that sustained combustion was possible when no particles were in the bed.

5.4.5. Fluidising Trials. Three hot trials and several cold tests were conducted after a particulate bed had been placed in the combustor.

The combustor was charged with 83 kg of mullite giving a bed height under incipient fluidising conditions of approximately 0.16 m. The auxiliary air was used to provide a fluid from the gas tuyeres. Visual observation through a perspex window placed over the inspection port of the gas plenum chamber revealed that caution was required at start up and shut down in the regulation of the tertiary air and auxiliary

air, as at some flows, particles were blown down the gas tuyeres and could be seen raining into the gas plenum chamber where they settled. Inspection of the air tuyeres showed that after shut down, particles of mullite lodged on the mesh placed between the holding bar and ceramic tuyere (see Fig.4.3). These were blown out of the tuyere at the velocities encountered in normal operation.

The tertiary air flow was set at a maximum value determined by the blower, and it was observed that at volumetric flows of auxiliary air above 0.024 m^3/s, the blow back of particles did not occur. This flow gives a velocity of approximately 5 m/s in the vertical central duct and likewise in the horizontal ducts (see section 4.3.2). Under normal operating conditions, velocities in the duct are approximately 18 - 25 m/s and the viscosity of hot combustion gases is higher than that of air at room temperature, thus it is not likely that any blow-back will occur after start up. Blow-back through the gas tuyeres during start up was avoided by raising the tertiary air flow after the auxiliary air flow was fully established.

The solids in the gas plenum chamber at the end of this test were allowed to remain in position during a short test run to prove the gasifier ignition, and also during a second longer test prior to which 115 kg of mullite were added to the solids remaining in the combustor.

5.4.6. Fluidising Trials: Conclusions and Recommendations. It was found that the technique used to raise the combustor temperature sufficiently to avoid quenching the gases entering the bed during start up, was not directly applicable when the particulate bed was

in position (see Appendix 6B), as pressure fluctuations probably caused by bubbles in the bed endangered the floats in the rotameters metering the auxiliary air, and ignition in the fluidised bed was not verified.

Inspection of the contents of the solid separating cyclone catchpot revealed some soot, and also dust from the mullite charge, but no large particles of mullite. A sample of the effluent from the collecting tank of the liquid separating cyclone did not contain any mullite, but again soot was present. This soot was probably from two sources:

(a) Some soot already present in the gas feed by-passing the fluidised bed in bubbles, or by channelling through preferential gas paths. It is not thought that channelling occurred as the pressure drop between the gas tuyere ducts and the bed surface was similar for all tuyeres and exhibited the small fluctuations observed for ΔP_b measurements in bench scale experiments with bubbling beds.

(b) As it was not possible to raise the bed temperature sufficiently high to avoid quenching the gas feed, and is probable that some soot collected in the cyclone catchpots was produced in the reaction;

$$2CO \longrightarrow CO_2 + C$$

The start up and shut down routine for the operation of the plant is given in Appendix 6A, and technical recommendations made in a report drawn up at the conclusion of these trials (61) are listed in Appendix 6B.

The work was terminated at the stage when modifications to the

plant were well in hand. It is realised that no quantitative data were obtained in the commissioning trials, but sufficient experience was obtained so that the plant could be handed over for further operating trials leading to the next stage of this research.

CHAPTER SIX

SUMMARY

(i) The mechanisms of gas-air contacting in a fluidised bed have been assessed; it was concluded that when the complete combustion of unmixed reactants in a shallow bed is required, the air and gas inlets should be evenly distributed over the base of the bed, and mixing close to the distributor plate should be encouraged.

(ii) A novel distributor plate for a fluidised bed combustor in which hot gasified oil and air are mixed and burnt, has been designed to meet the above requirement. The plate consists of an array of nine tuyeres for the gasified oil, and twelve air tuyeres; each tuyere has four horizontally blowing orifices. The tuyeres are arranged so that each gas orifice is faced by an air orifice.

(iii) A simple model has been developed to study the effect of orifice separation and changes in gas and air flowrate and gas composition, on the combustion efficiency of two coalescing and reacting gas and air bubbles. This model demonstrates that orifice spacing, and a characteristic time existing between the commencement of bubbling at the orifices, the delay time, strongly affect combustion efficiency.

(iv) The coalescence model has been applied to the distributor designed in this work, for the case of a particulate phase equivalence ratio of one, and interstage heat removal by cooling tube only. It has been shown that soot in the bubbles formed at the distributor is not likely to burn when the number of air orifices is greater than the number of gas orifices. Large bubbles can be expected, and these could

lead to unsatisfactory fluidisation in theshallow fluidised bed necessitated by the low gas delivery pressure. A mean gas combustion efficiency has been defined for a partially operative distributor plate, and has been found in terms of the proportion of air orifices operating. Values of mean combustion efficiency less than 100% show that orifice non operation can considerably reduce combustion efficiency.

(v) A fluidised bed combustor has been designed and built, and has been incorporated into a pilot plant for the investigation of the fluidised bed combustion of fuel oil gasified in a high intensity combustor. The plant has been commissioned, and has been handed over for further experimental trials.

CHAPTER SEVEN

SUGGESTIONS FOR FURTHER RESEARCH

It is suggested that a small scale combustor should be designed, to be fed by gas taken from the gas plenum chamber through the inspection part there (see Fig. 4.1). This combustor could be used to assist in experiments aimed at investigating the effect of changes in design parameters on the performance of the second stage. It is recommendedthat particular attention be given to the diameter of the gas orifices, and also particle diameter.

The diameters of the orifices in the gas tuyeres have been made very large to attempt to avoid fouling of these orifices by carbonaceous matter contained in the gas feed. A significant reduction in orifice diameter would allow the number of orifices per unit area of the distributor to be increased, and this in turn could be beneficial to the quality of fluidisation in the combustor.

Under some conditions, the gas entering the bed will tend to form jets, and by analogy with the case of a spout forming in a bed of large particles, it is likely that the jet region will be very important in the capture of the solid carbon in the gas feed (26). The characteristics of a jet forming in a fluidised bed are largely determined by the fluid velocity and density at the orifice and particle diameter and density. Hence, in the collection of suspended matter in a given gas/solid system, particle diameter and the number and size of the orifices will be important.

CHAPTER EIGHT

APPENDICES

APPENDIX I

SPECIFICATION OF MINISTRY OF DEFENCE (NAVY) REFERENCE FUEL OIL VANILLA (62)

Fuel composition:

Constituent	% wt.
Carbon	86.1
Hydrogen	11.0
Sulphur	2.4
Ash	0.083
Water	0.21
Unaccounted	0.207

Ash composition:

Determined in an oxygen atmosphere.

TABLE A.1.1. RESIDUAL FUEL OIL ASH COMPOSITION

Oxide	% in Ash
V_2O_5	78.4
Na_2O	7.0
Ni O	7.2
SO_3	7.2
Fe_2O_3	1.7
Al_2O_3	1.25
Mg O	1.20
Si O_2	0.9
Ca O	0.85
Zn O	0.2

The analysis exceeds 100% as V_2O_5 dissociated to V_2O_4 has been reported as V_2O_5.

Physical Properties:

Specific gravity: at 60 F (15.6 C)		0.9635
Gross Calorific value:		42.9 MJ/kg

Viscosity:

70 F (21 C)	0.432	N s/m^2
100 F (38 C)	0.145	N s/m^2
210 F (99 C)	0.012	N s/m^2

APPENDIX 2

STEPWISE METHOD FOR INTEGRATING ALONG THE LENGTH OF A COOLING TUBE.

See references (3), (5).

A list of the symbols used in this appendix is given at the end of the appendix.

The total heat transfer rate from the gas in the tube is the sum of the radiant and convective heat transfer rates.

$$M c_p dT = R_c dl + R_r dl \qquad \text{E.A.2.1.}$$

where;

$$R_c = \pi D_t h_t (T - T_w) \qquad \text{E.A.2.2.}$$

$$R_r = \pi D_t \sigma (T^4 - T_w^4) \qquad \text{E.A.2.3.}$$

$$h_t = 0.02 \frac{k_t}{D_t} Re^{0.8} \qquad \text{E.A. 2.4.}$$

The tube is divided into a number of sections. The inlet Temperature, T_{ni}, is selected and then the outlet temperature, T_{no}, from the first section is found. This becomes the inlet temperature to the next section. The process is repeated until the end of the tube is reached.

T_{no} is estimated as follows:

(i) An initial estimate is made, T_{no1}.

(ii) The mean radiant and convective temperatures T_{nr}, T_{nc} are found thus:

$$T_{nr} = (T_{ni}\ T_{no1})^{\frac{1}{2}} \qquad \text{E.A.2.5.}$$

$$T_{nc} = \frac{2\ T_{ni}\ T_{no1}}{(T_{ni} + T_{no1})} \qquad \text{E.A.2.6.}$$

(iii) The convective and radiant heat transfer rates are calculated.

$$R_{nc} = \pi D_t\ h_t\ (T_{nc} - T_w) \qquad \text{E.A.2.7.}$$

$$R_{nr} = \pi D_t\ h_t\ \sigma\ (T_{nr}^4 - T_w^4) \qquad \text{E.A.2.8.}$$

h_t is found from the correlation (3);

$$h_t = h_d\ (T_{nc}/T_d)^{0.301} \qquad \text{E.A.2.9.}$$

where;

$$h_d = 0.02\ \frac{k_d}{D_t}\ \left(\frac{\rho_d\ U_d\ D_t}{\mu_d}\right)^{0.8} \qquad \text{E.A.2.10.}$$

and T_d is some arbitrary temperature at which the physical properties are known.

(iv) A heat balance gives an outlet temperature, T_{no2}.

$$T_{no2} = T_{ni} - dl \frac{(R_{nr} + R_{nc})}{M C_p} \qquad \text{E.A.2.11.}$$

(v) A new value for T_{no1} is estimated using the expression:

$$T'_{no1} = \frac{T_{ni}\, T_{nc1}}{T_{ni} + T_{no1} - T_{no2}} \qquad \text{E.A.2.12.}$$

(vi) T'_{no1} is used to recalculate T_{nc}, T_{nr} and steps (iii) - (v) are repeated until the desired convergence of T_{no1} and T'_{no1} is achieved, when:

$$T'_{no1} = T_{no1} = T_{no} \qquad \text{E.A.2.13.}$$

The diameter of the tube was 76 mm and in this work, the integration was performed in 30 steps.

Notation used in Appendix 2.

Symbol	Significance	Dimensions (see p 13)
c_p	mean heat capacity of combustion gases.	$EM^{-1}\theta^{-1}$
D_t	diameter of tube	L
e	Emissivity	
h_d	Convective heat transfer coefficient at temperature T_d.	$PL^{-2}\theta^{-1}$

Symbol	Significance	Dimensions
h_t	Convective heat transfer coefficient at temperature T.	$PL^{-2}\theta^{-1}$
k_d	Thermal conductivity of gases at temperature T_d.	$PL^{-1}\theta^{-1}$
l	Length along tube.	L
M	Total mass flow rate of combustion gases.	MT^{-1}
R_c	Convective heat transfer rate per unit length of cooling tube.	PL^{-1}
R_{nc}	Convective heat transfer rate in increment of length.	P
R_{nr}	Radiant heat transfer rate in increment of length.	P
R_r	Radiant heat transfer rate per unit length of cooling tube.	PL^{-1}
Re	Reynolds number.	
T	gas temperature.	θ
T_d	Arbitrary temperature at which physical properties of combustion gases are known.	θ
T_{nc}	Convective mean temperature in increment of length.	θ
T_{ni}	Inlet temperature to increment of length.	θ
T_{no}	Outlet temperature from increment of length.	θ

Symbol	Significance	Dimensions
T_{no1}	Initial estimate of T_{no}.	θ
T'_{no1}	Improved value of T_{no1}.	θ
T_{no2}	Second estimate of T_{no}.	θ
T_{nr}	Radiant mean temperature in increment of length.	θ
T_w	Temperature of cooling tube surface.	θ
μ_d	Viscosity of combustion gases at temperature T_d.	FTL^{-2}
σ	Stephan-Boltzmann constant.	$PL^{-2}\theta^{-4}$

APPENDIX 3

ESTIMATION OF EXCHANGE COEFFICIENT BETWEEN BUBBLE AND PARTICULATE PHASE.

The following method was proposed by Kunii and Levenspeil (29), and has been described by Potter (44).

The overall volumetric exchange rate per unit volume of bubble between the bubble and particulate phase (k_{bp}) is estimated by considering transfer from the bubble to the cloud using equations due to Davidson and Harrison (43) (coefficient k_{bc}) and then transfer across the cloud boundary (coefficient k_{cp}).

$$\frac{1}{k_{bp}} \simeq \frac{1}{k_{bc}} + \frac{1}{k_{cp}} \qquad \text{E.A.4.1.}$$

$$k_{bc} = \frac{4.5\, U_{mf}}{D_b} + \frac{5.85\, D_{ig}^{\frac{1}{2}}\, g^{\frac{1}{4}}}{D_b^{\frac{5}{4}}} \qquad \text{E.A.4.2.}$$

$$k_{cp} = 6.78 \left(\frac{D_{ig}\, \epsilon_{mf}\, U_a}{D_b^3} \right)^{\frac{1}{2}} \qquad \text{E.A.4.3.}$$

For single bubbles rising in an incipiently fluidised bed, $U_a = U_b$, and U_b is given by E.3.10.

D_{ig}, the diffusion coefficient was estimated for carbon monoxide and hydrogen diffusing through nitrogen at 1000 C by the method of

Hirschfelder (63). For carbon monoxide D_{ig} was found to be 237 mm^2/s and for hydrogen 857 mm^2/s. The values of U_{mf} = 0.07 m/s, D_b = 75 mm and ϵ_{mf} = 0.55 were used in E.A.4.2 and E.A.4.3.

For the carbon monoxide bubble k_{bp} was 2.17/s and for the hydrogen bubble it was 3.8/s.

APPENDIX 4

FLOW CHART FOR BUBBLE COALESCENCE MODEL

A flow chart of the program used to simulate bubble growth and coalescence with chemical reaction is shown in Fig. A.3.1.

Bubble position was found by the numerical integration of equation 9 in Appendix 8. When the perimeters of two bubbles touched, it was assumed that they coalesced to form a single bubble which had the same centre of gravity and momentum as the two bubble system that formed it. This bubble then continued to grow, fed by the orifices that had previously fed its component bubbles.

Input data required by the program falls into three categories:

(i) Characteristics of the distributor plate:

  (a) The location of the orifices on the distributor in cartesian coordinates, and the number of each type of orifice.

  (b) Characterisation of orifice type (gas or air) by an integer array.

  (c) Characterisation of angular orientation of horizontally blowing orifices relative to reference axes.

(ii) Characteristics of reactants:

  (a) Gas mass flow. Initial gas composition expressed as an equivalence ratio, interstage heat removal, (thus gas density by the use of an equilibrium program).

(b) Air mass flow, density.

(iii) The time step.

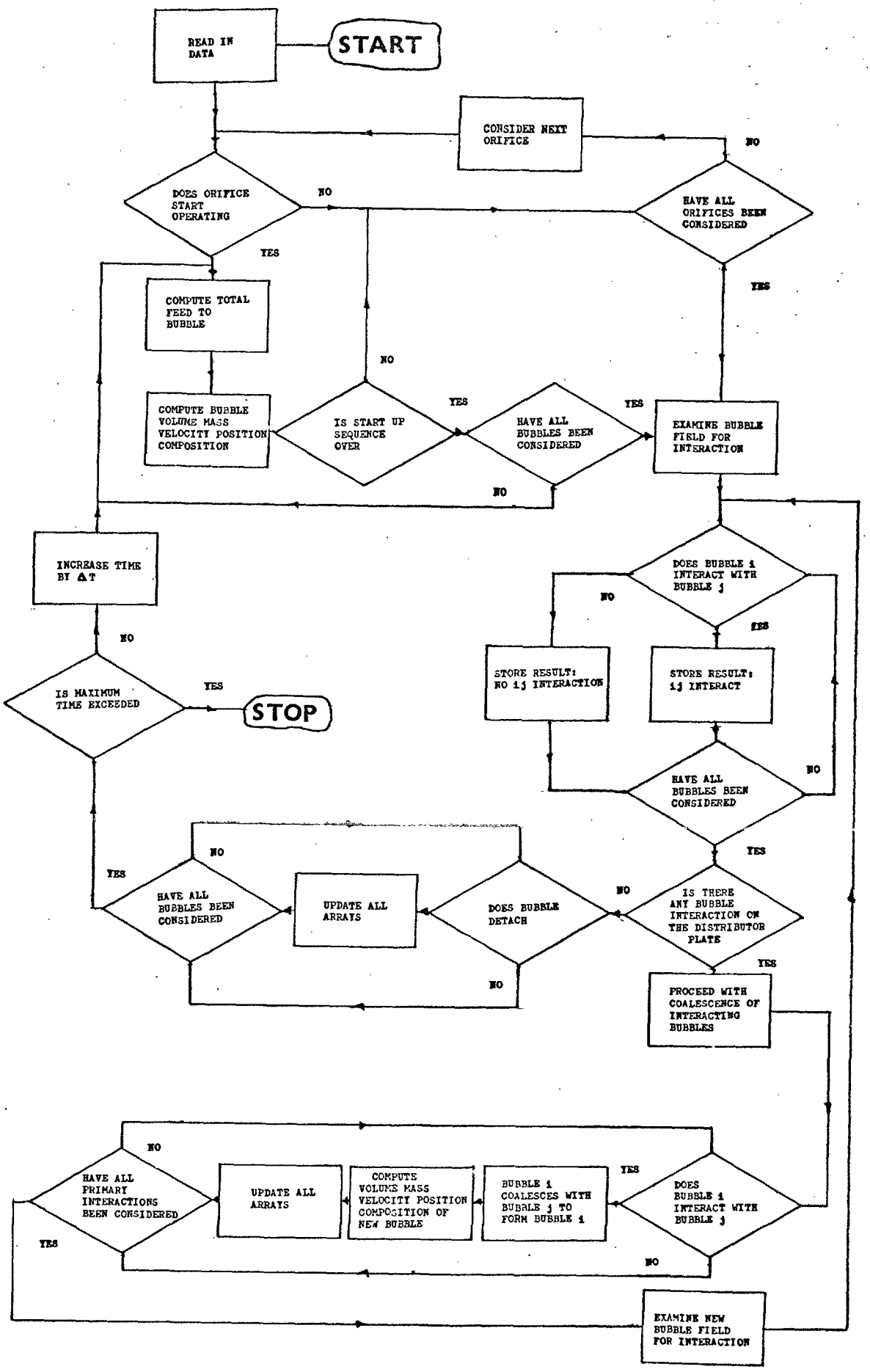

FIG. A.3.1: FLOWSHEET OF PROGRAM FOR BUBBLE COALESCENCE MODEL.

APPENDIX 5

PROPERTIES OF FUSED MULLITE

(i) Particle Sepcifications (64)

Chemical analysis.

Al_2O_3	76.4%
SiO_2	22.8%
Fe_2O_3	0.07%
TiO_2	0.01%
CaO	0.10%
MgO	0.03%
Na_2O	0.4%
K_2O	0.01%
Free iron	0.03%

Physical Properties.

Apparent porosity	0.5%
Refractoriness	Seeger cone 40, 1900C.
Specific gravity	3.14

(ii) Fluidising Properties

$$U_{mf} = 0.00001506\ d_p^{1.57}\ ,\ 240\,\mu m < d_p < 500\,\mu m$$

d_p , μm ; U_{mf} , m/s .

ϵ_{mf} = 0.54 - 0.57

Angle of repose 35^{o}

The cumulative size distribution of the material used in the first trials is shown graphically in Fig. A.5.1.

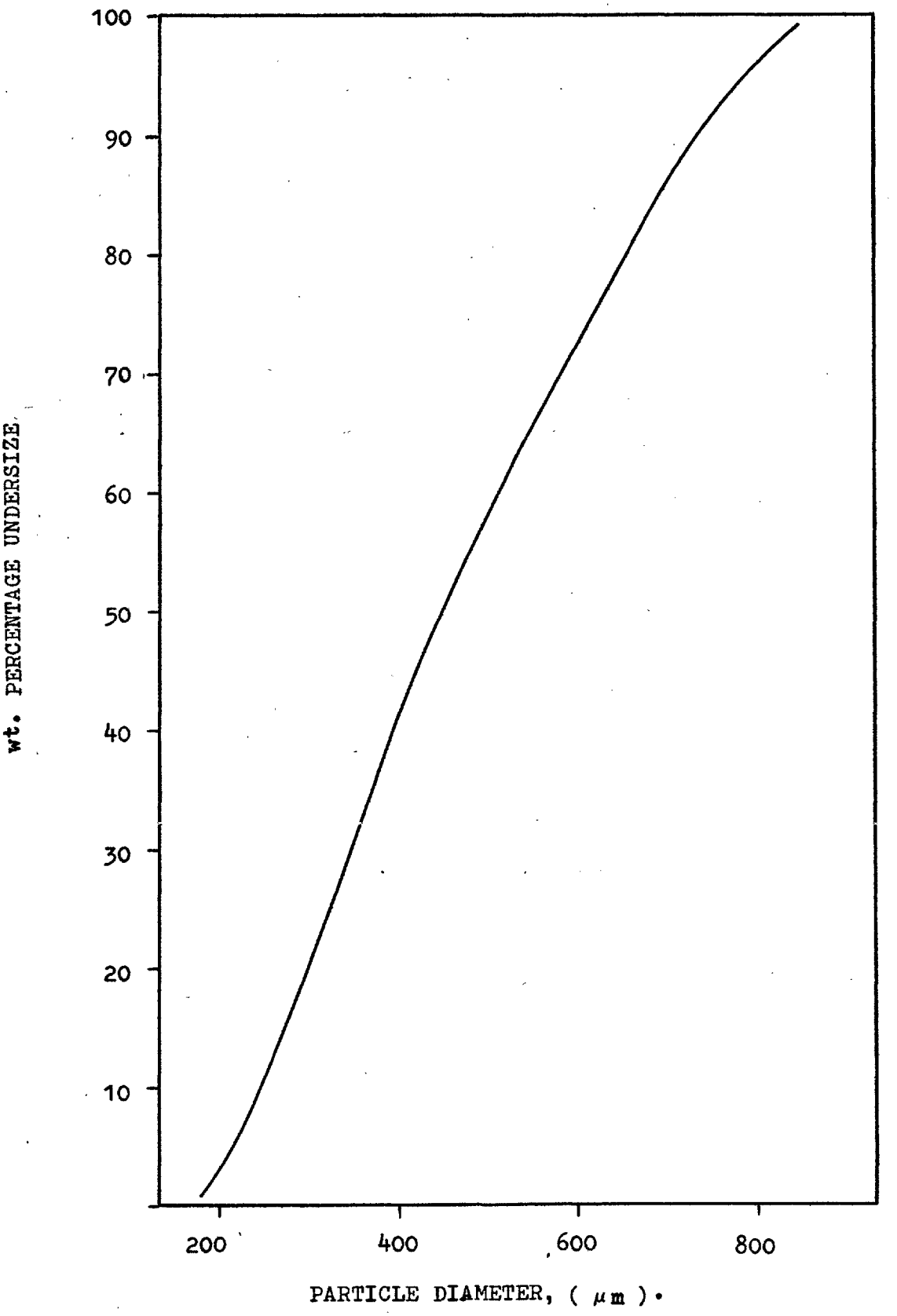

FIG. A.5.1: CUMULATIVE SIZE DISTRIBUTION OF FUSED MULLITE USED IN EXPERIMENTAL TRIALS.

APPENDIX 6: OPERATING PROCEEDURE AND TECHNICAL RECOMMENDATIONS

A. Operating proceedure.

(1) All valves closed.

(2) Check fuel supplies, drains, bursting discs.

(3) Make sure oil line to atomiser does not contain any air.

(4) Insert sampling probes if required.

(5) Insert igniter.

(6) Switch on A.C. and D.C. mains.

(7) Switch on mains water booster pump, (not shown in Fig. 5.2.)

(8) Set metering pump at 3 g/s.

(9) Open V44.

(10) Switch on primary air, E9.

Open V20, V25 and vent any liquid in the line thrɑgh V26.

Set P4 to desired atomising pressure using pressure reducing valve V25.

(11) Open valve isolating water reservoir, V37.

(12) Open V31, V32, V33.

Start cooling water booster pumps E5, E6, E7.

Set R_1 = 9.4 l/m

Set R_2 = 5 l/m

Set R_3 = 23 l/m

(13) Switch on secondary air, E8, and fully open V17, V18, V19.

(14) Open V38, V40, V41, V43, and

Switch on auxiliary air, E11.

Set air flow on R10, R11, to 3500 l/m.

(15) Open V54, V58, and switch on tertiary air, E10.

Set R8, R9 each at 440 l/m.

(16) Open V46, V47, V49, V50, V54, V55

Open V60, V62, V63, V64.

Set R4 = 10 gall/hr

Set R5 = 15 gall/hr

Set R6 = 45 gall/hr

Switch on cyclone outlet pump E13.

Maintain constant level in liquid collecting tank by adjusting V54.

(17) Open V9, V10, V11.

Switch on gas oil booster pump E3.

(18) Gasifier Ignition:

Switch on fuel metering pump E4.

When P2 reads 8 p.s.i.g. ignite pyrotechnic furnace igniter.

If igniter is successful open V16 immediately, and as soon as a flame is established reduce the oil flow to 2 g/s and set the total secondary air flow at 24 g/s with equal amounts going to the forward and reverse casings.

If the flame fails close V16 switch off E4 and fully open the secondary air lines. Allow any oil vapour in the system to be purged, and then insert a new igniter and repeat the gasifier ignition, step 18 in operating proceedure.

(19) Combustor Heatup:

When a flame is established, allow the gasifier to heat up for

½ hour then reduce the auxiliary air and at the same time raise the oil flow to ~3.5 g/s. Establish ignition of the gases entering the bed in the gas plenum chamber, and control their rate of temperature rise to 250C/hr by regulating the auxiliary air flow and observing the temperature response of T23, T22.

(20) Change over to fuel oil:

Open V1, V4 set P1 = 6 p.s.i.g..

Switch on residual oil booster pump E1.

Switch on oil heater and set to 100C.

When T1 is steady at 100C, close V9 and open V3.

Maintain P1 at 6 p.s.i.g.

(21) Proceedure for changing from air to steam atomisation:

Check steam pressure at supply is equal to 26 p.s.i.g.

Open V23, V22 and remove water condensed in line. Then crack V22 and switch on heating tapes (not shown in Fig. 5.2), and set steam temperature (T2), to give desired degree of superheat. Close V20 and at the same time open V26, V21. Maintain desired steam pressure using V23.

(22) Shut down:

If burning fuel oil close V3 and open V9 and allow oil line to atomiser to be purged with gas oil then switch off oil heater and allow the temperature of the gas oil to fall to ~30C.

If atomising with steam close V21, V26 opening V22, V20 and establish air atomised flame.

Switch off steam heating tapes.

Close V16 and switch off fuel metering pump.

Raise auxiliary air flow to 3500 l/m.

Switch off oil booster pumps.

Allow plant to cool for 1½ hrs.

Then switch off primary, secondary and tertiary air.

Switch off auxiliary air.

Switch off cooling water pumps and cyclone outlet pump.

Isolate all electrical supplies.

When plant is COLD close all valves.

B. Summary of technical recommendations.

(1) The Spray System. (see Fig. 5.2).

This should be redesigned with attention given to

(a) the prevention of accumulation of water at the places where the component sections of the tube are joined.

(b) the prevention of flowback of water into the solid separating cyclone.

If the existing system is to be used while a new one is being made all nozzles should be individually inspected and cleaned. All damaged nozzles should be replaced.

The angle the tube makes with the horizontal should be increased to discourage backflow of water into the solid separating cyclone.

(2) Prebed gas ignition.

A small venturimeter should be installed in parallel with R10, R11, to meter the low air flows required during the period of prebed gas ignition used to heat up the particles and refractory lining in the combustor.

(3) Oil line to Gasifier.

A small drain valve should be placed before V16 to allow the easy clearance of air in the oil supply line.

(4) Miscellaneous.

Extensive maintenance is advised for the first stage. The refractory lining of the gasifier should be inspected and if necessary replaced.

The steam supply system needs overhauling.

Steps should be taken to reduce the level of noise made by the air blowers, in particular the tertiary air blower, E10.

APPENDIX 7

TABULATED COMPUTER RESULTS

TABLE A.7.1. BUBBLE EQUIVALENCE RATIO.

ϕ_b	ϕ_1	
	E.3.38	Model
1.1	1.023	1.003
1.25	1.053	1.017
1.40	1.077	1.023
1.55	1.097	1.024

Conditions:

F_1 3.5 g/s

p_a 1

Interstage heat removal taken from Fig. 3.1.

TABLE A.7.2. COMBUSTION EFFICIENCY

F_1 (g/s)	ϕ_1 (-)	Combustion efficiency, $\bar{E}_p$, at different values of p_a: 0.6	0.7	0.8	0.9	1.0
2.5	1.1	82.1	93.3	100	100	100
	1.25	79.2	89.7	94.8	95.5	96.6
	1.40	77.3	88.6	93.0	94.2	95.1
	1.55	79.3	89.3	94.0	95.3	95.9
3.0	1.1	81	93	100	100	100
	1.25	76.8	88.0	92.0	92.0	93.6
	1.40	75.7	87.7	92.8	91.5	92.9
	1.55	75.8	87.6	93.5	91.8	94.0
3.5	1.1	79	89.9	96.0	94.6	96.2
	1.25	76	85.5	90.5	89.5	90.8
	1.40	75.5	85.9	90.3	88.8	90.8
	1.55	77.4	87.3	92.6	90.5	92.3

Interstage heat removal taken from Fig. 3.1.

TABLE A.7.3. HEAT RELEASE RATE

F_1 (g/s)	ϕ_1 (-)	Heat release rate $\bar{P}$ (kW) at different values of p_a. 0.6	0.7	0.8	0.9	1.0
2.5	1.1	1.6	1.8	1.9	1.9	1.9
	1.25	3.7	4.2	4.4	4.4	4.5
	1.40	5.2	5.95	6.3	6.3	6.4
	1.55	6.6	7.4	7.9	7.92	7.97
3.0	1.1	2.0	2.3	2.46	2.46	2.47
	1.25	4.43	5.1	5.3	5.3	5.4
	1.40	6.23	7.22	7.6	7.53	7.65
	1.55	7.7	8.9	9.4	9.34	9.55
3.5	1.1	2.4	2.73	2.92	2.87	2.93
	1.25	5.23	5.89	6.23	6.17	6.26
	1.40	7.4	8.4	8.84	8.69	8.89
	1.55	9.32	10.5	11.1	10.9	11.13

Interstage heat removal taken from Fig. 3.1.

TABLE A.7.4. DIAMETERS OF SINGLE GAS BUBBLES

All diameters found using E.2.3.

(i) Interstage heat removal by cooling tube only taken from Fig. 3.1.

ϕ_1 (-)	Bubble diameters in mm for different gasifier oil flowrates (g/s). 2.5	3.0	3.5
1.1	72	78	84
1.25	69	75	80
1.40	68	73.5	79
1.55	67	73	78

(ii) Interstage heat removal by cooling tube and water jacket round gas plenum chamber, (E.3.6). F_1 = 3.5 g/s.

ϕ_1 (-)	1.1	1.25	1.40	1.55
D_b (mm)	82	75	72	69.4

TABLE A.7.5. DIAMETERS OF PRODUCT BUBBLES.

F_1 (g/s)	ϕ_1 (-)	Diameters of product bubbles in mm for different values of p_a. 0.6	0.7	0.8	0.9	1.0
2.5	1.1	78	77.6	77.6	77	77
	1.25	83.4	83.2	82.6	82	82
	1.40	88.2	87.8	86.8	86	85.2
	1.55	93	92.2	91	89.8	88.6
3.0	1.1	85.2	85.2	84.8	84.6	84.2
	1.25	91	90.4	89.8	89	88
	1.40	96	95.4	94.6	93	92
	1.55	100	99.6	98.6	97	96
3.5	1.1	91.4	91.4	91	91	90
	1.25	98	97	96	95	95
	1.40	103	102	101	100	99
	1.55	108	107	105	104	103

Interstage heat removal taken from Fig. 3.1.

APPENDIX 8

A NOTE ON A HYDRODYNAMIC MODEL FOR GAS COMBUSTION ON THE DISTRIBUTOR PLATE OF A FLUIDISED BED

INSTITUTE OF FUEL SYMPOSIUM SERIES NO. 1: FLUIDISED COMBUSTION

A NOTE ON A HYDRODYNAMIC MODEL FOR GAS COMBUSTION ON THE DISTRIBUTOR PLATE OF A FLUIDISED BED.

C.E. Davies, Paul Eisenklam*

A simple model of a shallow fluidised bed with an orifice type distributor, previously treated by Harrison et al (1), is extended to deal with the introduction of two reacting gases individually through twin orifices. In particular, a fuel gas and air and their resulting combustion is considered. It is shown how the bubbling mode and the spacing of the orifices affect the combustion efficiency.

INTRODUCTION

When bubbling fluidised beds of small particles are operating with relatively large bubbles generated at an orifice type distributor, the volumetric flow of gas in excess of that percolating through the particulate phase can be considered to be the predominant phase, and the rate of conversion of a gas-phase reaction can be obtained from the contact time of the reacting species in this phase only. If the velocity of the rising bubbles is much larger than the incipient pore velocity, the gas circulates within the bubbles, and conversions can be calculated by considering only the gas enclosed by a bubble.

The model developed here, deals with such bubble voids generated at a twin-orifice type distributor on which two species of reacting gases (combustible fuel gas and air), are introduced through two individual orifices respectively. The single phase bubbles grow in size, and when their interfaces touch, they coalesce into a void containing a mixture which reacts if the temperature is suitably high. The void continues to be fed through the individual orifices and the reaction proceeds until it detaches and rises vertically. The bed considered is shallow and no further coalescence takes place before the bubble bursts at the surface and sheds its gaseous contents of reaction products into the free-board.

The combustion efficiency of this twin-orifice shallow fluidised bed is obtained from the composition of all bubbles, single ones in which no combustion takes place or coalesced bubbles in which continuous combustion occurs.

The postulated hydrodynamics of the model and of the reaction are described below and some computer results are given illustrating the use to which the model can be put. Extensions of this simple model to two practical cases are now being investigated, viz. multi-orifice distributor plates with vertical, and horizontally blowing nozzles, and deep beds with coalescence of voids after detachment. The simple models will be improved by the introduction of a random delay time between the start of operation of pairs of nozzles, the use of an ignition delay time and allowance for loss of mass on coalescence. No doubt, further sophistications will be attempted.

THE HYDRODYNAMICS OF BUBBLE GROWTH AND COALESCENCE

Davidson and Schüler (2) have derived equations describing the growth of a bubble on an orifice in an inviscid liquid by equating the bouyancy force of the growing bubble to the rate of change of momentum of the fluid surrounding it.

The equation of motion is:-

$$Vg = \frac{d}{dt}\left(k\, V \frac{ds}{dt}\right) \qquad (1)$$

*Department of Chemical Engineering and Chemical Technology, IMPERIAL COLLEGE, London, SW7 2BY.

The bubble is considered to be spherical at all times during its growth, and detaches from the orifice when the distance, s, of the bubble centre from the orifice is equal to the bubble radius. This is shown diagrammatically in Fig 1.

If the bubble is fed at a constant volumetric flowrate G, the volume of the bubble at any time is Gt, and equation (1) may be integrated with the boundary conditions $t = 0$, $\frac{ds}{dt} = 0$, $s = 0$, $V = 0$ to give:-

$$V = \left(\frac{48k^3}{\pi}\right)^{\frac{1}{5}} \frac{G^{\frac{6}{5}}}{g^{\frac{3}{5}}} \qquad (2)$$

Harrison and Leung (3) noted that the equations derived for single bubbles in an inviscid liquid were applicable to data obtained for bubbles growing on an orifice in a fluidised bed, and Watson and Harrison (1) extended the equations describing single bubbles to cover bubble interaction on a multi-orifice plate. They considered several situations that may arise when adjacent orifices are separated by a distance λ, the gas flowrate to each orifice is constant at G, and a time delay, t_d, exists between the start of operation of one orifice and that of the other.

In the present work, the equations of bubble growth and motion are not treated analytically, but are integrated numerically.

The Equations of Motion

At time $t = 0$, a bubble having volume V_o and upward velocity U_o is fed at the volumetric flowrate G. At time t, the volume of the bubble is:-

$$V = V_o + Gt \qquad (3)$$

Equating bouyancy force and momentum change of the displaced fluid and using $k = \frac{1}{2}$ from the theory of displacement of a steadily moving sphere in an inviscid fluid, one obtains for a bubble in a fluidised bed:-

$$\rho_p(1 - \varepsilon_{mf})(V_o + Gt)g = \frac{d}{dt}\left[\tfrac{1}{2}\rho_p(1 - \varepsilon_{mf})(V_o + Gt)\frac{ds}{dt}\right] \qquad (4)$$

On integration this becomes:-

$$2gV_ot + gGt^2 + \text{Const.} = (V_o + Gt)\frac{ds}{dt} \qquad (5)$$

Using the boundary condition

$t = 0$, $\frac{ds}{dt} = U_o$, equation (5) becomes:-

$$2gV_ot + gGt^2 + V_oU_o = (V_o + Gt)\frac{ds}{dt} \qquad (6)$$

For small time and distance intervals Δt, Δs, respectively, Equation (6) may be rewritten as follows:-

$$\Delta s = \frac{(2V_ogt + gGt^2 + V_oU_o)\Delta t}{V_o + Gt} \qquad (7)$$

A choice of suitable time interval Δt enables the bubble parameters to be monitored during growth. If the values of V_o and U_o refer to the beginning of any arbitrary interval Δt during growth, equation (7) becomes:-

$$\Delta s = \frac{(2gV_o\Delta t + gG(\Delta t)^2 + V_oU_o)\Delta t}{V_o + G\Delta t} \qquad (8)$$

In equation (8), G is the relevant value of the volumetric flow during the interval Δt.

The model for bubble coalescence before detachment. In order to simulate the behaviour of an assembly of bubbles coalescing on a distributor plate, most of the assumptions of Watson and Harrison (1) are adopted. It is assumed that the bubbles are spherical and that when their perimeters touch, the bubbles coalesce with conservation of mass and momentum. The bubble formed by the coalescence continues to grow and is fed by the orifices that feed the constituent bubbles. The position of the centre of gravity of the bubble formed by a coalescence is assumed to be the same as that of the constituent pair. The coalesced bubble detaches when it has grown to a radius equal to the distance of its centre from the line connecting the orifices. Both orifices feed the detached bubble until detachment occurs. The orifices are either continuously operating so that as soon as an original or coalesced bubble detaches, a new one is formed at each orifice that feeds it, or a delay time t_d is introduced. Only a pair of orifices of variable spacing, and different flow rates, G are considered here.

GAS COMBUSTION IN COALESCED BUBBLES ON A DISTRIBUTOR PLATE

When two bubbles containing the same chemical species coalesce isothermally, the density of the resulting bubble is the same as that of the original bubbles. However, when a bubble of air and a bubble of fuel gas coalesce and combustion follows, the density of the products of the reaction is different from that of the reactants because of temperature and mole changes.

If a fuel is mixed with air and combusted at a given pressure and at a specified heat removal, the equilibrium temperature and composition and consequently density of the products of the reaction are uniquely determined by an equivalence ratio, the temperature of the reactants, and the kinetics of the reaction. Thus if the temperature of given reactants and equivalence ratio are known, the density of the products can be found with or without heat removal.

When a single bubble is fed by more than one orifice of the same type, the total feed to the bubble is the sum of the individual orifice flow rates, or

$$G = \Sigma G_i \tag{9}$$

Equation (9) does not apply to a bubble in which combustion is taking place. However, an equivalent G may be found from the volume change experienced by the bubble over the time interval Δt. It is derived from a knowledge of bubble mass and density at the beginning and end of the interval Δt,

$$\text{viz.} \quad G = \frac{\Delta V}{\Delta t} = \frac{\frac{M_{\Delta t}}{\rho_{\Delta t}} - \frac{M}{\rho}}{\Delta t} \tag{10}$$

The fuel:air operating conditions considered are as follows: One orifice, called the gas orifice is considered to be fed with a lean fuel gas of given composition and equivalence ratio ϕ_g, at a given temperature T_g and mass flowrate R_g. The other orifice, called the air orifice, is fed by air at a given temperature T_a and mass flowrate R_a. The air flowrate is always such that overall stoichiometric combustion takes place. This does not mean that the equivalence ratio in a coalesced bubble ϕ_b will necessarily be unity. The reaction model used has been incorporated into a computer program and is fully described in Reference (4) and also outlined in Appendix I.

The density of the products formed from mixtures of any strength, and under adiabatic conditions are found from the model. The method of calculating the equivalence ratio of a bubble at the end of an interval Δt is given in Appendix II.

When two bubbles of different compositions coalesce, the density and hence the volume of the resulting bubble is found by the procedure described in Appendix III.

By using equations (8) and (10) and where necessary carrying out the material balances given in Appendices II and III, in conjunction with the use or neglect of the combustion model described in Appendix I, the position, volume and composition of combusting or non-combusting bubbles may be found.

THE COMBUSTION EFFICIENCY OF A SHALLOW FLUIDISED BED

The model described above requires stored values of bubble mass and equivalence ratio to generate G (equation (10)), which are used in equation (8) to obtain Δs. Further when

$$\Sigma(\Delta s) = \tfrac{1}{2}\sqrt[3]{\frac{6V}{\pi}} \tag{11}$$

the bubble detaches and its mass and ϕ are known.

The fuel gas entering the bed is of known equivalence ratio, and the gas rates are taken to be such that overall stoichiometric feed prevails. Because the products of a reaction are independent of path under given thermal conditions, the total amount of heat released by a bubble during its residence on an orifice is found from its mass and equivalence ratio at detachment, and the calorific value of the feed gas.

Let a gas bubble of equivalence ratio ϕ_g coalesce with an air bubble to form products of combustion at an adiabatic flame temperature T_b, and a heat release of ΔH per mass of fuel in the bubble, F. The maximum possible heat release would be the overall one at $\phi = 1$ i.e. $\Delta H_{overall}$. For a bubbling bed, the combustion efficiency E is therefore defined as:-

$$E = \frac{\Sigma(\Delta H_i\, F_i)100}{\Delta H_{overall}\Sigma F_i}\ \% \tag{12}$$

RESULTS

The specific examples deal with one feed rate of a fuel rich gas $G_g = 1{\cdot}4\ 10^{-3} m^3/s$ per orifice entering at the adiabatic temperature corresponding to its composition. For instance, the feed gas of equivalence ratio $\phi_g = 1{\cdot}35$ (a fuel rich gas, see definition of ϕ in the notations) has a feed temperature of 1994°K and a composition of 9·2% CO, 7·7% CO_2, 3·3% H_2, 11·6% H_2O and the remainder N_2, (see eqn. A1). The air feed rate is always stoichiometric which for a gas of $\phi_g = 1{\cdot}35$, comes to $G_a = 0{\cdot}4\ 10^{-3} m^3/s$ per orifice. Its temperature is always 298°K. The resulting combustion is taken to be adiabatic. The orifices either commence operating together or with a delay time of t_d which for the examples considered is the time delay between the commencement of operation of the air orifice after the gas orifice.

Computed results of combustion efficiency for various bubbling models and gas compositions were obtained as follows:

A. If there is a constant finite delay time between the operation of the twin orifices, the composition of a coalesced bubble is not given by the composition of the combined feed to both orifices. The resulting ϕ_b of the coalesced bubble is either greater or smaller than unity depending on the order of delay between the orifices and the magnitude of t_d. Both effects result in the lowering of the combustion efficiency as here defined. This efficiency remains essentially constant until the orifices are spaced so far apart that no coalescence and therefore no mixing and no combustion takes place.

This is also illustrated if $t_d = 0$ i.e. the start of the operation of an orifice occurs as soon as a bubble detaches. If the spacing, λ, is narrow, coalescence occurs and the efficiency will be 100% each bubble containing a gas of equivalence ratio $\phi_b = 1$. As soon as λ is large enough, no coalescence occurs and two individual bubbles of gas and air go through the bed with a resulting combustion efficiency of zero.

Fig 2 (Table i) shows the maximum orifice spacing beyond which the combustion efficiency drops to zero for various constant delay times. It is seen that a considerable variation of spacing over a narrow range occurs with change in gas composition, and that the effect of t_d is not very great. Thus, to achieve combustion, the spacing must be less than 28-38 mm.

B. If the spacing is such that combustion takes place, the efficiency will be influenced by the mode of bubbling. It is now considered that a varying delay time is introduced such that the second orifice begins to operate only when a bubble from the first has grown to a size which overlaps it. The results are shown in Fig 3 (Table ii) for three different gases. It is seen that quite low efficiencies are reached and that as soon as the spacing is wide enough no coalescence occurs and the efficiency drops to zero.

C. For a gas of one composition, the efficiency for a constant delay time remains essentially constant at any spacing. The results are shown in Fig 4 (Table iii) by such lines as ab for $t_d = 0$, de for $t_d = 10$ms and gh for $t_d = 20$ms. Each of these efficiencies of course drops to zero when the maximum spacing has been reached (lines bc, ef, hj respectively). It seems reasonable to postulate that if a bubble overlaps the second orifice within a period shorter than t_d it will begin to operate and thus the results shown in Fig 4 are obtained:

For a delay time of zero, the efficiency is 100% until the maximum spacing has been reached - line abc. For a delay time of $t_d = 10$, the efficiency is given by line adef. Correspondingly for $t_d = 20$ the line is aghj. It is of course clear that the curve adg is the respective line from Fig 3 and that the maximum λ's are obtained from Fig 2.

The three groups of examples only illustrate the model. Results for a random delay time or overlapping time, whichever is the shorter, will be presented at another occasion when other sophistications to the model have been carried out.

CONCLUSIONS

Gas combustion in shallow fluidised beds in a manner described here is likely to lead to a considerably reduced combustion efficiency or to complete unmixedness within the bed (with resulting combustion in the free board) unless the spacing of an orifice type distributor is below a critical value. The results of this paper give considerable insight into the effect of such distributors on combustion and into the likely benefits to be obtained from further sophistications to the model.

TABLES OF COMPUTED RESULTS

Gas Equivalence Ratio ϕ_g →	1.07	1.16	1.25	1.35	1.44	1.53	1.63	1.69	1.79
(i) Maximum orifice spacing (λ, cm) versus delay time (t_d) for combustion to take place									
Delay time t_d (ms) = 0		2.9	3.1		3.3	3.5			
5	2.8	3.0	3.2	3.4	3.4	3.6	3.6		
10	2.8	3.2	3.2	3.4		3.6			
15			3.3	3.5	3.5	3.7			
20			3.3	3.5	3.5	3.7	3.7	3.9	
(ii) Combustion efficiency (E,%) versus orifice spacing (λ) for a varying delay time such that the second orifice begins to operate as soon as a growing bubble from the first orifice overlaps it									
Orifice spacing λ = 0.5 cm			98.9	98.9	98.9	98.9	98.9		
1.0			98.9	98.9	98.9	98.9	98.9		
1.5			92.7	94.0	94.0	94.0	94.1		
2.0			86.7	86.8	87.0	88.2	88.4		
2.5			74.6	76.3	77.6	79.1	80.3		
3.0			57.3	60.5	63.5	64.9	66.6		
3.5						43.4	46.8		
(iii) Combustion efficiency (E,%) versus delay time (t_d)									
Delay time t_d (ms) = 0	100.0	100.0	100.0	100.0	100.0	100.0	100.0	100.0	100.0
5	93.7	93.8	93.9	94.0	94.0	94.1	94.1		
10	87.5	87.7	87.8	88.1	88.1	88.2	88.3		
15			81.8	82.1	82.4	82.6	82.8		
20			76.1	76.5	76.8	76.8	77.3	77.3	77.6

APPENDIX I: A MODEL FOR THE COMPLETE COMBUSTION OF A HYDROCARBON FUEL

A pure hydrocarbon vapour of a given C/H ratio is combusted with air to form a gas which is fed to the fluidised bed where further air is added, the whole operation being stoichiometric.

$$\frac{1}{n}(C\ H_y)_n + a(O_2 + 3{\cdot}76N_2) = bCO_2 + cCO + dH_2O + fH_2 + 3{\cdot}76aN_2 \qquad (A1)$$

The water gas shift equilibrium is assumed, and the following relations enable the constants in equation (A1) to be found for a given y.

Carbon balance: $1 = b + c$ (A2)

Hydrogen balance: $y = 2d + 2f$ (A3)

Oxygen balance: $2a = 2b + c + d$ (A4)

Water gas shift equilibrium constant: $K = \frac{b.f}{c.d}$ (A5)

The expression $a = \frac{1 + \frac{y}{4}}{\phi}$ relates a to ϕ, (for definition see notation).

K is obtained as a function of gas temperature T from data given by Gumz (5).

Gas temperature and product composition are found by an iterative heat balance thus:

A gas temperature T' is assumed and the total heat capacity of the combustion products is calculated thus:

$$C'_T = \Sigma x_i C_i \qquad (A6)$$

The sensible heat of the products is given by:

$$H'_s = C'_T(T' - T_a) \qquad (A7)$$

The heat released by combustion is given by:

$$H'_r = \Sigma x_i H_{Fi} - H_{FO} \tag{A8}$$

The combustion temperature T is found by comparing the sensible heat with the heat of reaction as follows:

If $T' = T$

$H'_r = H_r$, $H'_s = H_s$, $H_r = H_s$

$H_r = C_T(T - T_a)$

$$T = T_a + \frac{H_r}{C_T} \tag{A9}$$

This procedure is carried out until there is suitable agreement between T' and T, and in most cases three or four iterations are sufficient to give convergence to within 1°C.

APPENDIX II: THE CHANGE IN EQUIVALENCE RATIO OF A BUBBLE FED FROM A GAS AND AIR ORIFICE

Consider a coalesced bubble at time t, mass M and an equivalence ratio ϕ_b. The air mass feed rate to the bubble is R_a, and the gas mass feed rate is R_g, at a gas equivalence ratio ϕ_g.

By definition
$$\phi_b = \frac{F.w}{A} \tag{A10}$$

Also
$$M = F + A \tag{A11}$$

rearranging (A10), (A11):

$$F = \frac{M.\phi_b}{\phi_b + w} \tag{A12}$$

$$A = \frac{M.w}{\phi_b + w} \tag{A13}$$

At t + Δt, the amounts of fuel and air in the bubble are respectively:

$$F_{\Delta t} = F + \frac{R_g.\phi_g.\Delta t}{\phi_g + w} \tag{A14}$$

and
$$A_{\Delta t} = A + \frac{R_g.w.\Delta t}{\phi_g + w} + R_a\Delta t \tag{A15}$$

from (A14) and (A15), the equivalence ratio at t + Δt is

$$\phi_{b\Delta t} = \frac{F_{\Delta t}.w}{A_{\Delta t}} \tag{A16}$$

Substitution of this value of ϕ into the combustion model described in Appendix I enables $\rho_{\Delta t}$ to be found, and hence equation (10) gives G, and (8) gives the distance, Δs, moved.

APPENDIX III: EQUIVALENCE RATIO OF A COALESCED BUBBLE

The equivalence ratio of the bubble formed by the coalescence of two bubbles of different equivalence ratio is found by applying the equations derived in Appendix II.

Bubble h equivalence ratio ϕ_h, mass M_h, coalesces with bubble i equivalence ratio ϕ_i, mass M_i to form bubble j of equivalence ratio ϕ_j.

From (A14) and (A15)

$$\phi_j = \frac{(F_h + F_i).w}{(A_h + A_i)} \tag{A17}$$

NOTATION

a,b,c,d,f = stoichiometric coefficients (-).

A = mass of air in bubble (M).

C = heat capacity ($Q\ M^{-1}\theta^{-1}$).

D = diameter of bubble (L).

E = combustion efficiency of fluidised bed (-).

F = mass of fuel in bubble (M).

g = acceleration due to gravity ($L\ T^{-2}$).

G = volumetric flowrate to bubble (L^3T^{-1}).

ΔH = heat released in fluidised bed by combustion in bubble per mass of fuel in the bubble (QM^{-1}).

H_{Fi} = heat of formation of chemical species i per unit mass ($Q\ M^{-1}$).

H_{Fo} = heat of formation of hydrocarbon fuel per unit mass ($Q\ M^{-1}$).

H_r = heat released by combustion (Q).

H_s = sensible heat of combustion products (Q).

k = constant (-).

K = equilibrium constant for water gas shift reaction (-).

M = mass of bubble (M).

n = average number of carbon atoms per molecule of fuel (-).

R = mass flowrate of air or gas ($M\ T^{-1}$).

s = distance measured vertically above distributor plate (L).

T = temperature (θ).

t = time (T).

U = velocity of bubble in vertical direction ($L\ T^{-1}$).

V = volume of bubble (L^3).

w = air to fuel mass ratio at stoichiometric conditions (-).

x = mole fraction(-).

y = hydrogen to carbon ratio of hydrocarbon fuel (-).

Greek letters

ε = voidage of fluidised bed (-).

ρ = density ($M\ L^{-3}$).

ϕ = equivalence ratio defined as ratio of stoichiometric to actual air used (-).

Subscripts

a = air.

b = bubble.

d = delay.

g = gas.

h,i,j, = species h,i,j, respectively.

m_f = state of incipient fluidisation.

p = particulate mass.

Δt = at end of interval Δt.

T = temperature.

0 = at t = 0 or at beginning of time interval Δt.

Superscripts

' = estimated.

REFERENCES

1. Watson, P.R., and Harrison, D., 1974, Instn. Chem. Engrs. Symp. Series No.38, (Paper F4). Multi-phase Flow Systems.

2. Davidson, J.F., and Schüler, B.O.G., 1960, Trans. Instn. Chem. Engrs., 38, 335.

3. Harrison, D., and Leung, L.S., 1961, Trans. Instn. Chem. Engrs., 39, 409.

4. Archer, John S., and Eisenklam, Paul, 1970, J. Inst. Fuel, 43, 397.

5. Gumz, W., 1950, "Gas Producers and blast furnaces - theory and methods of calculation." Chapman and Hall Ltd. (London).

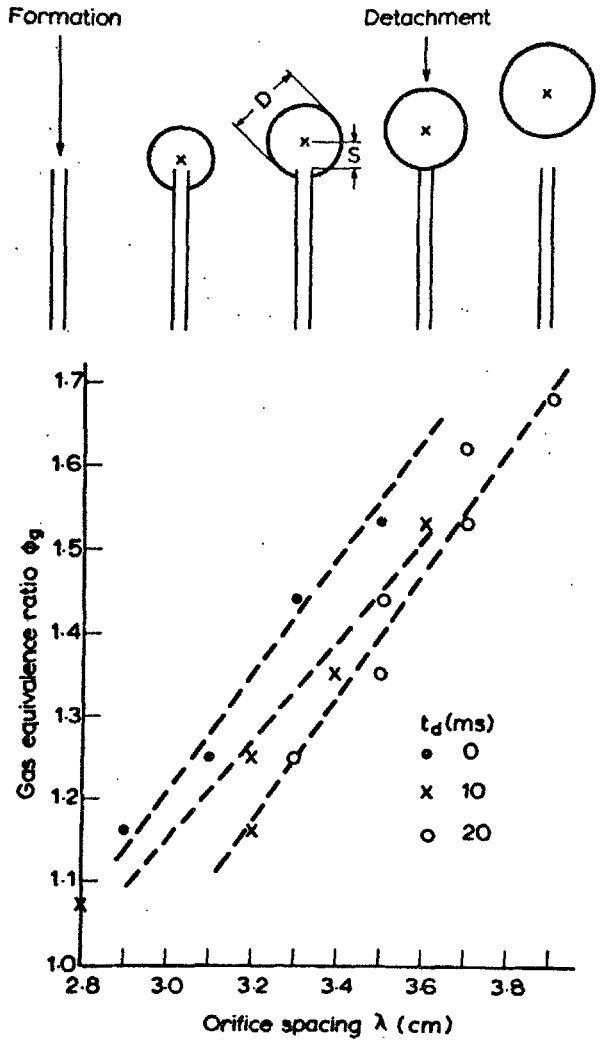

Fig 2: Orifice Spacing beyond which no mixing and hence no combustion takes place.

←Fig 1: Position and growth of bubble on single orifice with time.

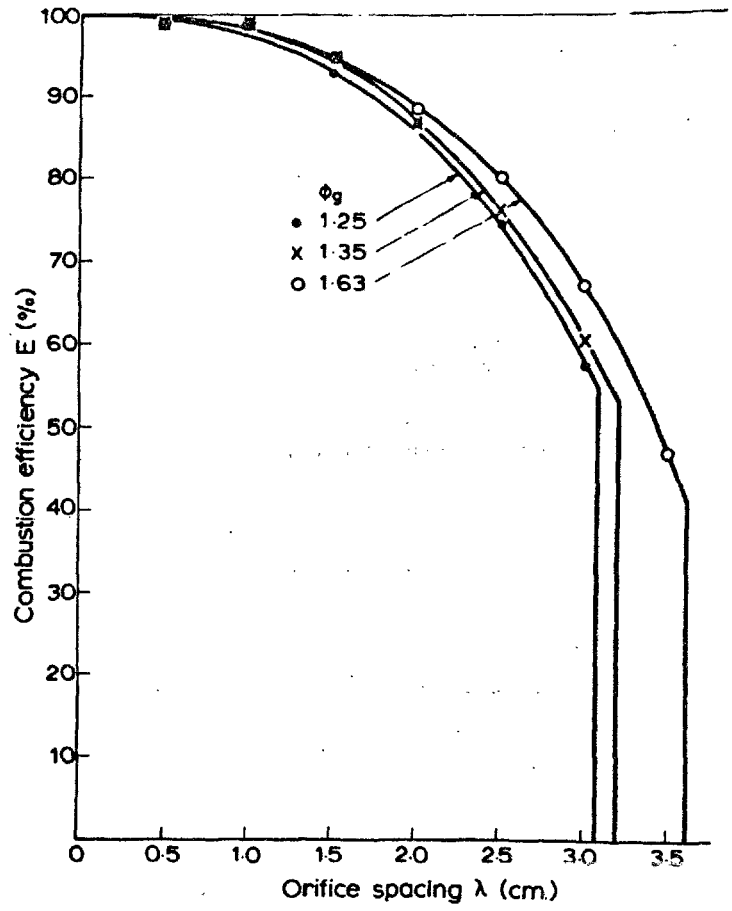

Fig 3: Combustion Efficiencies for varying delay times (bubble from one orifice overlapping the second).

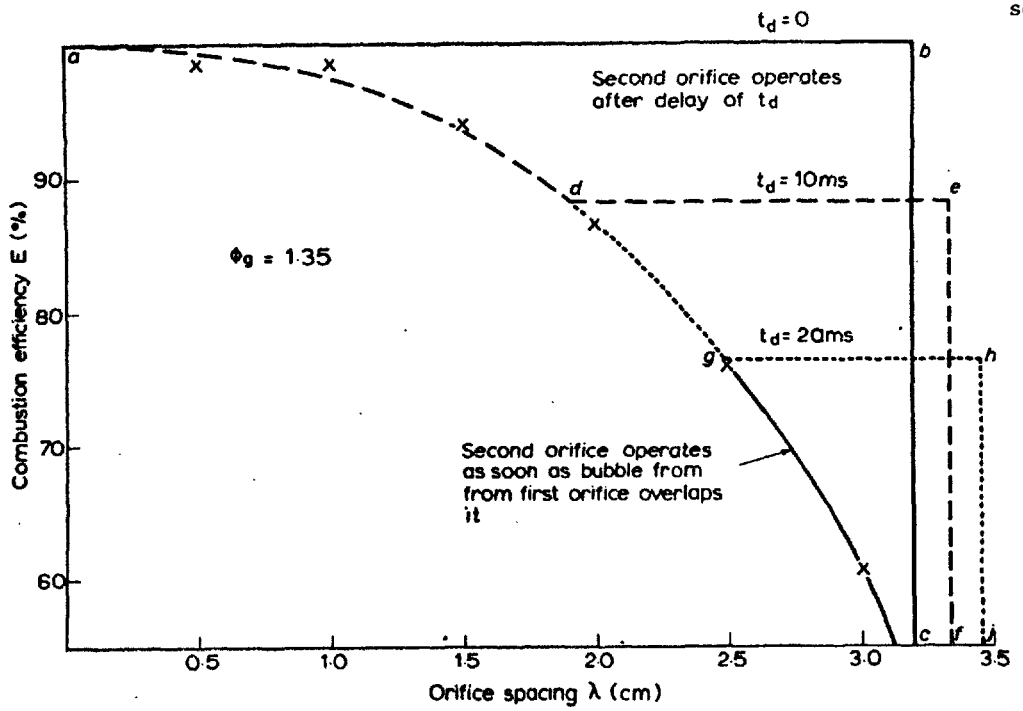

Fig 4: Combustion Efficiencies for various delay times for a gas of one composition.

REFERENCES

1. Archer, John S., and Eisenklam, Paul, 1970, "Multistage combustion of residual fuel oil, Part 1: The effects of using air or steam for the atomisation of residual fuel oil in a high intensity first stage gasifier," J. Inst. Fuel, 43, 397.
2. Ewings, H.A., 1969, "High Intensity and Two Stage Combustion," The Combustion Engineering Association, Document No. 8580.
3. Johns, W.R., 1965, "Residual Fuel Oil Combustion : The Effect of Air/Fuel Ratio on the Temperature of Combustion," Ph.D. Thesis, University of London.
4. Htun, Maung Nay, 1966, "Residual Fuel Oil Combustion : The Effect of Air/Fuel Ratio on Combustion Products Formed," Ph.D. Thesis, University of London.
5. Dombrowski, N., and Johns, W.R., 1969, "Thermal properties of Combustion gases from a residual-oil-fired high intensity combustion chamber," J. Inst. Fuel, 42, 194.
6. Rodriguez-Polanco, D., 1975, "Spray Combustion of Residual Fuel-Oil : Particulate and Gaseous Emission in a Two Stage System," Ph.D. Thesis, University of London.
7. Ministry of Housing and Local Government, 1967, "Grit and dust : The measurement of emissions from boiler and furnace chimneys," H.M.S.O., London.
8. Grout, Peter David, 1970, "Combustion of Residual Fuel Oil : Modelling

and Optimisation of a Two Stage System," Ph.D. Thesis, University of London.

9. Bartok, W., Crawford, A.R., and Skopp, A., 1971, "Control of NO_x emissions from stationary sources," Chem. Engng. Prog., 67, 64.

10. Eisenklam, Paul, and Archer, John Stuart, 1972, "Methods of an apparatus for burning fuel," Brit. Patent 1, 296, 057.

11. Skinner, D.G., 1970, "The Fluidised Combustion of Coal," The National Coal Board.

12. First, Second, Third International Conference on Fluidised Bed Combustion, 1968, 1970, 1972, U.S. Environmental Protection Agency.

13. Fluidised Combustion Conference, 1975, Inst. Fuel Symp. Series No. 1, Proceedings Vol. 1.

14. Stubington, J.F., 1973, "The Combustion of Oil in Fluidized Beds," Ph.D. Dissertation, University of Cambridge.

15. Craig, J.W.T., Johnes, G.L., Moss, G., Taylor, J.H., and Tisdall, D.E., 1972, "Study of Chemically active fluid bed gasifier for reduction of sulphur oxide emissions," Esso Research Centre.

16. Lunn, H.G., Roberts, A.G., and Locke, H.B., 1973, "Combustion of residual fuel oils in fluidised beds," Proceedings of Third International Conference on Fluidised-bed Combustion, EPA - 650/2 - 73 - 053, (paper V - 5).

17. Town, Joseph W., Paige, Jack I., and Russell, James H., 1970, "Sorption of sulphur dioxide by alkalised alumina in a fluidised-bed reactor," Chem. Eng. Prog. Symp. Series No. 105, 66, 260.

18. Jarry, R.L., Anastasia, L.J., Carls, E.L., Jonke, A.A., and Vogel, G.L., 1970, "Comparative emissions of pollutants during combustion of natural gas and coal in fluidised beds," Proceedings of Second International Conference on Fluidised-bed Combustion, U.S. Environmental Protection Agency Publication No. AP - 109, (paper I - 5).

19. Elliot, D.E., and Virr, M.J., 1973, "Small-scale applications of fluidised-bed combustion and heat transfer," Proceedings of Third International Conference on Fluidised-Bed Combustion, EPA - 650/2 - 73 - 053, (paper IV - 1).

20. Broughton, J., 1975, "Gas Combustion in shallow fluidised beds," Applied Energy, 1, 61.

21. Cole, W.E., and Essenhigh, R.H., 1973, "Studies on the combustion of natural gas in a fluid bed," Proceedings of Third International Conference on Fluidised-Bed Combustion, EPA - 650/2 - 73 - 053, (paper II - 5).

22. Tamalet, M., 1968, "The application of fluid-bed heat transfer to metallurgical processes," Instn. Chem. Engrs. Symp. Series No. 31, 105.

23. Reh, L., 1970, "Combustion of oil or gas in fluidised beds," Proceedings of Second International Conference on Fluidised-Bed Combustion, U.S. Environmental Protection Agency Publication No. AP - 109, (paper V - 6).

24. Evans, Bruce Ronald, 1973, "Gas distributors for fluidised beds," Brit. Patent 1, 341, 617.

25. Singh, B., Rigby, G.R., and Calcott, T.G., 1975, "Combustion of gaseous fuels in a fluidised bed," Inst. Fuel Symp. Series No. 1, (paper C5).

26. Meisen, A., and Mathur, K.B., 1974, "The spouted bed aerosol collector : A novel device for separating small particles from gases," Inst. Chem. Engrs. Symp. Series No. 38, (paper K3).

27. Suzukawa et al., 1973, "Process for treating gaseous products obtained by thermal cracking of hydrocarbons," United States Patent 3, 719, 029.

28. Whitehead, A.B., 1971, in "Fluidization" Ed. Davidson, J.F., and

Harrison, D., Academic Press, (chapter 19).

29. Kunii, Dazio, and Levenspeil, Octave, 1969, "Fluidization Engineering" John Wiley and Sons Inc..

30. Johnson, T.W., and Davison, J., 1964, "Reduction of iron ore by the flame-smelting process," Jnrl. Iron and Steel Inst., 202, 406.

31. Harrison, D., and Leung, L.S., 1961, "Bubble formation at an orifice in an inviscid liquid," Trans. Instn. Chem. Engrs., 38, 335.

32. Davidson, J.F., and Schuler, B.O.G., 1960," Bubble formation at an orifice in an inviscid liquid", Trans. Instn. Chem. Engrs., 38, 335.

33. Leung, L.S., 1972, "Design of gas distributors and prediction of bubble size in large gas-solids fluidised beds," Powder Technol., 6, 189.

34. Whitehead, A.B., and Young, A.D., 1967, "Fluidisation performance in large scale equipment : Part 1," Proc. Int. Symp. Fluidisation, Ed. Drinkenburg, A.A.H., Netherlands Univ. Press, 284.

35. Watson, P.R., and Harrison, D., 1974, "The influence of gas distributor design on the bubbling behaviour of a fluidised bed," Instn. Chem. Engrs. Symp. Series No. 38, (paper F4).

36. Whitehead, A.B., and Dent, D.C., 1967, "Behaviour of multiple tuyere assemblies in large fluidised beds," Proc. Int. Symp. Fluidisation, Ed., Drinkenburg, A.A.H., Netherlands Univ. Press, 802.

37. Fakhimi, S., and Harrison, D., 1970. "Multi-orifice distributors in fluidised beds : a guide to design," Chemeca '70, Butterworths of Australia, 29.

38. Whitehead, A.B., Gartside, G., and Dent, D.C., 1970, "Flow and pressure maldistribution at the distributor level of a gas-solid fluidised bed," Chem. Engng. Jrnl., 1, 175.

39. Gregory, S.A., 1967, "The distribution plate problem," Proc. Int. Symp. Fluidisation, Ed., Drinkenburg, A.A.H., Netherlands Univ. Press, 751.

40. Hiby, J.W., 1964, "Untersuchungen über den kritischen Mindestdruckverlust des Anströmbodens bei Fluidalbetten (Fliessbetten)," Chemie - Ing. Techn., 36, 228.

41. Zuiderweg, F.J., 1967, "Report, Session 9," Proc. Int. Symp. Fluidisation, Ed., Drinkenburg, A.A.H., Netherlands Univ. Press, 739.

42. Archer, John S., Grout, Peter D., and Eisenklam, Paul, 1970, "Multistage combustion of residual fuel oil, Part 2 : The characteristics of a second stage combustion chamber and a two stage combustion system," J. Inst. Fuel, 43, 451.

43. Davidson, J.F., and Harrison, D., 1963, "Fluidised Particles," Cambridge University Press.

44. Potter, O.E., 1971, in "Fluidization" Ed., Davidson, J.F., and Harrison, D., Academic Press, (chapter 7).

45. Davies, C.E., and Eisenklam, Paul, 1975 "A note on a hydrodynamic model for gas combustion on a distributor plate in a fluidised bed," Inst. Fuel Symp. Series No. 1, (paper A4).

46. Kozin, V.E., and Baskakov, A.P., 1966, Izv. Vysshikh Uchebn. Zavedenii, Khim. i Khim. Technol., 9, 137; quoted by Whitehead, A.B., in reference 28.

47. Zenz, Frederick A., 1968, "Bubble formation and grid design," Instn. Chem. Engrs. Symp. Series No. 30, 136.

48. Merry, J.M.D., 1971, "Penetration of a horizontal gas jet into a fluidised bed," Trans. Instn. Chem. Engrs., 49, 189.

49. Singh, B., Rigby, G.R., and Calcott, T.G., 1973, "Measurement of minimum fluidisation velocities at elevated temperatures," Trans. Instn. Chem. Engrs., 51, 93.

50. Svehla, Roger A., 1962, "Estimated viscosities and thermal conductivities of gases at high temperatures," NASA TR - R - 132, N 63 - 22 862.

51. Toth, H.E., 1968, "Equilibrium compositions and physical properties of products of combustion of methane and natural gases with air," Special Report No. 6, The Gas Council Industrial Marketing Committee.

52. Toth, H.E., and Francis, W.E., 1964, "The physical properties of town gas and its combustion products," The Gas Council Industrial Gas Development Committee.

53. Lever, G., Urquhart's Engineering Limited, Perivale, Middlesex, Private Communication.

54. Leva, Max, 1959, "Fluidisation," McGraw-Hill Book Co. Inc., 158.

55. Stairmand, C.J., 1951, "The design and performance of cyclone separators," Trans. Instn. Chem. Engrs., 29, 356.

56. Coates, N.H., and Rice, R.L., 1970, "Fluid-bed combustion of various U.S. coals," Proceedings of Second International Conference on Fluidised-Bed Combustion, U.S. Environmental Protection Agency Publication No. AP - 109, (paper I - 2).

57. Davies, C.E., 1973, Drng.No. F0118 - F137, Combustion Engineering Laboratory, Dept. of Chem. Eng., Imperial College.

58. Turner, B., G R - Stein Refractories Limited, Monolithics Division, Deepcar, Sheffield, Private Communication.

59. Wilson, H., 1974, "Investigation as to structural feasibility of building a 'fluidised-bed reactor' on an existing suspended floor," Civil Engineering Consultation to Imperial College Buildings Officer.

60. Archer, John S., 1969, "An Experimental Investigation of Spray Combustion in a Two Stage System," Ph. D. Thesis, University of London.

61. Davies, C.E., 1975, "Technical Recommendations following commissioning trials with fluidised bed combustor," Combustion Engineering Laboratory, Dept. of Chem. Eng., Imperial College.

62. Composition of 'Vanilla' residual fuel oil, Admiralty - NTGE Communication, 1955.

63. Hirschfelder, J.O., 1958, in "The properties of gases and liquids," by Reid, Robert C., and Sherwood, Thomas K., McGraw-Hill book Company Inc., 267.

64. Anon., "Product Data," Cawoods Refractories Ltd., Crabtree Manorway, Belvedere, Kent.